

RCA REVIEW

a technical journal

**RADIO AND ELECTRONICS
RESEARCH • ENGINEERING**

VOLUME XIX

MARCH 1958

NO. 1

RADIO CORPORATION OF AMERICA

DAVID SARNOFF, *Chairman of the Board*

FRANK M. FOLSOM, *Chairman of the Executive Committee*

JOHN L. BURNS, *President*

E. W. ENGSTROM, *Senior Executive Vice-President*

DOUGLAS H. EWING, *Vice-President, Research and Engineering*

JOHN Q. CANNON, *Secretary*

ERNEST B. GORIN, *Vice-President and Treasurer*

RCA LABORATORIES

J. HILLIER, *General Manager*

RCA REVIEW

C. C. FOSTER, *Manager*

C. H. VOSE, *Business Manager*

PRINTED IN U.S.A.

RCA REVIEW, published quarterly in March, June, September, and December by RCA Laboratories, Radio Corporation of America, Princeton, New Jersey. Entered as second class matter July 3, 1950 at the Post Office at Princeton, New Jersey, under the act of March 3, 1879. Subscription price in the United States and Canada; one year \$2.00, two years \$3.50, three years \$4.50; in other countries: one year \$2.40, two years \$4.30, three years \$5.70. Single copies in the United States, \$.75; in other countries, \$.85.

RCA REVIEW

a technical journal

RADIO AND ELECTRONICS
RESEARCH • ENGINEERING

Published quarterly by

RCA LABORATORIES

in cooperation with all subsidiaries and divisions of

RADIO CORPORATION OF AMERICA

VOLUME XIX

MARCH, 1958

NUMBER 1

CONTENTS

	PAGE
Tropospheric Scatter Propagation—A Summary of Recent Progress H. STARAS	3
A Solid-State Amplifying Fluoroscope Screen B. KAZAN	19
Hollow-Cathode Glow Discharge in Mercury Vapor K. G. HERNQVIST	35
Some New Structure-Type Targets for the Vidicon—An Analysis of Their Operation S. A. OCHS AND P. K. WEIMER	49
Differential Method of Lag Compensation in Photoconductive Devices H. BORKAN AND P. K. WEIMER	62
A Hysteresis Effect in Cadmium Selenide and Its Use in a Solid-State Image Storage Device F. H. NICOLL	77
An Electrostatically Focused Traveling-Wave-Tube Amplifier K. K. N. CHANG	86
Large-Area Germanium Power Transistors B. N. SALDE AND JANE PRINTON	98
Considerations Affecting the Rise and Decay of Cathode Currents in Receiving Tubes E. R. SCHRADER	109
RCA TECHNICAL PAPERS	128
AUTHORS	132

© 1958 by Radio Corporation of America
All rights reserved

RCA REVIEW is regularly abstracted and indexed by *Industrial Arts Index*, *Science Abstracts* (I.E.E.-Brit.), *Electronic Engineering Master Index*, *Chemical Abstracts*, *Proc. I.R.E.*, and *Electronic & Radio Engineer*.

RCA REVIEW

BOARD OF EDITORS

Chairman

R. S. HOLMES
RCA Laboratories

D. D. COLE
RCA Victor Television Division

M. C. BATSEL
Defense Electronic Products

I. F. BYRNES
Industrial Electronic Products

O. E. DUNLAP, JR.
Radio Corporation of America

E. W. ENGSTROM
Radio Corporation of America

G. H. BROWN
Industrial Electronic Products

H. H. BEVERAGE
RCA Laboratories

G. L. BEERS
Radio Corporation of America

D. H. EWING
Radio Corporation of America

A. N. GOLDSMITH
Consulting Engineer, RCA

A. L. HAMMERSCHMIDT
National Broadcasting Company, Inc.

O. B. HANSON
Radio Corporation of America

E. W. HEROLD
RCA Laboratories

J. HILLIER
RCA Laboratories

C. B. JOLLIFFE
Defense Electronic Products

E. A. LAPORT
Radio Corporation of America

C. W. LATIMER
RCA Communications, Inc.

H. W. LEVERENZ
RCA Laboratories

G. F. MAEDEL
RCA Institutes, Inc.

L. MALTER
Semiconductor Division

H. F. OLSON
RCA Laboratories

D. S. RAU
RCA Communications, Inc.

D. F. SCHMIT
Radio Corporation of America

S. W. SEELEY
RCA Laboratories

G. R. SHAW
Electron Tube Division

L. A. SHOTLIFF
Radio Corporation of America

I. WOLFF
RCA Laboratories

Secretary

C. C. FOSTER
RCA Laboratories

REPUBLICATION AND TRANSLATION

Original papers published herein may be referenced or abstracted without further authorization provided proper notation concerning authors and source is included. All rights of republication, including translation into foreign languages, are reserved by RCA Review. Requests for republication and translation privileges should be addressed to *The Manager*.

TROPOSPHERIC SCATTER PROPAGATION — A SUMMARY OF RECENT PROGRESS*

BY

HAROLD STARAS

RCA Laboratories,
Princeton, N. J.

Summary—During the past decade, one of the major breakthroughs in the field of communication has occurred because of our ability to understand a new mode of propagation through the atmosphere of radio signals in the 50-5,000 megacycle range. This new mode has come to be called tropospheric scatter propagation. The great interest in it arises from the fact that it provides a highly reliable means of establishing a point-to-point communication system over distances up to about 600 miles.

This paper gives a short history of this new mode of propagation and then presents an explanation of many of its characteristics in terms of simple physical pictures rather than detailed mathematics. It is hoped that this presentation will provide a theoretical foundation for those who may become active workers in this new and exciting field as well as satisfying the scientific curiosity of many other readers.

INTRODUCTION

ONE of the most significant achievements in the communications field during the past decade has been the utilization of the scattering of electromagnetic radiation by the random inhomogeneities in the atmosphere for long-range point-to-point communication systems in the frequency range 50-5,000 megacycles. With the aid of this new mode of propagation, it is now possible to communicate between distant points separated by rugged terrain, barren wastes or water barriers.

Like many other notable achievements in science or engineering, scatter propagation was discovered by pure chance. Although there had been occasional reports of very strong signals being received beyond the horizon during World War II, the detailed study of scatter propagation did not begin in the United States until commercial television had become firmly established. At this time, it was discovered that the signals from one transmitter would frequently interfere with those of a co-channel transmitter almost 200 miles away. A detailed investigation of these strong interference signals (strong compared to previous theoretical predictions), indicated that they were present

* Manuscript received November 4, 1957.

all the time, but were subject to rather severe and rapid fading. This had suggested to many workers in the field of propagation that some sort of scatter mechanism was responsible. The first reasonably accurate mathematical statement of the phenomenon was made by Booker and Gordon,¹ who used a formulation originally suggested by Pekeris² in connection with the scattering of sound by a turbulent fluid.

Although there have been many improvements in the theory since it was first presented by Booker and Gordon, the broad outlines of it remain substantially intact. The usual concept of the scatter phenomenon can be described somewhat as follows. The major part of the radiation from a transmitting antenna illuminates that part of the atmosphere above the horizon of the transmitter which lies within the antenna beamwidth. Within this volume there are irregular variations of the refractive index of the atmosphere so that the atmosphere can be considered as consisting of "blobs" of different dielectric constant randomly distributed. The average dimension of a blob, l , in any direction is substantially greater than the wavelengths of the radiation in the 50-5,000 megacycle under consideration.

These irregularities in the refractive index of the atmosphere re-radiate a portion of the incident electromagnetic energy. Because the irregularities are large compared to the wavelength of the radiation, the scattered radiation is concentrated in a fairly narrow cone angle around the forward direction of the incident energy. A portion of the energy scattered by the atmospheric irregularities in that part of the atmosphere which is within the antenna beams of both the transmitter and receiver arrives at the receiver. The sketch shown in Figure 1, which by now has become the symbol of the "scatter propagationist," depicts the phenomenon just described. The volume of air space inside the heavy lines represents the common volume visible to both the transmitting and receiving antennas. In this volume are depicted several typical blobs of atmosphere having a refractive index somewhat different from the average. Each of these blobs scatters a portion of the incident radiation in all directions but, as mentioned earlier, *not* in all directions equally, i.e., the intensity of the scattered radiation from each blob is a function of the scattering angle, θ . Some of the scattered radiation from each of the blobs arrives at the receiving antenna. The total received scattered signal is then the sum of the signals scattered from each of the blobs to the receiver.

¹ H. G. Booker and W. E. Gordon, "A Theory of Radio Scattering in the Troposphere," *Proc. I.R.E.*, Vol. 38, p. 401, April, 1950.

² C. L. Pekeris, "Note on the Scattering of Radiation in an Inhomogeneous Medium," *Phys. Rev.*, Vol. 71, p. 268, February, 1947.

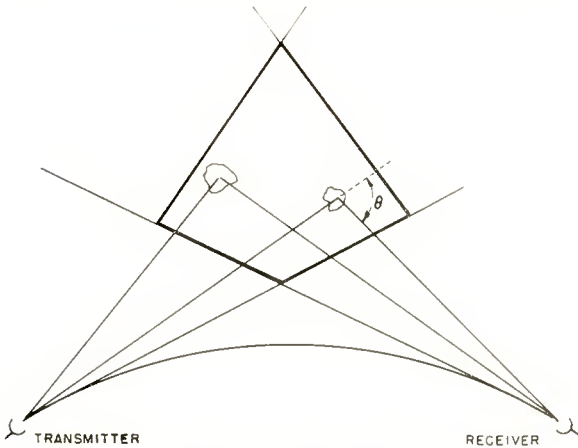


Fig. 1—Schematic of the scatter-propagation phenomenon.

Angular and Frequency Dependence of the Scattered Radiation

Figure 2 shows a typical atmospheric blob whose dielectric constant differs from the average dielectric constant, ϵ , by $\Delta\epsilon$. Impinging on this blob is incident radiation from a transmitter and emerging from it is the scattered radiation. The energy scattered in the forward direction is a maximum and, as the scattering angle increases, the scattered energy decreases. From considerations of electromagnetic theory, it can be shown that the frequency and angular dependence of the scattering from a blob are interconnected. In particular, the *average* scattered power from a blob, P_s , is proportional to $(\Delta\epsilon/\epsilon)^2 k^4 S (k l \sin \theta/2)$, where $(\Delta\epsilon/\epsilon)^2$ is the mean square of the refractive index variations (this might be referred to as the intensity of the turbulence) and $k = 2\pi/\lambda$ (λ being the wavelength of the radiation) and l the dimension typical of the blob size. The function S might be called the scattering function. For $l/\lambda \ll 1$ (which does not apply to radio scattering in the troposphere), the function S is a constant and the scattering is called Rayleigh scattering, which has the character-

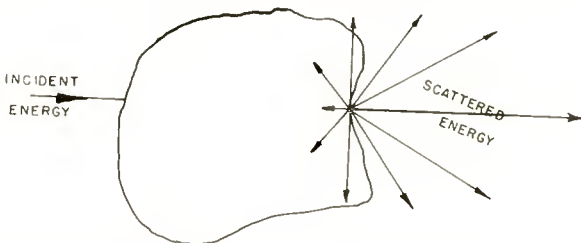


Fig. 2—The angle dependence of scattering from a blob.

istics of being independent of angle and having an $1/\lambda^4$ frequency dependence. For $l/\lambda \gg 1$, a condition which is satisfied in the phenomenon of radio scattering in the troposphere, the functional form of S must be determined either from experimental data, especially data bearing on the frequency dependence of the scattered radiation, or by an analysis of the hydrodynamics of atmospheric turbulence. This latter point is discussed later.

Another important property of the scattering function is that it represents the normalized three-dimensional Fourier transform of the autocorrelation function of the dielectric constant fluctuations. If we represent the autocorrelation function by $N(\rho)$ defined by

$$N(\rho) = N(\mathbf{r} - \mathbf{r}') = \overline{(\Delta\epsilon/\epsilon)(\mathbf{r}, t) (\Delta\epsilon/\epsilon)(\mathbf{r}', t)}$$

then

$$\overline{(\Delta\epsilon/\epsilon)^2} S = \int \int_{-\infty}^{\infty} N(\rho) e^{j\mathbf{k}\cdot\rho} d\rho$$

where $|\mathbf{k}| = 2k \sin \theta/2$. Thus, a knowledge of S implies a knowledge of $N(\rho)$. This relation between S and N has received considerable attention in the literature.*

The experimental data gathered over many years over many different scatter paths and throughout the frequency band of 50-5,000 megacycles suggest that there is a frequency dependence proportional to wavelength.³ Since the scattering angle, θ , is quite small throughout the important part of the scattering volume, the sine function may be replaced by its argument and S becomes proportional to $(kl\theta)^{-5}$. Furthermore, since the scattering angle, θ , is proportional to the path length between the transmitter and receiver, the functional form of S plays a significant role in determining the distance dependence of the scattered signal. However, the θ^{-5} relation does not adequately explain the experimentally measured distance dependence. In order to accommodate the experimental data as to both frequency and distance dependence, one must also assume that the intensity of turbulence, $\overline{(\Delta\epsilon/\epsilon)^2}$, decreases with height with somewhere between an h^{-1} and h^{-2} dependence.⁴ This is consistent with data obtained by von Rosen-

* See, for example, References (1) and (9).

³ K. Bullington, "Characteristics of Beyond the Horizon Radio Transmission," *Proc. I.R.E.*, Vol. 43, p. 1175, October, 1955.

⁴ W. E. Gordon, "Radio Scattering in the Troposphere," *Proc. I.R.E.*, Vol. 43, p. 23, January, 1955.

berg, Crain and Straiton,⁵ of the University of Texas, using an airborne microwave refractometer,^{6,7} an instrument which measures directly the dielectric constant of the air to which it is exposed.

In the previous discussion on the distance and frequency dependence of the scattered signal, consideration was restricted to long time averages of these quantities. Since the scattering phenomenon is related to atmospheric irregularities, there must be time variations associated with it. Broadly speaking, there are two general classes of fading associated with scattering, namely, "fast" and "slow" fading. The slow fading results from the gross changes of atmospheric conditions, changes which take place on a diurnal and seasonal basis. These slow signal level variations are presumably caused by changes in the magnitude of the intensity of turbulence and in its spatial distributions. It may also be caused by changes in the internal blob structure as defined by the autocorrelation function, $N(\rho)$. To date, there has been little success in using weather information to predict radio signal data with any degree of accuracy on an hourly basis or even on a daily basis. There are, however, certain crude generalizations which may be made; summer signal levels average 10 decibels higher than those in winter, while midafternoon signals, when the atmosphere is reasonably well mixed, are 5 decibels or so lower than morning or evening signals. In addition, the longer scatter paths exhibit less variability over the year than the short paths. This is explained by the fact that the scatter volume for the longer paths is located at higher altitudes where there is less meteorological variability.

The fast fading occurs because the total received signal is the phasor sum of many signals coming from different blobs in the atmosphere. Since these blobs are in constant turbulent motion, the phase angles between the different signal components coming from the different blobs are constantly changing. The resultant amplitude variations are well described by a Rayleigh distribution. Another characteristic of the fast fading which is consistent with theory is that the average fading rate is proportional to path length and f^n , where f is the frequency of the radiation and n lies between 2/3 and 1. According to theory, the time variations of the received signal due to a steady

⁵ C. E. von Rosenberg, C. H. Crain, A. W. Straiton, "Atmospheric Reference Index Fluctuations as Recorded by an Airborne Microwave Refractometer," *Elec. Eng. Res. Lab., U. of Texas*, Report 6-01 (1953).

⁶ C. Birnbaum, "A Recording Microwave Refractometer," *Rev. Sci. Instr.*, Vol. 21, p. 169, February, 1950.

⁷ C. M. Crain, "Apparatus for Recording Fluctuations in the Refractive Index of the Atmosphere at 3.2 cm Wavelength," *Rev. Sci. Instr.*, Vol. 21, p. 456, May, 1950.

drift of the blobs as they are borne along by the wind would give rise to an f dependence, while the random self-motion of the blobs would contribute an $f^{2/3}$ dependence. A typical rate for the fading is one cycle per second over a 100 mile path at 1,000 megacycles.

As stated earlier, the phenomenon of scatter propagation was discovered accidentally from experimental data. Then other experiments were carried out to define more accurately the distance and frequency dependence of the scattered radiation even before the theory became well established. For a summary of the experimental evidence, see Bullington.³ By now, however, a reasonably accurate and consistent theory has been established and has been used to predict other important parameters concerning scatter circuits before conclusive experimental evidence became available. Probably the first analytical estimates of system parameters on a scatter circuit were presented by Gordon,⁴ who employed heuristic reasoning to obtain estimates of such parameters as the correlation distance between spaced receiving antennas, the height-gain function, and the bandwidth that the scatter medium can support with negligible distortion. Continuing with the same type of heuristic reasoning, Booker and de Bettencourt,⁵ obtained estimates of the antenna-to-medium coupling loss, which is discussed later. Extensions of these ideas were presented by the present author.⁹⁻¹² In these references, more detailed mathematical formulas for many of the important scatter circuit parameters are given and, in addition, the effect of anisotropy* on these parameters has been incorporated.

BANDWIDTH CAPABILITIES OF THE SCATTER MEDIUM

The bandwidth which the scatter medium can support without serious distortion is intimately related to the multipath delays which are experienced. These, in turn, depend on the effective size of the

³ H. G. Booker and J. T. de Bettencourt, "Theory of Radio Transmission by Tropospheric Scattering Using Very Narrow Beams," *Proc. I.R.E.*, Vol. 43, p. 281, March, 1950.

⁹ H. Staras, "Forward Scattering of Radio Waves by Anisotropic Turbulence," *Proc. I.R.E.*, Vol. 43, p. 1374, October, 1955.

¹⁰ H. Staras, "Diversity Reception with Correlated Signals," *Jour. of Appl. Phys.*, Vol. 27, p. 93, January, 1956.

¹¹ H. Staras, "The Statistics of Combiner Diversity," *Proc. I.R.E.*, Vol. 44, p. 1057, August, 1956.

¹² H. Staras, "Antenna-to-Medium Coupling Loss," *Trans. I.R.E.*, PGAP, p. 228, April, 1957.

* Anisotropy here refers to the fact that the characteristic length of a scattering blob in the horizontal dimension may be different from its length in the vertical dimension.

scatter volume. The effective size of the scatter volume is determined by a combination of antenna beamwidths and the beamwidths of the scattering blobs. Assuming for the moment that we have broadbeam antennas, a very large volume of air space above the horizons of both transmitter and receiver becomes visible to both (see Figure 3). Consider further, two points, P_1 and P_2 from which scattering to the receiver takes place. From the geometry of the situation, it is evident that the scatter angle θ_2 , at the point P_2 is larger than the scatter angle θ_1 , at the point P_1 . Since the scattered energy decreases as the scatter angle increases, the signal component decreases as the height above the intersection of the horizon planes between transmitter and receiver increases. By similar reasoning, it can be shown that as one moves away from the great-circle plane between transmitter and receiver, the scattered energy also decreases. Thus, even when using very broad-beam antennas, there is an effective size to the scatter volume

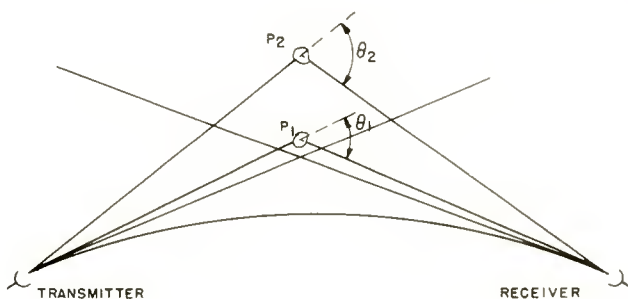


Fig. 3—Effective size of scatter volume.

which is much smaller than the volume within the beamwidths of the two antennas. Quantitative estimates of the size of the volume assuming isotropic scattering were first presented by Gordon.⁴ He also showed that the longest time delay is introduced by the ray that travels to the receiver via the highest point in the scatter volume lying in the great circle plane rather than from the point at the edge of the volume perpendicular to the great circle plane. In other words, the vertical dimension of the scatter volume is the determining factor in the maximum time delay encountered. The effect of anisotropic turbulence as developed by the present author is to make the effective horizontal dimension even smaller than it is for isotropic turbulence, thus making it even more likely that the vertical dimension is the determining factor in the maximum time delay encountered.

A qualitative physical description of the phenomenon of selective fading can be obtained by considering that the received signal arrives

over two paths, one via the shortest path through the scatter volume and the other via the longest path (i.e., passing through the upper edge of the scatter volume). Since the phase between these two rays is a function of frequency, the amplitude of the resultant signal is a function of frequency and appears as sketched in Figure 4. The separation between nulls is, of course, a function of time delay. On a scatter circuit using broad-beam antennas and neglecting the effect of aircraft in the scatter path, the frequency separation is approximately $\Delta f = 30/d^3$, where Δf is measured in megacycles and d in hundreds of miles. Since the scatter medium is in constant turbulent motion, we assume that the curve in Figure 4 jitters back and forth along the frequency axis as a random function of time, i.e., the position where the maxima and the minima occur is a random function of time. If we now consider a fixed intermediate-frequency bandwidth in the receiver equal in magnitude to that indicated by BC , we would expect

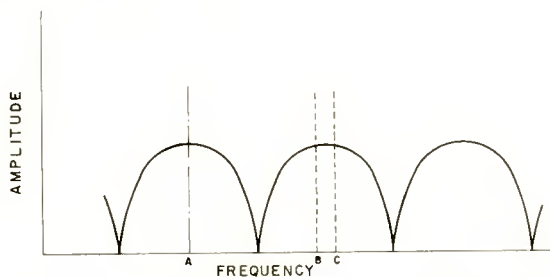


Fig. 4—Bandwidth limitation due to multipath.

no selective fading except when a null passes near or through the intermediate-frequency band. But, under these conditions, a substantial drop in signal would also occur and the diversity action in the receiving system would operate so as to attain a signal from another antenna, it being extremely unlikely that there, too, the received signal would pass through a null. On the other hand, if the bandwidth were as wide as AC , then the average signal level would remain reasonably high and even if diversity action did take place, it would be very likely that a null would also appear somewhere within the band at the second receiver, although at a different frequency.

The above qualitative discussion also applies when narrow-beam antennas are used (i.e., antenna beamwidths which are narrower than the inherent beamwidth associated with the scatter phenomenon) or when aircraft are in the propagation path. The only difference is that the frequency separation between the nulls in Figure 4 becomes a function of the antenna beamwidths and the geometry of the path.

Another interesting and useful way to look at the question of the

bandwidth that can be supported on a scatter circuit is to consider the correlation of the signal components at either end of the frequency band being used. If the correlation is high it means that the signal components are behaving essentially in unison and little or no distortion is expected. If correlation is low, then the signal components at either end of the band behave more or less independently and distortion is expected to occur quite often. Using the correlation approach just discussed, the present author arrived at the conclusion that the effective bandwidth of the medium is approximately $\Delta f = 4/d^3$, where Δf is in megacycles, and d in hundreds of miles. In arriving at this conclusion it was assumed that no diversity was being used and that the antenna beamwidths were broad compared to the beamwidth of the scatter medium. With the use of diversity, however, it is felt that the effective bandwidth of the scatter circuit may be as large as one-half to the full frequency separation between nulls on the sketch of Figure 4.

Another interesting aspect of scatter propagation is the instantaneous bandwidth of the system.¹³ This subject may be approached by posing the following question. If it is known that one frequency component of a signal is at a certain level, what is the probability that another frequency component Δf away will be at least 3 decibels (or some other such criterion) different due to the effects of propagation. An analysis of this problem was made based on the following assumptions: (1) fading followed a Rayleigh distribution, (2) diversity action could be ignored, and (3) distortion would result when propagation effects caused two signal components at opposite ends of the band to be more than 3 decibels apart for at least 1 per cent of the time. Based on these assumptions it was concluded that the instantaneous bandwidth is a function of instantaneous signal level. For example, if one signal level is 10 decibels above its median, the scatter medium bandwidth is about four times as wide as it would be if that signal level were at its median. On the other hand, if one signal level is 10 decibels below its median, the scatter medium bandwidth would be about one-fifth as wide as it would be if the signal level were at its median. For the case of a signal level 20 decibels below its median, the bandwidth is even lower. This conclusion can be visualized qualitatively from the amplitude-versus-frequency diagram shown in Figure 4, where it is seen that at low signal levels only a fairly small frequency change is necessary to obtain a 3-decibel change in signal level. At high signal levels, a much larger frequency change is required before a 3-decibel change in signal level is obtained.

¹³ "Study and Investigation of Tropospheric Scattering," Part A, Sec. 5.2.1.1, Final Report performed for U. S. Army Sig. Corps. Eng. Labs. by RCA under contract No. DA-36-039-SC-64555.

Before discussing the experimental results bearing on this question, it should be pointed out that aircraft in the propagation path will modify the maximum usable bandwidth when the antenna beamwidths are broader than the beamwidth of the scatter medium. In this case, the maximum time delay is determined by the antenna beamwidths rather than by the scatter medium beamwidth and the maximum usable bandwidth may become smaller than the estimate given by either Gordon⁶ or Staras.⁹ In the case of aircraft in the path, the bandwidth (with diversity) may be taken as approximately one-half the reciprocal of the maximum time delay over the circuit. This must be determined from the geometry of the situation and the antenna beamwidths.

COMPARISON WITH EXPERIMENT

The first set of data to which reference is made is presented in an RCA report.¹³ The data indicates that there exists appreciable pulse distortion and breakup (1.5-microsecond pulse) on a 153-mile path when broad antenna beams are used (about 5 degrees). This distortion apparently occurs even when no aircraft are in the path but is almost always accompanied by a short-time fade of at least 10 decibels below the local median. This result is consistent with the earlier discussion on "instantaneous" bandwidth.

The second experimental effort to which we make reference is that presented by Tidd,¹⁴ who reported that on a 188-mile path, no distortion was discovered on a television picture so long as signal strength was high enough to permit viewing. Examination of his experimental setup, however, shows that a frequency of 5,000 megacycles was being used with 28-foot parabolic antennas at either end of the path. Since for this path length and antenna beamwidths a time delay of only 0.01 microsecond is expected, it is not surprising that no bandwidth difficulties were encountered.

Another significant experimental test of the bandwidth capabilities of the scatter medium was reported by Ames and Rogers.¹⁵ In their test, Ames and Rogers observed the transmission of a commercial television test pattern from a distance of 196 miles. On the basis of observing about 600 photographs of the transmitted test pattern, they conclude that the scatter mechanism can support television bandwidths. However, a word of caution must be introduced concerning these con-

¹⁴ W. H. Tidd, "Demonstration of Bandwidth Capabilities of Beyond-Horizon Tropospheric Radio Propagation," *Proc. I.R.E.*, Vol. 43, p. 1297, October, 1955.

¹⁵ L. A. Ames and T. F. Rogers, "Available Bandwidth in 200 Mile VHF Tropospheric Propagation," *Trans. I.R.E.*, Vol. AP-3, p. 217, October, 1955.

clusions because of what has here been called "instantaneous" bandwidth. It is to be noted that Ames and Rogers operated at a median signal level of about 7 decibels above threshold, but a signal level of at least 30 decibels above threshold is necessary to get a picture sufficiently good to determine whether or not there is a noticeable multipath distortion. It would appear, therefore, that, by the very nature of their experiment, Ames and Rogers were able to measure the instantaneous bandwidth *only when signal level was instantaneously high*. From the earlier discussion, it was estimated that when the signal level is 10 decibels above the median, the bandwidth might be 20 times greater than when signal level is instantaneously 10 decibels below the median. Thus, the data of Ames and Rogers might lead one to an overly optimistic estimate of the bandwidth capacity of the scatter medium.

Another item of experimental evidence is presented in a report of the Pine Tree Project.¹⁶ In this report there are two experiments pertinent to this discussion. In one, a 160-kilocycle tone was used to frequency modulate a transmitter. Substantial sidebands appeared out to about 1 megacycle from the carrier. The intermediate-frequency signal from the receiver was fed through a spectrum analyzer and instantaneous photographs taken of the spectrum. The report states that quite often there appeared a fade of 20-30 decibels in a band only several hundred kilocycles wide, and that this fade would move through the radio-frequency band of the transmitted signal. This particular test suggests that the effective bandwidth on this path (about 170 miles) is only several hundred kilocycles wide without diversity. This result is consistent with the RCA results¹³ on AM pulse distortion and is more in line with the estimate presented by Staras⁹ (i.e., bandwidth = $4/d^3$, where bandwidth is in megacycles and d in hundreds of miles) rather than the estimate presented by Gordon⁶ (i.e., bandwidth = $30/d^3$). It should be emphasized, however, that these experimental results were obtained without diversity. Just how much diversity would improve the bandwidth capabilities is still a moot question.

The other experiment of interest in the Pine Tree Project report is the cross-talk experiment and the results presented in their Figure 12. In this experiment a baseband from 40 to 120 kilocycles was noise loaded and used to frequency modulate a transmitter with peak deviations up to 2 megacycles. After transmission over a 150-mile path,

¹⁶ H. J. von Baeyer, "Principles of Design and Operation of a Communication System Based on Tropospheric Scatter Propagation," report from Pine Tree Project Office, Ottawa, Canada, July, 1955.

the noise in an inactive channel was monitored and the cross-talk measured. The published curves in their Figure 12 indicated very little cross-talk added because of the propagation medium. Unfortunately, it would appear that this test cannot be used to draw significant conclusions concerning the bandwidth of the medium. It should be remembered from the discussion of instantaneous bandwidth that if a system encounters any bandwidth difficulties they are most likely to occur during a fade. A typical fade might last for a tenth of a second and occur only once every few seconds. The average cross-talk introduced by such a situation might hardly be measurable. It is of interest to note that in a verbal conversation, Dr. von Baeyer, the author of The Pine Tree Project report, indicated that he noticed occasional rises in channel noise simultaneously with a fade of the signal and these he did attribute to propagation bandwidth limitations.

It is felt that the problem of bandwidth limitations is one of the more serious ones yet to be resolved by a concerted effort of both analytical and experimental investigations. An interesting detail of this problem concerns the question of an FM system in which case it would be highly desirable to decide conclusively by an appropriate analysis whether the bandwidth limitation refers to the baseband, the r-f band, or something in-between.

CORRELATION DISTANCES

The correlation distance is the minimum spatial separation between antennas which will give rise to independent fading of the received signals. From a communications system standpoint, the significance of obtaining quantitative estimates of this parameter lies in the fact that space diversity is almost always utilized to obtain greater reliability. Conversely, from measurements of correlation distances, some conclusions can be drawn concerning anisotropy in atmospheric turbulence.

Estimates of the correlation distances in three mutually perpendicular directions (assuming isotropic turbulence) were first presented by Gordon.⁴ More refined estimates, including the effects of anisotropic turbulence, were obtained by the present author.⁹ From measurements taken by RCA,¹³ it appears that the effects of anisotropy are present at all times. More specifically, the anisotropy parameter (which is defined as the ratio of the scale of turbulence in the vertical dimension to the scale of turbulence in the horizontal dimension) was measured to have a median value of $\frac{1}{4}$.

This estimate of the anisotropy parameter was obtained indirectly by measuring the correlation between the signals received on two

spaced antennas as a function of the separation of the two antennas and then adjusting the anisotropy parameter so that the analytical curves match the data reasonably well. When the same procedure is used with Kurihara's data,¹⁷ an anisotropy parameter of about $\frac{1}{3}$ results.

As might be expected the measured estimates of the correlation distances and the anisotropy parameter are highly variable. Variations in these parameters involving a factor of two or three from day to day or even from hour to hour are not unusual. A crude estimate of the separation, s , in either the vertical dimension or horizontal dimension transverse to the plane of propagation required to give essentially independent fading is given by the formula $s = \lambda/\theta$, where λ is the wavelength of the radiation and θ is the angle, measured in radians, between horizon planes from the transmitter and receiver.

ANTENNA-TO-MEDIUM COUPLING LOSS

A somewhat more important parameter than the correlation distances discussed previously, and one which has been on occasion incorrectly evaluated from experimental data, is the antenna-to-medium coupling loss. This parameter was first evaluated by Booker and de Bettencourt⁸ and later by Staras.¹² In the latter paper, curves are presented which permit evaluation of the coupling loss when non-conical, nonidentical antennas are used at either end of the scatter circuit and which also permit taking the anisotropy parameter into account. For equivalent conditions, Staras' estimate for the coupling loss is substantially lower than the estimate of Booker and de Bettencourt.

The coupling loss phenomenon arises from the fact that the scattered signal arriving at the receiver does not come from a point source but rather from an extended volume subtending a measurable solid angle at the receiver. Thus, if the transmitting antenna is very highly directional it will illuminate a volume of air space smaller than the effective size of the scatter volume when a broad beam antenna is used. Since the scatter volume is decreased when a very-high-gain transmitting antenna is used, the signal arriving at the receiver will not increase in the same proportion as it would under free-space propagation conditions. This difference between the free-space expected gain of a highly directional antenna and its measured gain on a scatter circuit is called the antenna-to-medium coupling loss.

¹⁷ Y. Kurihara, "Trans-Horizon Microwave Propagation Over Hilly Terrain," *Proc. I.R.E.*, Vol. 43, p. 1362, October, 1955.

Conversely, if a very highly directional antenna is used on the receiving end of a scatter circuit, it will not "see" the entire effective scattering volume that is visible to a lower gain antenna. Again, the increase in signal will not be as large as under free-space conditions and again an antenna-to-medium coupling loss will be experienced. If two identical very-high-gain antennas are used on both ends of a circuit, the total coupling loss will be only a little larger than the coupling loss for any one of them individually.

COMPARISON WITH EXPERIMENT

Recent data from the Lincoln Laboratories of M.I.T. (unpublished) indicates that on the average, no noticeable coupling loss has been observed on a 618-mile path utilizing a 60-foot dish (frequency = 400 megacycles) at the transmitting and while comparing a 60-foot dish with a 28-foot dish on the receiving end. For this particular situation, it is not possible to utilize the Booker-de Bettencourt⁸ estimates properly since their estimates are for identical antennas at each end of the scatter circuit. However, their estimate for the coupling loss between two 60-foot antennas on this path is about 13 decibels, while the present author's estimate (Figure 2, Reference (12)) for this experiment is 2.5 decibels and appears to be more consistent with Lincoln Laboratory data. Furthermore, to evaluate experiments such as this one accurately, it is essential to be able to estimate coupling loss for dissimilar antennas at either end of the scatter circuit.

Another source of interest in this connection is the Bell Laboratory data¹⁸ obtained on a Labrador path. In this experiment, a coupling loss of 2.5 decibels was measured (650 hours of observations) at 4,000 megacycles when a 28-foot transmitting antenna was used, and a comparison between the received signal on a 5-foot and 28-foot antenna was made at the receiving end. For this particular situation the present author's estimate (as obtained from Figure 2, Reference (12)) is 2 decibels. Again it appears to be in substantial agreement with experiment.

ANGULAR DIVERSITY

Recently the desirability of using angular diversity (or scatter-angle diversity) has been under consideration. The intriguing aspect of this type of diversity is that the diversity action can be achieved

¹⁸ K. Bullington, W. J. Inkster, and A. L. Durkee, "Results of Propagation Test at 505 mc and 4,090 mc on Beyond-Horizon Paths," *Proc. I.R.E.*,

by use of only one large antenna at each terminal of a scatter circuit. The diversity action is achieved by the use of multiple radiators in a single reflector, each radiator giving rise to a narrow beam (i.e., narrow with respect to the beamwidth of the scatter medium itself) and these beams irradiate, or look at, different parts of the scatter volume. A simple two-dimensional schematic is shown in Figure 5. In the following discussion, it is explicitly assumed that all antenna beamwidths are broad in the horizontal dimension (i.e., in the dimension perpendicular to the plane of the drawing). In Figure 5, both antennas are assumed to be sufficiently large in the vertical dimension so that any one radiator in the antenna structure will give rise to a pattern which is substantially narrower than the angle subtended by the effective scattering volume. Figure 5 shows two beams, T_1 and T_2 , originating at the transmitter and two beams, R_1 and R_2 , associated with the receiver. The diversity action is obtained by virtue of the fact that the T_1R_1 propagation path is expected to behave independently

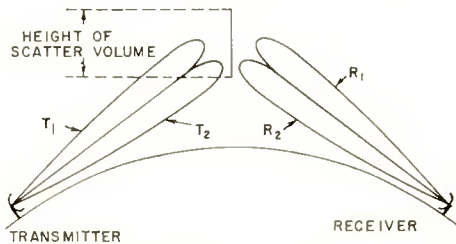


Fig. 5—Angular diversity diagram.

of the T_2R_2 path. A closer look at the situation reveals the following. For a fixed amount of power available for the transmitter, about one-half of it would have to be put into each of the transmitter radiators (see Figure 5). The question then arises: Why not put the total available power into one antenna half the size (twice the beamwidth)? The resulting power density in the scatter volume would remain the same. It would thus appear unnecessary to have an extremely large antenna with two radiators at the transmitting end. Consider now the merits of a very large antenna with two radiators at the receiving end. To be sure, the improvement of dual diversity will be realized in this case; however, the signal arriving at each radiator will have suffered a coupling loss and will be approximately equal to the signal strength received on an antenna half the size. The important decision to be made then is whether it is preferable to use one antenna sixty feet in diameter, say, with two radiators operating on angular diversity or two antennas thirty feet in diameter operating on the more conven-

tional space diversity. From this analysis it appears that angular diversity is not as exciting as a first estimate would indicate.

TURBULENT MIXING THEORY AND RADIO SCATTERING

During the past three years the most prominent progress in the theory of scatter propagation has occurred in the area of the hydrodynamics of atmospheric turbulence. There are at the moment two popular and conflicting theories. One is known as the Obukhov Mixing Theory and its application to radio scattering is discussed by Silverman¹⁹ and Bolgiano.²⁰ The other is referred to as the Mixing-in-Gradient Theory. It was first presented by Villars and Weiskopf²¹ and later extended by Wheelon.²² Both of these theories recognize that humidity fluctuations are primarily responsible for the refractive index variations in the troposphere and temperature fluctuations predominate in the stratosphere. Furthermore, in both theories, the analysis is fundamentally concerned with the spectrum of the turbulent irregularities, $S(k)$. Electromagnetic theory points out that the spectrum function, S , is the same as the scattering function mentioned earlier. Therefore, the scattered signal may be looked at as the result of applying a narrow-band filter centered about the point $k l \sin \theta/2$ in the spectrum of the turbulence. The two theories, however, lead to different estimates of the frequency dependence of the scattered radiation. The Obukhov Theory indicates a $\lambda^{-1/3}$ dependence while the Villars-Weiskopf Theory yields a λ dependence. On the basis of radio data only (i.e., no meteorological data is considered) the Villars-Weiskopf theory would appear to be more accurate.

¹⁹ R. A. Silverman, "Turbulent Mixing Theory Applied to Radio Scattering," *Jour. Appl. Phys.*, Vol. 27, p. 699, July, 1956.

²⁰ R. Bolgiano, "Turbulent Mixing and its Role in Radio Scattering," Cornell Univ. EE Report 334, Ithaca, N. Y., 1957.

²¹ V. Villars and V. F. Weiskopf, "On the Scattering of Radio Waves by Turbulent Fluctuations of the Atmosphere," *Proc. I.R.E.*, Vol. 43, October, 1955.

²² A. D. Wheelon, "Spectrum of Turbulent Fluctuations Produced by Convective Mixing of Gradients," *Phys. Rev.*, Vol. 105, p. 1706, March, 1957.

A SOLID-STATE AMPLIFYING FLUOROSCOPE SCREEN*†

BY

B. KAZAN

RCA Laboratories,
Princeton, N. J.

Summary—By using photoconductive and electroluminescent materials, a thin solid-state panel has been developed which is comparable in form and size to the conventional fluoroscope screen. With X-ray intensities used in medical fluoroscopy, this produces a high-contrast image with a brightness of about one foot-lambert which can be viewed in moderate room light; however, seconds are required for image build-up.

In terms of dosage, 5 to 50 milliroentgens are required on the panel to produce the image. The bright picture persists for 30 seconds or longer with the X-rays cut off. Thus, when extended viewing of stationary images is needed, patient dosage is reduced compared to conventional fluoroscopy. By electrical means it is possible to erase the persistent image in a fraction of a second. Using a shorter pulse of higher intensity X-rays, a transient image may also be recorded for extended viewing.

INTRODUCTION

DURING the past decade a number of electron-tube devices have been developed for reducing the X-ray dosage and increasing the image brightness.¹⁻⁴ These have successfully demonstrated that a reduction in X-ray dosage of about 10 times⁵ is possible without loss of information content from the fluoroscope screen, and that dark adaptation can be eliminated by the many orders of magnitude brightness increase. However, the complexity, bulk, expense, and operating problems associated in varying degrees with these systems have until now imposed limitations on their widespread use.

* Manuscript received November 22, 1957.

† Presented at the 58th Annual Meeting of the American Roentgen Ray Society, Washington, D. C., October 1-4, 1957; to be published in the Journal of that Society. The exhibit described in this paper was awarded first prize at the meeting.

¹ J. W. Coltman, "Fluoroscopic Image Brightening by Electronic Means," *Radiology*, Vol. 51, p. 359, September, 1948.

² R. H. Morgan and R. E. Sturm, "The Johns Hopkins Fluoroscopic Screen Intensifier," *Radiology*, Vol. 57, p. 556, 1951.

³ M. C. Teves and T. Tol, "Electronic Intensification of Fluoroscopic Images," *Philips Technical Review*, Vol. 14, p. 33, August, 1952.

⁴ J. E. Jacobs and H. Berger, "Large-Area Photoconductive X-ray Pickup-Tube Performance," *Electrical Engineering*, Vol. 75, p. 158, February, 1956.

⁵ T. Tol, W. J. Oosterkamp, and J. Proper, "Limits of Detail Perceptibility in Radiology Particularly When Using the Image Intensifier," *Philips Research Reports*, Vol. 10, p. 141, April, 1955.

The objectives of the present work are to increase the image brightness and reduce the X-ray dosage by using solid-state techniques. This approach allows the retention of many of the desirable features of the conventional fluoroscope screen since it permits the construction of the entire amplifying system in the form of a thin, large-area panel which can be easily viewed and manipulated, and which is free of complex auxiliary equipment.

The work described stems from earlier work on solid-state light amplifiers.^{6,7} With such panels it was demonstrated that a very dim image of visible light could be intensified by more than 100 times. The success in obtaining large gains in radiant energy with panels comparable in size to fluoroscope screens led to this extension of the work into the field of fluoroscopy.

PRINCIPLE OF OPERATION

The basic principle of the amplifier is shown in Figure 1, which depicts a single picture element. A photoconductor and an electroluminescent phosphor are connected electrically in series, and a voltage is applied across them. Photoconductive materials have the property of increasing their conductivity when excited by radiation. When unirradiated, many of these materials act as insulators. When excited with low levels of radiation, they increase their conductivity by many orders of magnitude. Depending on the particular material, they are sensitive to different types of radiation such as visible light, infrared, or X-rays in varying degrees. Electroluminescent phosphors are materials which emit light when voltage is directly applied to them, with the color of the light depending on the composition of the phosphor.

In the combination, the photoconductor acts as a valve or variable resistor controlling the flow of electrical power into the phosphor element. With sensitive photoconductors, a low-level X-ray beam can control a high level of output light. By comparison, in the case of the conventional fluoroscope phosphor, the output light is relatively low, deriving its energy from the conversion of the low-level energy in the X-ray beam. Using the amplifying principle, a picture device can be made with the materials in the form of thin layers. In Figure 2 the cross section of such an amplifier is shown in idealized form. Two adjacent layers are used with an opaque insulating layer between them to prevent output light from feeding back to the photoconductor.

⁶ B. Kazan and F. H. Nicoll, "An Electroluminescent Light-Amplifying Picture Panel," *Proc. I.R.E.*, Vol. 43, p. 1888, December, 1955.

⁷ B. Kazan, "An Improved High-Gain Panel Light Amplifier," *Proc. I.R.E.*, Vol. 45, p. 1358, October, 1957.

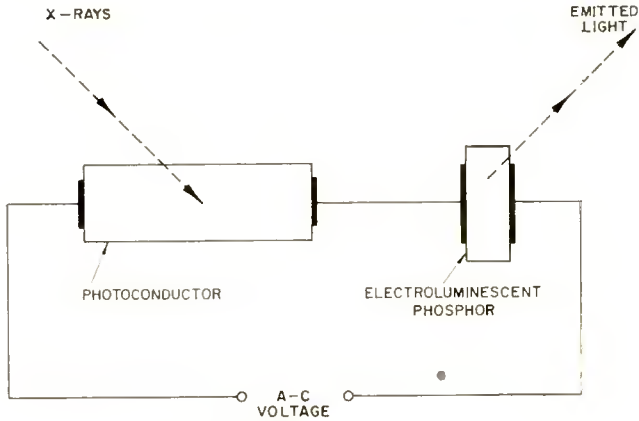


Fig. 1—Single-element amplifier.

Electrodes are provided on the outer surfaces, the electrode on the viewing side being transparent to visible light. Since the layers are very thin, X-rays exciting a local area of the photoconductor cause a flow of a-c current which is restricted to the adjacent phosphor area. This allows a pattern of X-rays to be converted to a pattern of light.

AMPLIFIER DESIGN

Because of the special properties of the photoconductive and electro-luminescent materials used, the actual panel design differs from the

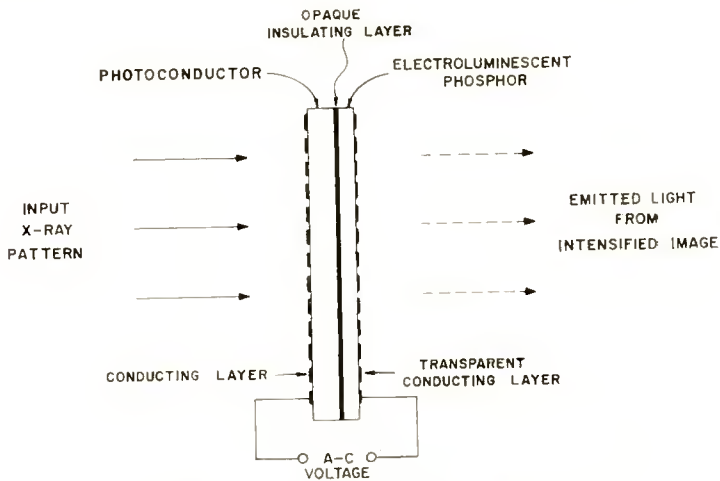


Fig. 2—Double-layer image intensifier.

idealized double-layer amplifier. Before describing the panel design, some of the properties of the materials will be discussed.

The phosphor is a Zn(S:Se) copper-activated material⁸ emitting a yellow-green light. Typical of most electroluminescent phosphors, it is in powder form bonded with plastic. For operation, such phosphor layers require a-c voltage to produce light. With d-c, there is only a negligible current flow and no light emission. Operation is possible over a wide range of audio frequencies, for example, from 60 to over 10,000 cycles, with the light output increasing almost linearly with frequency in this range. Figure 3 shows a log-log plot of the light output as a function of voltage for a fixed frequency of 420 cycles. The slope shows the light output to vary roughly as the third power of the applied voltage.

The photoconductor is a CdS powder⁹ also bonded with plastic. This powder was selected because it can easily be formed into uniform layers of arbitrary size and thickness.¹⁰ In addition, it has a sensitivity to X-rays and light comparable to the best photoconductive materials.

Although the photoconductive powder can be operated with a-c voltage, its sensitivity is as much as 10 times greater when operated with d-c or pulsed d-c voltage.^{6,7} Since the phosphor layer requires a-c voltage, being inoperative with d-c, this difference cannot be reconciled by the simple series circuit shown for the double-layer type of intensifier. One method of overcoming the problem is shown in Figure 4, which depicts a single amplifier element. Instead of a single photoconductor, two smaller photoconductors are used, both of which are assumed to be equally irradiated. Bias voltages of opposite polarities are in series with the photoconductors, and an a-c voltage is across the entire combination. Since the bias voltages are equal to the peak a-c voltage, pulsating d-c voltages of opposite polarity are produced as indicated to the right. Because of the very nonlinear current-voltage characteristic of the photoconductor, the current pulses are narrow, as indicated by the dashed curves. Since the current pulses are of opposite polarity and phase, the phosphor element is charged positive during one half cycle and negative during the next half cycle. In this way the phosphor is excited with a-c while pulsating d-c voltage

⁸ I. J. Hegyi, S. Larach, and R. E. Shrader, "Electroluminescence of Zinc Sulfo-Selenide Phosphors with Copper Activator and Halide Coactivator," *Jour. Electrochem. Soc.*, Vol. 104, p. 717, December, 1957.

⁹ S. M. Thomsen and R. H. Bube, "High-Sensitivity Photoconductor Layers," *Rev. Sci. Instr.*, Vol. 26, p. 664, July, 1955.

¹⁰ F. H. Nicoll and B. Kazan, "Large-Area High-Current Photoconductive Cells Using Cadmium Sulfide Powder," *Jour. Opt. Soc. Amer.*, Vol. 45, p. 647, August, 1955.

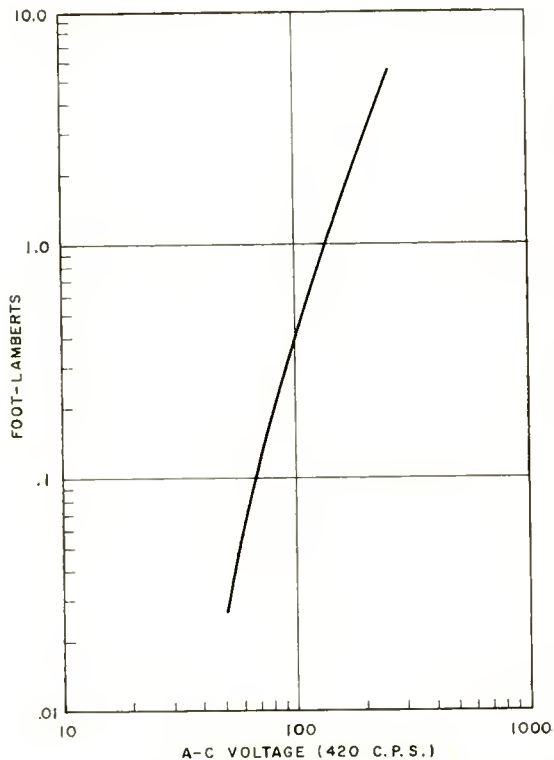


Fig. 3—Phosphor output light versus applied voltage.

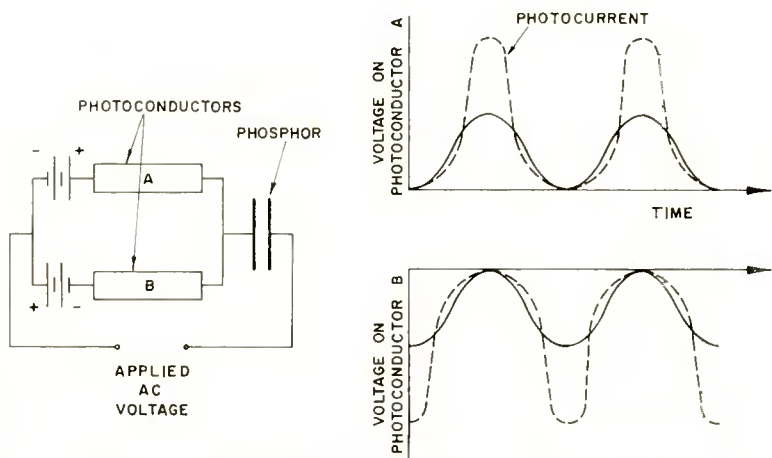


Fig. 4—Amplifier element with biased a-c operation.

is used to obtain high sensitivity from the photoconductor. In practice, two rectifier elements can be substituted for the d-c supplies to obtain the pulsed d-c. Such operation is almost as efficient, requiring only an a-c voltage source.

To use the pulsed d-c method of operation, the amplifier design shown in the cross section of Figure 5 is employed. For illustrative purposes the thickness of the layers is greatly exaggerated. As a base, a glass plate is used whose upper surface has a transparent conducting electrode. On this surface a thin layer of electroluminescent phosphor is deposited. The photoconductive layer is on the side facing the X-ray beam; the layer has grooves cut into it and has narrow conducting lines

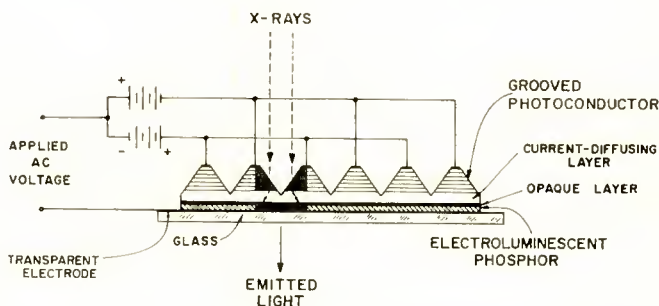


Fig. 5—Cross section of amplifying fluoroscope screen.

along the top. Between the phosphor and photoconductive layers are two other auxiliary layers. One is a thin opaque insulating layer to block feedback light from the phosphor. The other, called the current-diffusing layer, has a conductivity sufficient to allow current to flow from the photoconductor to the phosphor layer and from the base of a photoconductive ridge to its neighbor. At the same time the conductivity is not great enough to allow spreading of the photocurrents more than about one groove width.

By connecting the conducting lines into two interdigital groups, opposite polarity voltage pulses are applied to adjacent photoconductor ridges. The darkened areas of Figure 5 show a single picture element excited, with the two irradiated portions of photoconductor and the associated phosphor area corresponding to the single element of the preceding figure.

INPUT-OUTPUT CHARACTERISTICS

When excited with an X-ray image the amplifier does not respond instantly but has a build-up characteristic determined by the photo-

conductive material. Figure 6 shows build-up curves of the amplifier output as a function of time for different levels of X-rays. These show that the time required to reach a specified light level decreases as the X-ray level is increased. For a given time of excitation, the output light can be determined as a function of input X-ray level from these

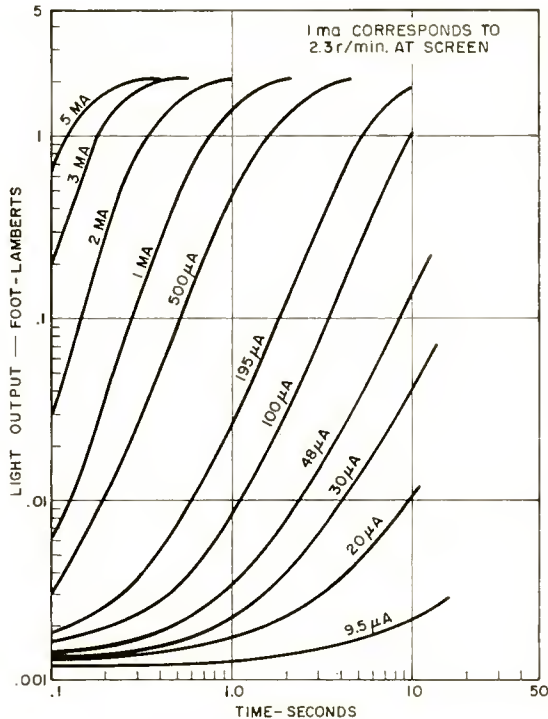


Fig. 6—Light output versus time for various X-ray currents.

curves. Figure 7 shows an input-output characteristic for a 10-second excitation of the amplifier. The input level is shown in terms of X-ray current and also milliroentgens per minute. For comparison, the output light of a conventional fluoroscope screen (Patterson Type CB-2) is also plotted. The 45-degree slope of the conventional screen indicates its linear output. The much higher slope of the amplifier characteristic indicates it to have a gamma of about 3. These curves show the amplifier output to be as much as 100 times brighter than the conventional screen for equal levels of X-ray excitation.

Examination of the amplifier characteristics with other exposure times shows that the output light level reached is a function of the milliamperere-second product of the X-ray source. Figure 8 shows the

amplifier characteristic in terms of the milliampere-second input with a target-to-amplifier distance of 24 inches and a $\frac{1}{2}$ -millimeter aluminum filter. The equivalent exposure of the amplifier in milliroentgens is also shown along the abscissa. The horizontal lines through the

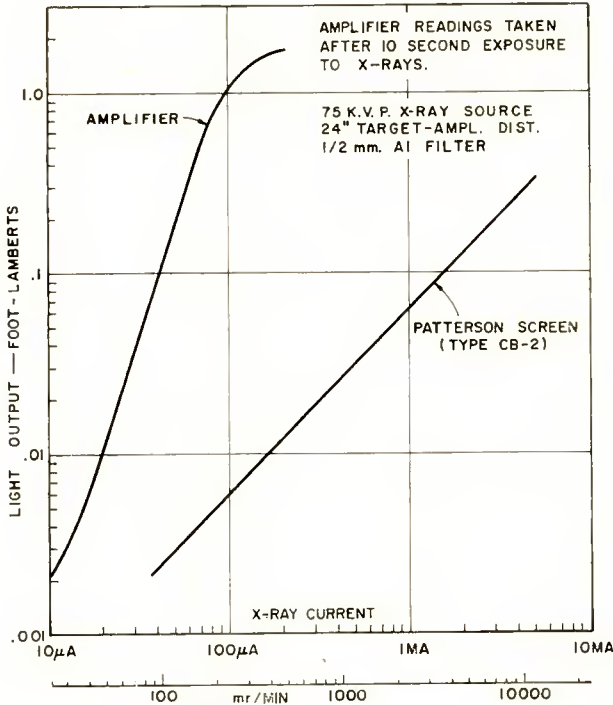


Fig. 7—Input-output characteristics of amplifier and conventional screen.

curve show the range of experimental variations in input for a given output (neglecting the 9.5 and 20 microampere curves of Figure 6). As shown, an exposure of between 5 and 50 milliroentgens is required to excite the amplifier. By comparison, about 60 milliroentgens are required to obtain a density of 1 on medical X-ray film (Kodak Blue Brand).¹¹ At the conventional levels used in fluoroscopying a human chest (posteroanterior view) about 10 seconds of exposure are required for image build-up on the amplifier. The high gamma of the amplifier and its latitude are similar to the medical film used with calcium tungstate screens. The curve of this film is shown in Figure 9 for comparison, with the density and exposure in relative values. The

¹¹ R. B. Wilsey, "The Use of Photographic Films for Monitoring Stray X-rays and Gamma Rays," *Radiology*, Vol. 56, p. 229, February, 1951.

straight-line portion similarly has a high gamma, and the latitude is also about 10.

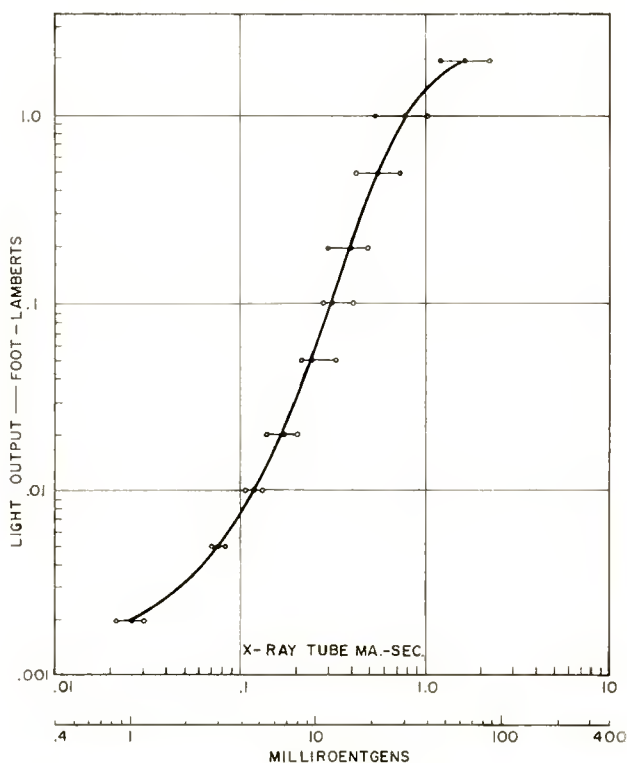


Fig. 8—Light output versus X-ray dosage on amplifier.

DECAY PROPERTIES

In addition to its build-up, the amplifier has long decay properties. This is shown by the curves of Figure 10 obtained by exciting the amplifier for a 1-second period with different X-ray levels. These curves show the amplifier output to decay slowly over a 15-30 second period. Because of internal heating of the photoconductor, the 200-milliroentgen curve, shown dashed, has a more rapid decay rate. The time of decay depends on the photoconductive material, in some instances being of the order of minutes. Because of this long decay, a picture previously excited can be viewed with the X-rays cut off. In such cases a fixed image can be observed for an extended time with a saving in dosage of X-rays. If the object being X-rayed is not stationary, a short pulse of X-rays can be used to produce a "tempo-

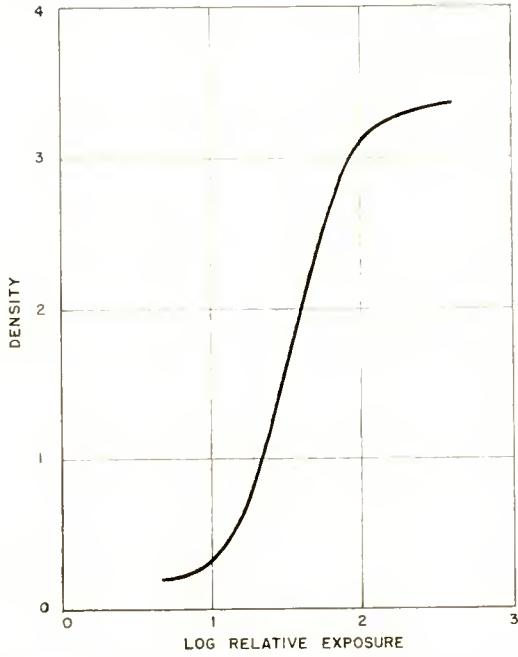


Fig. 9—Characteristic curve of medical X-ray film with calcium tungstate intensifying screens.

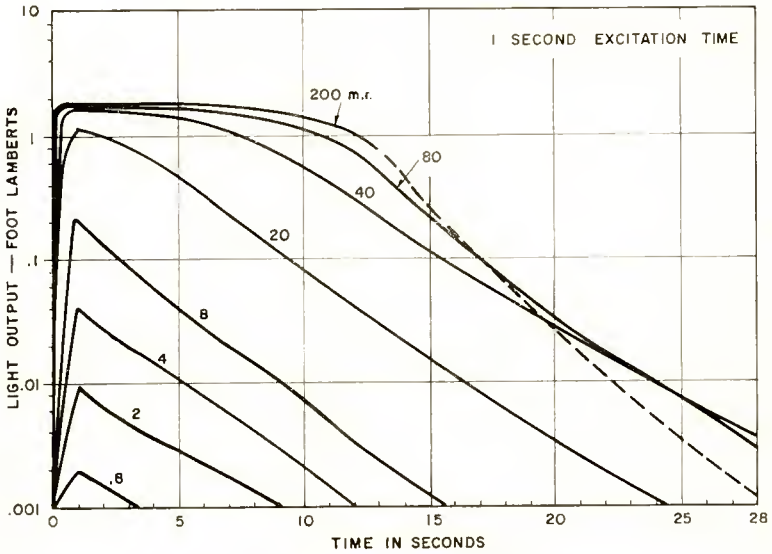


Fig. 10—Build-up and decay for various X-ray input levels.

rary photograph" for extended viewing. Since in addition the highlights of the output picture may exceed one foot-lambert, the image can be comfortably viewed with moderate room illumination.

Because of the long decay of the bright image, the time-integrated light is relatively high. This is of interest in applications where the output of the screen is to be photographed. From the decay curves

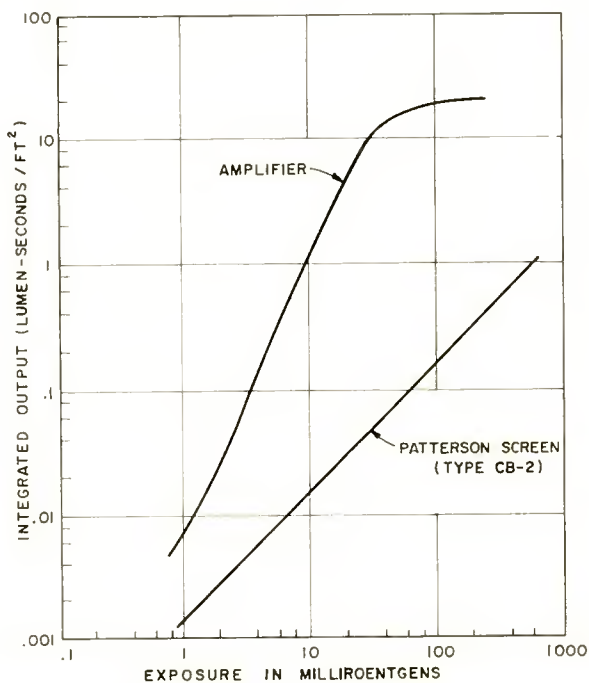


Fig. 11—Time-integrated light output of amplifier.

the time-integrated light was determined, and in Figure 11 this integrated light is shown as a function of X-ray input in milliroentgens. By comparison, the integrated light output produced from a conventional CB-2 screen with the same excitation is also plotted. This shows the integrated output of the amplifier to be about 100 times that of the conventional screen at inputs of about 10-20 milliroentgens. However, because of the high gamma of the characteristic and the rapidly decreasing output of the amplifier at low X-ray exposures, its advantage at these levels is reduced. With more sensitive materials and longer decay, it is hoped that the amplifier can be used for reducing the X-ray dosage in photofluorography.

IMAGE ERASING

Unless special erasing means are used, the long decay of the photoconductor prevents the viewing of a new image for a period of many minutes or more. If the photoconductor is not allowed to decay sufficiently, the new image will re-excite portions of the old image. However, by using a special property of the photoconductive powder, erasure of an old image can be accomplished in a fraction of a second

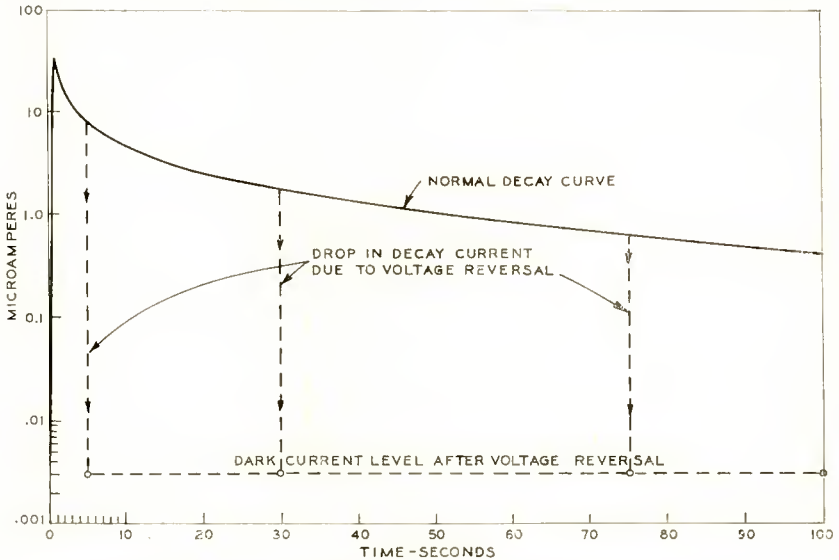


Fig. 12—Effect of voltage reversal on photocurrent decay.

at any desired moment during the decay. The panel can then be used instantly for viewing a new image.

Figure 12 shows the d-c decay curve of a photoconductive sample initially excited for a 1-second period. Although the decay current is shown up to 100 seconds, the current continues to drop slowly beyond this time. To reach the level of the lower dashed line an hour or more is required. If instead of allowing the photoconductor to decay normally, the applied voltage is suddenly reversed, the photocurrent (neglecting the polarity change) instantly drops to a low level many orders of magnitude less than its normal level. As shown, the voltage can be reversed at an arbitrary time during the decay, driving the photocurrent down to the same low current level. Immediately after being erased the photoconductor can be excited again with an X-ray signal to a new current level.

This type of erasing can be applied to the amplifying panel in

several ways. The simplest method is to reverse the polarity of the bias voltages on the panel at the moment erasure is desired. With reversed polarity the panel can be then excited with a new X-ray image. For successive images, this procedure can be continued.

In the voltage-reversal process a relation exists between the photocurrent reached during excitation and the dark current level which results after voltage reversal. In some cases the higher the photocur-

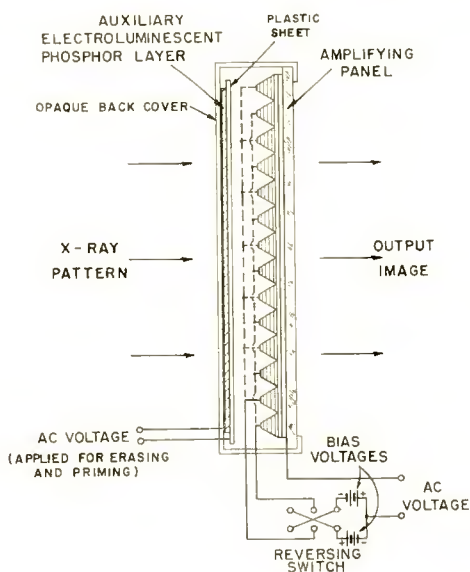


Fig. 13—Arrangement for erasing image.

rent the lower the dark current after erasing. Because of this, erasing by voltage reversal alone may be nonuniform or incomplete. An improved operation is possible with the arrangement shown in Figure 13. Here an auxiliary, thin electroluminescent layer on a plastic sheet is provided on the inner surface of the light-tight back cover of the amplifier. In operation, the X-ray image passes through the cover and the auxiliary phosphor layer. Since the phosphor layer is about 1 mil thick, its attenuation of the X-rays can be neglected. After the amplifier has been excited by the X-ray image and the picture viewed, erasing is accomplished by reversing the bias voltages connected to the photoconductive grooves and simultaneously switching on the auxiliary phosphor to flood the photoconductor for a fraction of a second. The bias voltages are then reversed again, leaving the photoconductive layer at a uniformly low dark level over the entire surface. The amplifier is now ready to be excited with a new X-ray image. In some cases

the dark current level is so low after erasure that the panel has reduced sensitivity for a new image. This can be overcome by a priming action whereby the auxiliary phosphor layer is momentarily switched on again during or just preceding the excitation with the new X-ray image.

EXCITATION BY FLUOROSCOPE SCREEN

Since the photoconductive layer is sensitive to visible light as well

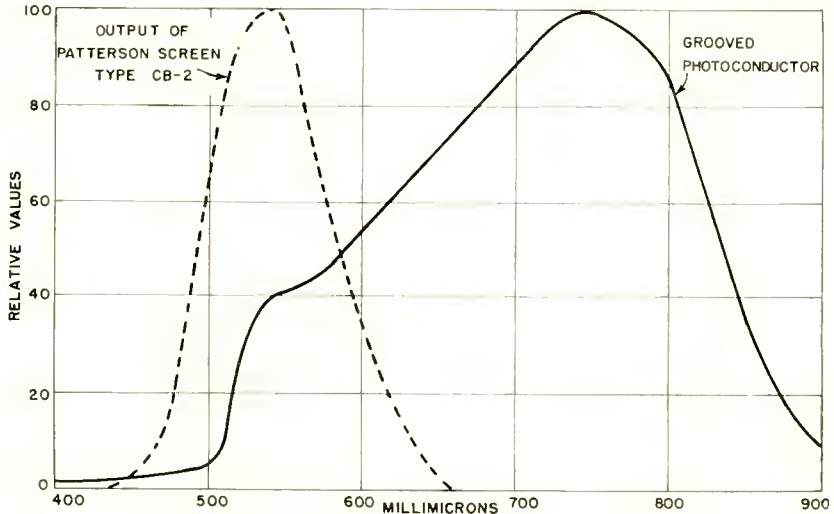


Fig. 14—Spectral response curve of grooved photoconductor.

as X-rays, the amplifier can be used to intensify the visible image of a fluoroscope screen. To avoid optical losses, the fluoroscope screen can be placed in contact with the photoconductive layer or, alternatively, the phosphor material can be deposited in the groove spaces of the photoconductor. Tests with the conventional screen and the amplifier indicate that about the same gain or slightly less is obtained by this method of operation compared to exciting the photoconductor. As shown in Figure 14 the peak sensitivity of the grooved photoconductor is at about 750 millimicrons in the deep red, while the peak emission of the phosphor is at about 550 millimicrons in the green. The value of this type of operation is dependent on the future availability of better matched new materials having comparable efficiencies.

RESOLUTION AND CONTRAST SENSITIVITY

The resolution of the amplifier is limited by several factors. Since the photoconductive layer has grooves cut into it with a 25-mil spacing

between centers, picture details smaller than this cannot be observed in the direction across the grooves. In order to absorb a large fraction of the X-rays and to efficiently control the output phosphor, the photoconductive layer is made about 12 mils thick. This results in spreading of the photocurrents by roughly this amount along the grooves. Some loss in resolution is also caused if the current-diffusing layer has too high a conductivity. It is believed, however, that with improved design, amplifier panels can be made comparable in resolution to conventional fluoroscope screens.

Because of its high gamma, the amplifier is potentially useful for detecting small variations in object thickness or density. However, with the experimental fabrication techniques presently used, non-uniformities in amplification over the surface limit the contrast sensitivity. With $\frac{1}{2}$ -inch-thick aluminum, large-area variations in thickness of about 6 per cent can presently be detected. It is believed that with improved techniques, lower limits can be reached.

The output of an X-ray-excited 12-inch amplifier panel is shown in the photograph of Figure 15. Immediately above the amplifier is a conventional screen simultaneously excited with the same X-ray level. Because of its relatively low output, it is entirely dark in the photograph. For producing the image, a 5-inch-thick phantom of Presdwood* sheets was used between which were inserted a femur containing a Smith-Peterson nail as used for hip pinning, a hypodermic syringe, and a simulated section of intestine made of BaSO_4 in plastic. In addition, a number of metallic objects were inserted, some of which extend into the area of the Patterson screen. The distal half of the femur was cut off and placed above, allowing the shaft to extend also across the conventional screen. A thin amplifying screen identical to the one shown in operation is held by the author.

SUMMARY

The amplifying screen requires approximately the same X-ray exposure as Kodak Blue Brand medical X-ray film. Compared to the conventional fluoroscope screen, the output image is about 100 times brighter and has a gamma 3 times higher. In fluoroscopying a human chest, for example, an image of about .01 foot-lambert on a conventional screen is increased to about 1 foot-lambert on the amplifier. At the same time 2 to 1 variations in brightness of image details are increased to almost 10 to 1 variations by the amplifier. With its long persistence or storage the amplifier permits a stationary output

* Registered Trade Mark.

image to be viewed for an extended time with the X-rays off. This enables a reduction in dosage of several times or more.

Solid-state amplifying panels are relatively new devices. Although an accurate estimate of their ultimate possibilities is difficult, it is hoped that continuing research in the future will bring sufficient improvements so that they can be used for the viewing of moving objects. For this purpose, however, several orders of magnitude of improve-

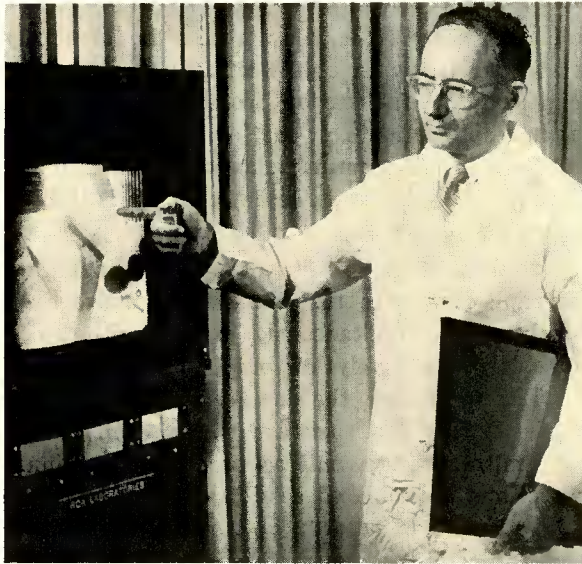


Fig. 15—Photograph of amplifier screen in operation.

ment in materials are possibly required. In addition to the long-term objectives, it is also hoped that the relatively smaller improvements occurring along the way will enable such amplifiers to gradually find uses in specific applications.

ACKNOWLEDGMENTS

The author wishes to acknowledge the support and advice of E. W. Herold in this work as well as discussions with D. W. Epstein of these Laboratories, and E. W. Godfrey of the Princeton Hospital. The helpful suggestions of J. A. Reynolds of the Picker X-ray Corporation are appreciated and also the direct assistance of J. E. Berkeyheiser, J. Bernath, and G. H. Brown, Jr. of RCA Laboratories.

HOLLOW-CATHODE GLOW DISCHARGE IN MERCURY VAPOR*†

BY

K. G. HERNQVIST

RCA Laboratories,
Princeton, N. J.

Summary—The hollow-cathode glow discharge operates with a metal cathode having a spherical cavity and a small exit aperture. The main glow is situated inside the cathode cavity. This discharge has been operated in mercury vapor by keeping the inside of the cavity wetted with mercury. The volt-ampere characteristic does not exhibit any regions of negative resistance. An analysis based on the energy balance relation is shown to yield a volt-ampere characteristic which is in good agreement with experiment. Microwave measurements of the plasma density also corroborate the analysis. These studies indicate that plasma densities in excess of 10^{15} per cubic centimeter may be attained in this discharge.

INTRODUCTION

THE studies described in this paper were done as a part of a research program for generation of millimeter wave plasma oscillations. The natural frequency of electron oscillations of a plasma is given by the Langmuir-Tonks formula¹

$$f_e = 9000 \sqrt{N}, \quad (1)$$

where N is the number of electrons per cubic centimeter. Relation (1) has been tabulated in Table I for the wavelength range 1 to 3 millimeters. It is seen that the plasma density necessary for this range is 10^{14} to 10^{15} per cubic centimeter. Such a plasma then could take the place of conventional r-f structures which become very small and

Table I—Electron Plasma Frequency and corresponding Wavelength for Different Plasma Densities

f_e Mc	λ mm	N cm ⁻³
3×10^5	1	1.1×10^{15}
2×10^5	1.5	5×10^{14}
10^5	3	1.2×10^{14}

* Manuscript received October 15, 1957.

† This research was supported by the United States Army Signal Corps.

¹ L. Tonks and I. Langmuir, "Oscillations in Ionized Gases," *Phys. Rev.*, Vol. 33, p. 195, February, 1929.

their construction troublesome in this frequency range. The practical problem of generating millimeter waves by electron plasma oscillations is threefold: (1) To create the high plasma density required; (2) To excite oscillations in the plasma; (3) To provide means to extract the r-f energy from the plasma. The first of these is the subject of discussion in this paper.

The problem of creating plasmas of densities as high as 10^{14} to 10^{15} per cubic centimeter, which is a prerequisite for the success of this scheme for millimeter wave generation, has heretofore been given very little attention. A density of 10^{13} per cubic centimeter is considered extremely high for most gas discharge devices. Special types of discharge forms must therefore be sought for in which conditions for maintaining high plasma densities are satisfied. Furthermore, these discharge devices must have potentialities for incorporating means for plasma excitation and r-f power extraction. In practice, such a means for plasma excitation will consist of an electron stream from an auxiliary cathode either injected into the plasma or grazing its boundary.²⁻⁶ In general this calls for a low gas density within the plasma region, preferably not appreciably exceeding the plasma density (corresponding to a pressure of the order of 1 millimeter of mercury). In cases where a high beam velocity is called for in the exciting electron beam, a further requirement of good vacuum in the vicinity of the auxiliary cathode must be satisfied. This inevitably calls for some means to provide a differential pressure within the tube. In general these requirements limit the plasma generation devices to low-pressure discharges.

An attractive form of discharge for obtaining a high-density plasma is the hollow-cathode glow discharge.⁷ The basic geometry of the hollow-cathode glow discharge is shown in Figure 1. The cathode consists of a metal body having a spherical cavity and a small exit

² H. J. Merrill and H. W. Webb, "Electron Scattering and Plasma Oscillations," *Phys. Rev.*, Vol. 55, p. 1191, June, 1939.

³ A. A. Sluzkin and A. P. Maydanov, "Factors Determining the Intensity of Oscillations in the Plasma of Gaseous Discharge," *Jour. Phys. U.S.S.R.*, Vol. 6, p. 7, January-February, 1942.

⁴ E. B. Armstrong and K. G. Emeleus, "The Generation of High-Frequency Oscillations by Hot-Cathode Discharge Tubes Containing Gas at Low Pressure," *Proc. I.E.E.*, Part III, Vol. 96, p. 390, September, 1949.

⁵ G. Wehner, "Electron Plasma Oscillations," *Jour. Appl. Phys.*, Vol. 22, p. 761, June, 1951.

⁶ D. H. Looney and S. C. Brown, "The Excitation of Plasma Oscillations," *Phys. Rev.*, Vol. 93, p. 965, March, 1954.

⁷ A. D. White, "A Novel Form of Hollow Cathode and Its Discharge Characteristics," presented as paper D-4 at the Ninth Annual Gaseous Electronics, Pittsburgh, Pa., November, 1956.

aperture. When the discharge is operated, the main glow plasma is situated inside the spherical cavity with no visible glow at the outside surface of the cathode. This mode of operation has the following advantages: (1) Material sputtered away from the cathode surface is instantly redeposited on other parts of the cathode leading to a stable geometry and a very long tube life; (2) The plasma inside the cavity is well confined and of simple geometry; (3) Since the geometry essentially constitutes an electron trap for electrons emitted from the cathode, the kinetic energy carried by the electrons is effectively utilized for ionization; (4) Essentially all ions leaving the plasma contribute to the secondary electron emission process at the cathode surface. When operated with a noble gas this discharge requires quite a high gas pressure (of the order of 100 mm Hg). This is a drawback from the

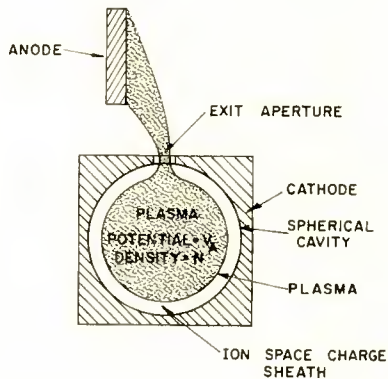


Fig. 1—Cross section of basic structure for hollow cathode glow discharge.

point of view of plasma oscillation excitation. It is the purpose of this paper to describe a special form of the hollow-cathode glow discharge which is operated in mercury vapor and in which the vapor pressure is high only within the spherical cathode cavity.

PLASMA ENERGY BALANCE RELATION OF HOLLOW-CATHODE GLOW DISCHARGE

The following simplified model of the hollow-cathode glow discharge will be analyzed based on an energy balance equation for the glow plasma: The main plasma located within the cathode cavity is of uniform density and at a potential approximately equal to the anode voltage. It will be assumed that the plasma has spherical geometry and is separated from the cathode by a very thin positive-ion space-charge sheath.

The following symbols are used:

- V_A = anode voltage,
 I_A = anode current,
 I_p = ion current leaving the plasma and arriving at the cathode surface,
 I_c = electron current leaving the cathode,
 N = plasma density,
 V_i = ionization potential of the gas,
 e = electronic charge,
 v = plasma volume,
 k = Boltzmann's constant,
 T_e = electron plasma temperature,
 \bar{c}_p = average Maxwellian ion velocity,
 T_p = ion plasma temperature,
 M = atomic weight of ions,
 A = total boundary surface of the plasma,
 α = ion-electron recombination constant,
 γ = number of electrons leaving the cathode per ion striking the cathode,
 d = diameter of spherical plasma.

Referring to Figure 1, the energy balance for an observer in the plasma is as follows: The input power, $I_c V_A$, is the kinetic energy carried into the plasma per second by the electrons leaving the cathode after being accelerated through the ion space-charge sheath. The energy losses are (1) Recombination losses $P_{\text{rec.}} = \alpha N^2 e V_i v$, lost as heat and radiation; (2) Energy for generating ions $I_p V_i$; (3) Energy carried away to the anode⁸ by electrons leaving the plasma $(2kT_e/e)I_A$; (4) Energy lost in exciting (but not ionizing) atoms $P_{\text{ex.}}$. This last energy is quite difficult to estimate but can be approximately represented as a constant fraction, κ , of the input energy, thus $P_{\text{ex.}} = \kappa I_c V_A$. Thus the energy balance equation reads

$$I_c V_A = \alpha N^2 e V_i v + I_p V_i + 2 \frac{kT_e}{e} I_A + \kappa I_c V_A. \quad (2)$$

Further, neglecting secondary processes which cause some electron emission at the cathode, $I_c = \gamma I_p$ and

$$I_A = I_c + I_p = I_p (1 + \gamma). \quad (3)$$

⁸G. Herrmann and S. Wagener, *The Oxide-Coated Cathode*, Vol. 2, Chapman and Hall Ltd., London, England, 1951, p. 78.

The average ion space current at the plasma boundary is equal to I_p , or

$$\frac{Ne\bar{c}_p}{4} A = I_p. \quad (4)$$

Inserting N from Equation (4) into Equation (2) and using Equation (3), one obtains

$$V_A = \frac{16\alpha V_i v}{(1-\kappa)\gamma e A^2 \bar{c}_p^2 (1+\gamma)} I_A + \frac{V_i + \frac{2kT_e}{e} (1+\gamma)}{(1-\kappa)\gamma}. \quad (5)$$

This relation can be written as

$$V_A = R I_A + V_0, \quad (6)$$

where

$$R = \frac{1}{(1-\kappa)\gamma} \frac{16\alpha V_i v}{e A^2 \bar{c}_p^2 (1+\gamma)}, \quad (7)$$

and

$$V_0 = \frac{1}{(1-\kappa)\gamma} \left[V_i + \frac{2kT_e}{e} (1+\gamma) \right]. \quad (8)$$

For a range where the factors in Equations (7) and (8) do not change much with V_A and I_A , the idealized volt-ampere characteristic as given by Equation (6) is a straight line with slope R . Since the values of κ and γ are uncertain, comparison with the experimental results may be facilitated by combining Equations (7) and (8), yielding

$$R = \frac{16V_0\alpha v}{\left[1 + \frac{2kT_e}{V_i e} (1+\gamma) \right] e A^2 \bar{c}_p^2 (1+\gamma)}. \quad (9)$$

Assuming a spherical geometry and $\gamma \ll 1$, and inserting

$$\bar{c}_p = 1.455 \times 10^4 \sqrt{\frac{T_p}{M}},$$

one obtains
$$R \cong 2.5 \times 10^{10} \frac{V_0 \alpha M}{\left(1 + \frac{2kT_e}{V_i e}\right) dT_p} . \quad (10)$$

Further, it is of interest to find the relations between the different energy sinks. Of the total power input to the discharge, $I_A V_A$, a large fraction (approximately $1 - \gamma$ according to Equation (3)) is carried into the cathode by the ions. This results in cathode heating, evaporation, sputtering, and secondary electron emission. Only a fraction equal to γ of the input energy is carried into the plasma. Equation (2) can be written as

$$\gamma I_A V_A = P_{\text{rec}} + P_{\text{diff}} + P_{\text{ex}} , \quad (11)$$

where

$$P_{\text{diff}} = I_p V_i + \frac{2kT_e}{e} I_A .$$

Using Equations (7) and (8) it can be shown that

$$\frac{P_{\text{rec}}}{P_{\text{diff}}} = \frac{R I_A}{V_0} = \frac{V_A}{V_0} - 1 . \quad (12)$$

Thus recombination losses, P_{rec} , equal diffusion losses, P_{diff} , when $V_A = 2V_0$. Further,

$$\frac{P_{\text{diff}}}{P_{\text{ex}}} = \frac{V_i + \frac{2kT_e}{e} (1 + \gamma)}{\gamma \kappa V_A} . \quad (13)$$

The plasma density determined by Equation (4) can be written as

$$N = \frac{4I_p}{e\bar{c}_p A} = 1.72 \times 10^{15} \sqrt{\frac{M}{T_p}} J_p = 1.72 \times 10^{15} \sqrt{\frac{M}{T_p}} \frac{I_A}{A} , \quad (14)$$

where J_p is the ion current density at the cathode. J_p is related to the electric field at the cathode,⁹ E_c , by

⁹ S. S. Mackeown, "The Cathode Drop in an Electric Arc," *Phys. Rev.*, Vol. 34, p. 611, August, 1929.

$$E_c^2 = 3.25 \times 10^7 J_p \sqrt{V_A M}. \quad (15)$$

It has been found¹⁰ that glow-to-arc transitions usually occur when E_c exceeds a value of about 9×10^5 volts per centimeter. Thus from Equations (14) and (15) the upper limit for the plasma density is

$$N_{\max} = 0.43 \times 10^{20} (T_p V_A)^{-1/2}. \quad (16)$$

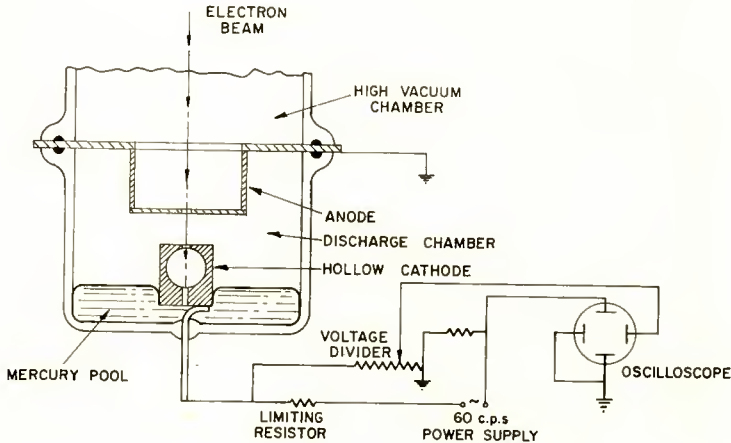


Fig. 2—Schematic drawing of tube and circuits for study of the volt-ampere characteristic of the hollow cathode glow discharge.

EXPERIMENTAL STUDIES OF HOLLOW-CATHODE GLOW DISCHARGE IN MERCURY VAPOR

Description of Tube

The tube used in these studies is shown schematically in Figure 2. The tube is continuously pumped and consists of two chambers, the upper, high-vacuum chamber and the lower, glow-discharge chamber. The two chambers are separated by a stainless-steel disc and communicate only through a 2-millimeter-diameter hole. A high-voltage electron-gun assembly which is surrounded by a liquid nitrogen cold trap is located in the upper chamber. The lower chamber contains the hollow cathode which is partly immersed in a mercury pool. The cathode is machined of nickel and has a spherical cavity of 4-millimeter diameter. The exit aperture has a diameter of $\frac{3}{4}$ millimeter. At the bottom of the cavity is a narrow feed tube. The inside of the cavity

¹⁰ W. S. Boyle and F. E. Haworth, "Glow-to-Arc Transition," *Phys. Rev.*, Vol. 101, p. 935, February, 1956.

and feed tube are prewetted with mercury. The cathode communicates with the mercury pool so as to provide a mercury film on the inside of the cavity continuously replenished through the feed tube. The plate separating the two chambers also serves as the anode for the glow discharge.

Several kilovolts potential can be applied between the cathode and the anode without starting a discharge. However if a high-voltage electron beam (e.g., 15 kilovolts beam voltage and 0.5 milliampere beam current) is fired through the exit aperture into the cavity, the local vapor pressure within the cavity is raised and a hollow-cathode glow discharge starts. A very bright glow is present within the cavity. There is no visible light on the outside of the cathode except a very faint glow where the current is conducted from the exit aperture to the anode. Once fired, the discharge is sustained when the high-voltage beam is switched off.

Volt-Ampere Characteristic

The volt-ampere characteristic of the hollow-cathode glow discharge was swept out at a 60-cycle rate using the circuit shown in Figure 2. Figure 3 shows the characteristic replotted from an oscilloscope picture. The theoretical relation given by Equation (6) is fitted to the experimental curve yielding values of $R = 1,070$ ohms and $V_0 = 560$ volts. As seen from Figure 3, the experimental curve is quite well represented by Equation (6). Assuming¹¹ $\gamma \ll 1$, $T_c = 10,000^\circ\text{K}$, $T_p = 400^\circ\text{K}$, $V_i = 10.4$ volts for mercury, $d = 0.4$ centimeter, and taking the experimental values for V_0 and R , Equation (10) yields a value for the recombination coefficient $\alpha = 7 \times 10^{-9}$ cubic centimeter per second. Considering the assumptions made in the analysis, this can be considered a good agreement with $\alpha = 2.3 \times 10^{-10}$ found by Mohler¹² and $\alpha = 5.5 \times 10^{-9}$ found by Dandurand and Holt.¹³

For comparison of the various losses of energy, a knowledge of γ for mercury ions is essential. Measurement of γ for mercury ions on mercury¹¹ indicates that γ is of the order of 0.1 or less for voltages of interest. Thus it is seen that 90 per cent or more of the total power input to the tube is dissipated in the cathode. The other 10 per cent is delivered to the plasma and is lost due to recombination, diffusion,

¹¹ M. Schwarz and P. L. Copeland, "Secondary Emission by Positive Ion Bombardment," *Phys. Rev.*, Vol. 96, p. 1466, December, 1954.

¹² F. L. Mohler, "Recombination in the Afterglow of a Mercury Discharge," *Jour. Res. of the National Bureau of Standards*, Vol. 19, p. 559, November, 1937.

¹³ P. Dandurand and R. B. Holt, "Electron Removal in Mercury Afterglow," *Phys. Rev.*, Vol. 82, p. 868, June, 1951.

and excitation. Since κ is probably¹⁴ of the order 0.2, Equation (13) indicates that P_{ex} is of the same order of magnitude as P_{diff} . Finally, Equation (12) indicates that over the current range shown in Figure 3, P_{rec} does not exceed $0.3 \times P_{diff}$. The relative magnitude of these different energy sinks is shown schematically in Figure 4.

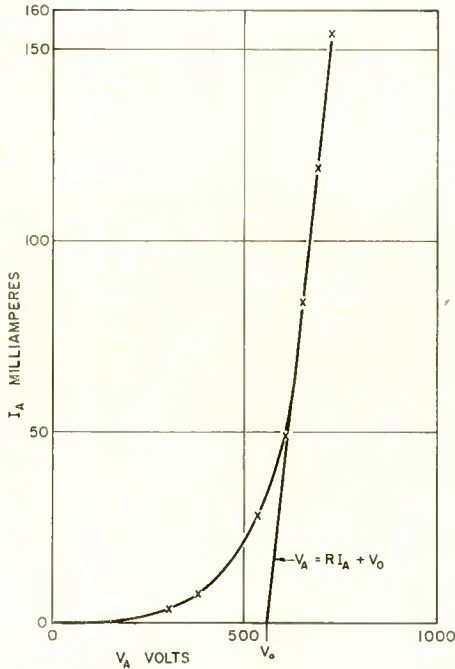


Fig. 3—Volt-ampere characteristic of hollow cathode glow discharge.

Plasma Density Measurements

The theoretical expression given by Equation (14) relating plasma density, N , to discharge current, I_A , is plotted in Figure 5 for mercury, assuming $T_p = 400^\circ\text{K}$. In Figure 5 the electron plasma frequency, f_e , from Equation (1) is also shown.

One method of measuring the plasma density is through the use of microwave techniques. It is well known that a plasma becomes nearly opaque to a microwave signal whose frequency, f , is larger than the electron plasma frequency, $f_e (= 9,000 \sqrt{N})$. This fact allows

¹⁴E. O. Johnson, "Studies of Externally Heated Hot Cathode Arcs, Part IV—The Low-Voltage Form of the Ball-of-Fire Mode (The Low-Voltage Arc)," *RCA Review*, Vol. XVI, p. 498, December, 1955.

plasma density measurements to be made in a range where available signal sources cover the corresponding plasma frequency range. The problem of microwave propagation through a plasma has been dealt with by several workers.¹⁵⁻¹⁷ The essential facts that have come out of these studies are:

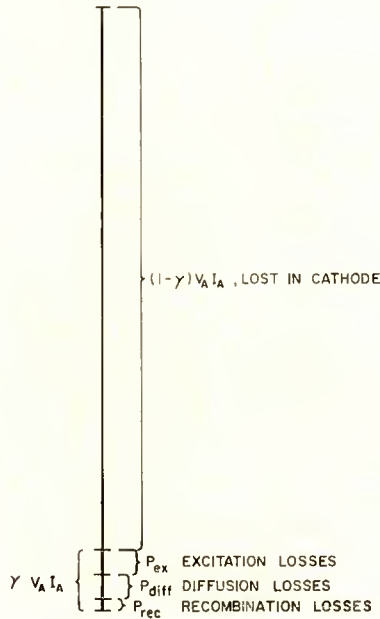


Fig. 4—Diagram showing relative magnitude of different energy sinks for hollow-cathode glow discharge.

- (1) For $f \cong f_c$, the plasma is almost opaque;
- (2) For $f \ll f_c$, the plasma is transparent;
- (3) For f nearly equal to but less than f_c , the transparency of the plasma depends strongly on the collision frequency of the plasma.

When the plasma frequency is less than the signal frequency, the behavior is essentially that of a spherical cavity filled with a dielectric whose dielectric constant is

¹⁵ C. G. Montgomery, R. H. Dicke, and E. M. Purcell, *Principles of Microwave Circuits*, McGraw-Hill, New York, New York, 1949.

¹⁶ L. Goldstein, "Electrical Discharge in Gases and Modern Electronics," *Advances in Electronics and Electron Physics*, Vol. III, Academic Press Inc., New York, New York, 1955.

¹⁷ H. Steele and P. Walsh, "Effect of Moving Striations on Microwave Conductivity of a Coaxial Discharge," *Jour. Appl. Phys.*, Vol. 25, p. 1435, November, 1954.

$$C = 1 - \frac{f_c^2}{f^2} \quad (17)$$

where f is the signal frequency. The resonant frequency, f_r , of the cavity filled with a plasma¹⁸ is given by

$$f_r^2 = f_c^2 + f_0^2, \quad (18)$$

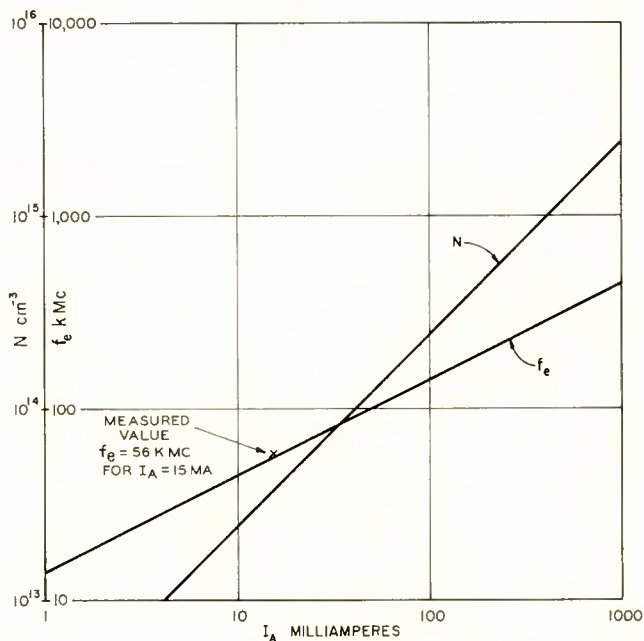


Fig. 5—Plasma density, N , and electron plasma frequency, f_e , as functions of anode current.

where f_0 is the resonant frequency of the resonator without plasma. The effect of the plasma is thus to increase the resonance frequency.

Figure 6 shows schematically the experimental setup used for measuring the plasma density of the hollow-cathode glow discharge. A microwave signal from a klystron source (QK-295) was transmitted through the cathode cavity to a bolometer detector using RG 98/U waveguide components. The cavity is provided with slits and tapered waveguide sections for transmission of the microwave signal. The

¹⁸ O. Schumann, "Über Sphärische Elektromagnetische Eigenschwingungen in Räumen, die Plasmen Enthalten," *Zeitschr. für Naturf.*, Vol. 4a, p. 486, August, 1949.

resonance frequency of the empty cavity (diameter = 4 millimeters) is 66×10^9 cycles for the TM_{101} mode. The signal frequency used was 56×10^9 cycles, which is far from the resonance frequency. The transmission of the signal through the cavity is thus simply due to leakage through the cavity, and from Equation (18) it is seen that no resonance effects will occur due to the plasma detuning the cavity. In the experiment, the signal frequency was held constant at 56×10^9 cycles and the signal amplitude modulated by a 1,000-cycle square wave. The detector signal was fed through an amplifier and displayed on an oscilloscope. The discharge current was varied from zero to a high value at a 60-cycle repetition rate. The horizontal sweep of the oscilloscope displaying the detector signal was proportional to the discharge current. Figure 7 shows an oscillogram of detector signal versus discharge current. Complete cutoff of the transmitted signal occurred

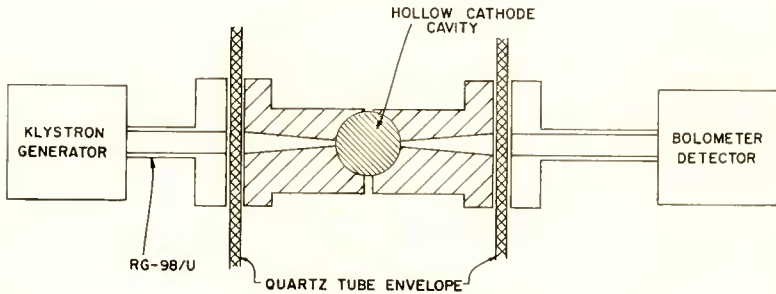


Fig. 6—Schematic diagram showing experimental set-up for plasma-density measurements on hollow-cathode glow discharge.

at a discharge current of 15 milliamperes. The remaining amplitude at higher currents is due to leakage of the microwave signal outside of the cavity. This experiment then yields one point on the plasma frequency versus discharge current curve. It is seen in Figure 5 that the experimental point agrees quite well with the theory. The good agreement between theory and experiment both for the volt-ampere characteristic and for the density measurements would seem to make the extrapolation of Equation (14) to higher currents permissible. Discharge currents up to 400 milliamperes have been drawn without arcing. This indicates the plasma densities in excess of 10^{15} per cubic centimeter ($f_c = 300 \times 10^9$ cycles) may be obtained in the hollow-cathode glow discharge. The maximum plasma density predicted by Equation (16) is about 10^{16} per cubic centimeter. Glow-to-arc transitions occurred at lower values of plasma density at the sharp edges of the exit aperture.

Collision Frequency

An important parameter of the plasma for millimeter wave plasma oscillations is the collision frequency, f_c . This determines the r-f losses of the plasma. The collision frequency is given by

$$f_c = \frac{\bar{c}_e}{\lambda}, \quad (19)$$

where \bar{c}_e is the average electron velocity in the plasma and λ is the electron mean free path. For mercury,¹⁹ $\lambda = 0.015$ centimeter at a pressure of 1 mm Hg. An electron temperature of 10,000°K, yields $\bar{c}_e = 6.23 \times 10^7$ centimeters per second or, from Equation (19),

$$f_c = 4 \times 10^9 p, \quad (20)$$

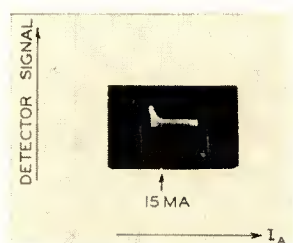


Fig. 7—Oscillogram showing transmission of a 56,000-megacycle microwave signal through the plasma as a function of discharge current I_A .

where p is the vapor pressure in mm Hg. The pressure p can be estimated from the evaporation rate at the cathode. Assume that the power input to the cathode resulting in evaporation is P_c . If η is the energy required to evaporate one atom of mercury from the cathode surface, then the particle flux from the cathode surface is P_c/η . The particle flux from the gas into the cathode is $1/4 AN\bar{c}$ where A is the cathode area, N is the particle density of the gas, and \bar{c} the average thermal velocity of the gas. In equilibrium

$$\frac{P_c}{\eta} = \frac{1}{4} AN\bar{c},$$

or

$$N = \frac{4P_c}{\eta A\bar{c}}. \quad (21)$$

¹⁹ K. T. Compton and I. Langmuir, "Electrical Discharges in Gases," *Rev. Mod. Phys.*, Vol. 2, p. 123, April, 1930.

For the conditions used in the experiment described in the previous section $P_c = 60$ watts, $A = 0.5$ square centimeter, and $\bar{c} \cong 2 \times 10^4$ centimeters per second. Further, $\eta = 1.13 \times 10^{-10}$ joule for mercury,²⁰ yielding $N = 2 \times 10^{17}$ per cubic centimeter. This corresponds to a vapor pressure of about 5.6 mm Hg. Thus from Equation (21) $f_c = 22 \times 10^9$ cycles.

One way to obtain an experimental value for f_c is to examine in detail the curve of Figure 7. This, however, requires knowledge of the uniformity of plasma density as well as the type of wave propagation through the plasma. The relatively broad cutoff characteristic of Figure 7 may be partly due to a high collision frequency.

ACKNOWLEDGMENTS

The author wishes to thank R. W. Peter for many helpful discussions and J. J. Thomas for assistance in performing the experiments.

²⁰ T. B. Douglas, A. F. Ball, and D. C. Ginnings, "Heat Capacity of Liquid Mercury Between 0° and 450°C; Calculation of Certain Thermodynamic Properties of the Saturated Liquid and Vapor," *Jour. Res. of the National Bureau of Standards*, Vol. 46, p. 334, April, 1951.

SOME NEW STRUCTURE-TYPE TARGETS FOR THE VIDICON—AN ANALYSIS OF THEIR OPERATION*

BY

S. A. OCHS AND P. K. WEIMER

RCA Laboratories,
Princeton, N. J.

Summary—Severe physical requirements are imposed on the photoconductive layer used in the conventional Vidicon camera-tube target. In particular, its resistivity must be of the order of 10^{12} ohm-centimeters for frame storage operation and its thickness must be sufficient to prevent capacitive lag. New Vidicon targets of a complex structure permit a relaxation of these requirements on the photoconductor. Two types of targets are discussed:

- (1) An experimental "lateral-flow" structure in which the photocurrent flows parallel to the target plane instead of transversely as in the standard Vidicon.
- (2) An experimental "bridge-type" structure in which each picture element provides an internal closed circuit so that the charge pattern is established independently of the scanning beam.

Both types of targets can make use of sensitive photoconductors having too low a resistivity for the standard Vidicon. An interesting feature of the bridge target is that it can be made self-discharging, thus removing the usual restrictions on beam impedance and target capacitance which apply for conventional targets. The full sensitivity of the photoconductor cannot be utilized in the bridge target since only a fraction of the photocurrent appears as video signal. The efficiency of utilization of photocurrent is less for bridge-type targets of lower resistance.

Structure-type targets are more difficult to fabricate than conventional layer-type targets. Experimental targets capable of several hundred lines resolution have been built.

INTRODUCTION

THE sensitivity of photoconductive television camera tubes usually falls considerably short of that obtained in simple photoconductive cells. While such a difference is not surprising in view of the more sophisticated function of the camera tube, it should not be inherent.

The usual approach to the camera-tube problem has been to choose the simplest possible target structure and then to search for a photoconductive material suitable for this structure. As the following discussion shows, a thin layer of photoconductor deposited on a transparent conducting support, as now done, must satisfy rather precise requirements for camera-tube operation. Although this simple structure has many desirable characteristics, alternative approaches

* Manuscript received October 15, 1957.

involving more complex structures may ease some of the requirements on the photoconductor and, in some cases, offer certain operational advantages.

Early workers in television had considered various complicated structures for camera-tube targets. The present interest in structure-type targets arises from the recent development of techniques for depositing very fine strips of conducting and insulating materials.¹ It is now possible to build targets of considerable complexity on a sufficiently fine scale to give adequate resolution for many purposes. Some of these structures provide a more favorable geometry for the usual mode of operation, while other structures permit entirely new modes of operation.

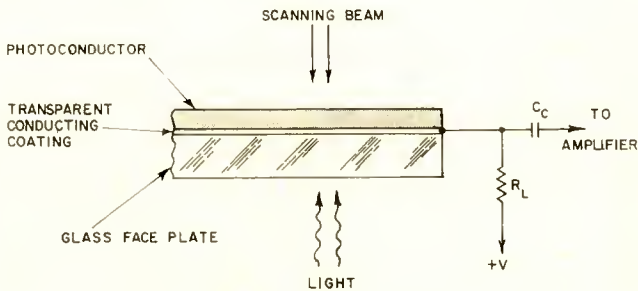


Fig. 1A—Cross section of Vidicon target.

PHOTOCONDUCTOR REQUIREMENTS FOR STANDARD VIDICON TARGET

The target structure in the commercial form of Vidicon consists of a thin layer of antimony sulfide photoconductor deposited over the signal plate, a transparent conducting coating on the inside face of the tube (see Figure 1A). In the usual mode of operation, charge is stored on the surface of the photoconductor for the 1/30-second interval between successive scans; electrons from the low-velocity beam scanning the photoconductor land in sufficient quantity to maintain its surface potential near that of the gun cathode. The conducting signal plate is biased 10 to 100 volts above cathode potential so that a high field is built up across the thin layer of photoconductor. The resistivity of the photoconductor is sufficiently high in the dark that a very small amount of beam current landing on the target will balance the leakage current.

¹ P. K. Weimer, S. Gray, H. Borkan, S. A. Ochs and H. C. Thompson, "The Tricolor Vidicon—an Experimental Camera Tube for Color Television," (Abstract) *Proc. I.R.E.*, Vol. 43, p. 370, March, 1955.

When light from the scene is imaged on the target, the increased current flow across the photoconductor causes the scanned surface to rise in potential. Conditions are chosen so that the potential rise in the brightest areas of the picture may reach several volts above cathode potential in the interval between scans. The thin layer of photoconductor is equivalent to an array of elemental capacitors in which the accumulated charge for each element is stored until it is neutralized by the scanning beam. The photoconductive layer should be thin enough that spreading of charge to adjacent elemental areas does not materially impair resolution.

At the instant the beam deposits electrons to return the scanned surface to cathode potential, an equal number of electrons are released from the signal plate and flow out through the load resistor as video signal. A high-gain amplifier, connected to the signal plate through the coupling capacitor, C_c , responds to the small voltage changes developed across the load resistor, R_L , by the video signal. Alternatively, the video signal can be derived as in the image orthicon from an

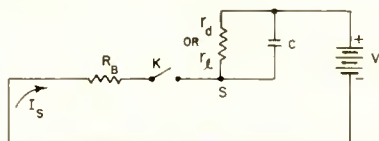


Fig. 1B—Equivalent circuit for one element of Vidicon target.

electron multiplier which collects the unused beam returning from the target.

The equivalent electrical circuit for one element of the commercial Vidicon is shown in Figure 1B. The photoconductive resistance is represented by r_i in the light and r_d in the dark. c is the capacitance existing between an elemental area S of the scanned surface and the signal plate. The photoconductive element is connected in series with a voltage supply V and an electron beam of resistance R_B . The periodic arrival of the beam is represented by switch K which is normally open but closes momentarily each $1/30$ second for a period of $1/(30N)$ second, where N is the total number of picture elements. The beam resistance is actually a nonlinear resistance whose value is a function of the potential of S relative to the gun cathode. When K is first closed, S may be 3 or 4 volts above cathode potential and R_B would be several megohms, but as the surface potential approaches that of the cathode, R_B increases toward infinity. In the qualitative discussion which follows, a constant effective value of R_B of 10 megohms will be assumed.

The load resistor which is very small compared to r_d , and the stray capacitance of S directly to ground which is much less than C , will be neglected.

The following conditions must be satisfied for satisfactory charge-storage operation in the manner outlined above:

1. The time constant for storage, given by the product $r_d c$, must exceed 1/30 second in order to keep the dark current down to a practical value. In terms of the total photoconductive resistance (in the dark), R_d , and the total target capacitance, C , where $R_d = r_d/N$ and $C = Nc$, this condition is $R_d C > 1/30$ second.

2. The time constant for the charging of each element by the beam, given approximately by $R_B c$, must be much less than 1/(30N) second, so that the beam can charge the target sufficiently in one scan; or, $R_B C \ll 1/30$ second.

3. The total charge stored by the target, given by NcV_s (where V_s is the desired potential rise of the scanned surface) must provide sufficient video signal I_s to be much greater than the equivalent r-m-s input noise current of the preamplifier.

Condition 1 sets a lower limit on the volume resistivity of the photoconductor. The product $R_d C$ for the photoconductor is equal to $10^{-12} \rho_d K / (4\pi)$ seconds where ρ_d is its volume resistivity (in the dark) in ohm-centimeters and K is the dielectric constant. This is a function of the material alone and is independent of the thickness and area. Assuming a dielectric constant of ten, the resistivity required for a time constant of one second is 10^{12} ohm-centimeters. A lower dielectric constant will require a higher resistivity for the same time constant.

Condition 2 sets an upper limit for C at about two thousand micro-microfarads assuming an effective beam resistance of 10 megohms. This prescribes a thickness of not less than four microns for a target area of one square centimeter and dielectric constant of ten. A larger area target would require a thicker photoconductor for the same capacitance.

Condition 3 sets a lower limit on C depending on the value determined for minimum acceptable signal current. Owing to amplifier-noise considerations, the minimum value of I_s is set at 0.2 micro-ampere. If the voltage swing of the target is restricted to ten volts, the minimum value for C is then about 600 micromicrofarads. If an electron multiplier is used, I_s may be reduced considerably and the target capacitance may be a fraction of the above value.

The advantages of the simple Vidicon target lie in its greater ease

of fabrication and its lack of any structure which would degrade the resolution of the picture. However, it is also true that:

(a) A photoconductor dark-resistivity of 10^{12} ohm-centimeter required by condition (1) has been difficult to attain with high-sensitivity materials.

(b) To satisfy condition (2), the photoconductive layer may have to be too thick for optimum sensitivity or greatest ease of deposition.

(c) The excessively high resistance of a low-velocity beam near cutoff potential causes a tendency for lag at low signal levels.

The latter considerations led to the investigation of some basically new target structures which might ease the requirements on the photoconductor. This approach was further encouraged by the development of highly sensitive photoconductive layers whose resistivity was too

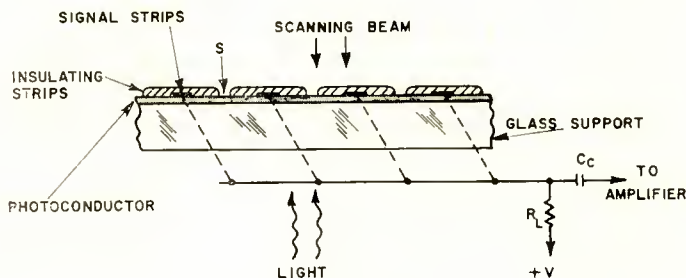


Fig. 2—Lateral-flow target structure.

low for the standard Vidicon target.² In the sections which follow, new structure-type Vidicon target designs are proposed and evaluated.

"LATERAL-FLOW" TARGETS

General Description

Structure-type targets in which the photoconductive current flows parallel to the plane of the target have been called "lateral-flow" targets. Many different target designs of this type are possible, a typical structure being shown in Figure 2.

The photoconductor in Figure 2 is deposited in a thin layer directly on a glass support, the usual transparent conducting coating being omitted. Narrow metallic strips, laid down by evaporation over the photoconductor, serve the same function as the signal plate in the

² S. M. Thomsen and R. H. Bube, "High-Sensitivity Photoconductor Layers," *Rev. Sci. Instr.*, Vol. 26, p. 664, July, 1955.

standard transverse-flow target. These strips are connected to a common output lead as indicated by the dotted lines and biased 10 to 20 volts above cathode potential for low-velocity operation. A set of somewhat wider insulating strips is deposited over the signal strips to prevent the beam from landing directly on the signal strips. The beam charges the exposed portion of the photoconductor, labelled S , down to cathode potential thereby establishing a lateral field in the photoconductor between the signal strips and S . Light from the scene falling on the section of photoconductor having the lateral field causes current to flow, leaving area S several volts positive in the bright parts of the picture. Neutralization by the beam of the charge stored on S induces a video signal which may be extracted by collecting the return beam or by connecting an amplifier to the signal strips. It is assumed, of course, that the number of strips is sufficiently large not to limit the desired resolution.

The equivalent circuit of Figure 1B describes the operation of the lateral-flow target of Figure 2 as well as that of the conventional target. The conditions a lateral-flow target must satisfy for satisfactory charge-storage operation are the same as outlined earlier, but the relative ease of meeting them is modified by the altered geometry.

The target capacitance, C , for the lateral-flow target of Figure 2 is that existing between the total storage area, S , and the interleaved coplanar signal strips. Its value may be influenced more by the dielectric constant of the support plate than by the relatively thin photoconductor and may be smaller than that of a standard transverse-flow target by a factor of 10. The magnitudes for the capacitance of different types of lateral-flow targets cover a range which extends above and below the values obtained with the standard target.

The total photoconductive resistance between the signal strips and the storage area S is, of course, strongly affected by the dimensions. R_d for a thin photoconductor can be made many times greater than would be obtained in a standard target with the same photoconductor.

Applications

Lateral-flow targets offer the following possible advantages in camera-tube design:

- (1) The storage-time constant, $R_d C$, can be made much larger than is possible for a standard transverse-flow target using a photoconductor of the same resistivity. This lowers the permissible dark-resistivity of the photoconductor to a value considerably less than 10^{12} ohm-centimeters. Lateral-flow targets can be readily built having a target capacitance external to the photoconductor, thereby offering

the possibility of raising the upper limit on maximum gain over the values which may exist³ in conventional Vidicon targets.

(2) The smaller target capacitance, C , here possible reduces capacitive lag at low signal levels and permits more effective use of an electron multiplier.

(3) The wide variety of photoconductor thicknesses and substrata permits the use of photoconductive materials and processing techniques not feasible in the more precisely defined standard target.

Lateral-flow targets must be uniform and sufficiently fine to avoid deterioration of the transmitted picture. Also, owing to their greater complexity, they require more fabrication art than does the standard Vidicon.

BRIDGE TARGETS

General Description

In contrast to the targets discussed thus far, bridge targets provide an internal closed circuit for each picture element permitting the photocurrent to establish a potential pattern independently of the scanning beam. Although the beam is modulated by the potential pattern,* it is not necessarily required to reduce the voltage of the scanned area to cathode potential or to carry the entire photocurrent as is customary. Many circuits are possible and many target structures have been proposed utilizing transverse or lateral flow of current or a combination of the two.

Figure 3A shows the equivalent circuit of one element of a bridge-type target. The photoconductor resistance, r_d in the dark and r_l in the light, is connected in series with a fixed resistance r_f across a voltage source 2V. The values of r_d and r_f are so chosen that in the dark the potential of the center S equals that of the gun cathode. In the light the potential of S rises due to the reduced resistance of r_l , causing a redistribution of charge in the capacitances c_1 and c_2 . The scanning beam will deposit charge on S depending on its potential, but need not reduce S to cathode potential since it will return automatically when the light is removed.

³ A. Rose in a recent paper entitled "Maximum Performance of Photoconductors," *Helvetica Physica Acta*, Vol. 30, p. 242, August, 1957, has given a theoretical argument which indicates that the maximum photoconductive gain in a conventional transverse-flow Vidicon target is unity for photocurrents not greatly exceeding the dark current.

* It is assumed that the velocity distribution of the beam electrons covers an energy spread greater than that of the potential pattern on the target.

A cross-sectional view of a bridge target employing the circuit of Figure 3A is shown in Figure 3B. In this example, the photoconductor operates in transverse flow and the fixed resistor is a lateral-flow semiconductor, but other combinations are possible. In Figure 3C, the fixed resistor is a portion of the photoconductor itself which is shielded from the light by the opaque strips. The center, *S*, of the bridge is a thin layer of semiconductor connecting the variable and fixed resistors.

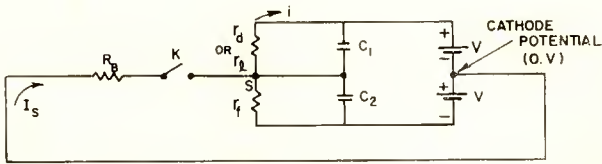


Fig. 3A—Equivalent circuit of one element of bridge target.

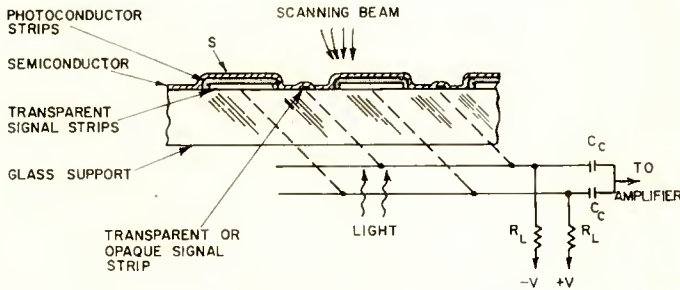


Fig. 3B—Bridge-type target structure.

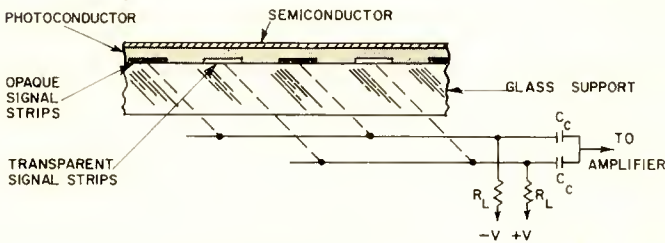


Fig. 3C—Bridge-type target structure.

Analysis of Operation

The chief benefits of bridge and lateral-flow targets are similar; they permit the use of photoconductors of relatively small dark-resistivity and they can reduce capacitive lag. A bridge target can have a high sensitivity without any charge storage, and it can be

designed to give zero signal current in the dark, regardless of the photoconductor resistivity. In addition, as mentioned above, the potential of the storage area S of each element of a bridge target (see Figure 3A) can change automatically in response to a change in illumination. If this change occurs sufficiently fast, such a target will reproduce a moving object as a series of separate, sharp images rather than the smeared-out picture which is produced when a tube stores charge throughout each frame time.

The part of the photocurrent which flows through the fixed resistance of the bridge generates no useful output. Only the current delivered to an element by the beam is available for producing the video signal. In the conventional Vidicon the useful current comprises the whole photocurrent produced by the target, while in a bridge target it may be a small fraction of the total. The question therefore arises as to the sensitivity realized by such a target. In particular, it seems desirable to compare the performance of a bridge target with that of a simple photocell using the same photoconductive element. The photocell circuit, consisting of the photoconductive resistance connected in series with a voltage source V and a current-measuring device, will provide the greatest change in total current which the photoconductor can contribute under a given amount of illumination. The photocell current is approximately equal to the corresponding current passing through the photoconductive resistance of the bridge target, i.e., the sum of the i 's (Figure 3A) of all elements.

We can now define the "efficiency" of a photoconductive target as the ratio of its signal current to the photocurrent passed, at the same light level, by the comparison photocell. A conventional Vidicon having full charge storage has a sensitivity close to that of the corresponding photocell. Its efficiency, therefore, is near unity. In Figure 4 the efficiency of the bridge target is plotted as a function of R_d , the dark-value of the photoconductive resistance for the whole target. R_f , the total fixed resistance of the target, is made equal to R_d . The computation was based on the equivalent circuit of Figure 3A, assuming practical operating conditions, with V equal to 10 volts and a 2-volt potential rise in the lighted area. The target was considered as scanned at low-velocity with the output signal taken from the modulation of the return beam. Curves were drawn for four values of the total target capacitance, C , the sum of the values of c_1 and c_2 for the whole target. The details of the computation are outlined in the Appendix.

Applications

Bridge-type targets offer the following new features in camera-tube design:

(1) They permit the use of photoconductors having dark-resistivities lower than permissible in a simple lateral-flow structure and considerably lower than can be used in the conventional transverse-flow target of the commercial-type Vidicon. The efficiency curve of Figure 4 shows, however, that the low-resistivity materials must be capable of a sensitivity considerably exceeding that of high-resistivity materials, in order to make up for the inherently low efficiency of the bridge for low-resistance targets. Since it is possible to achieve higher sensitivities with materials of lower resistivity, the resulting bridge-type targets may still exhibit a higher operating sensitivity than a conventional Vidicon.

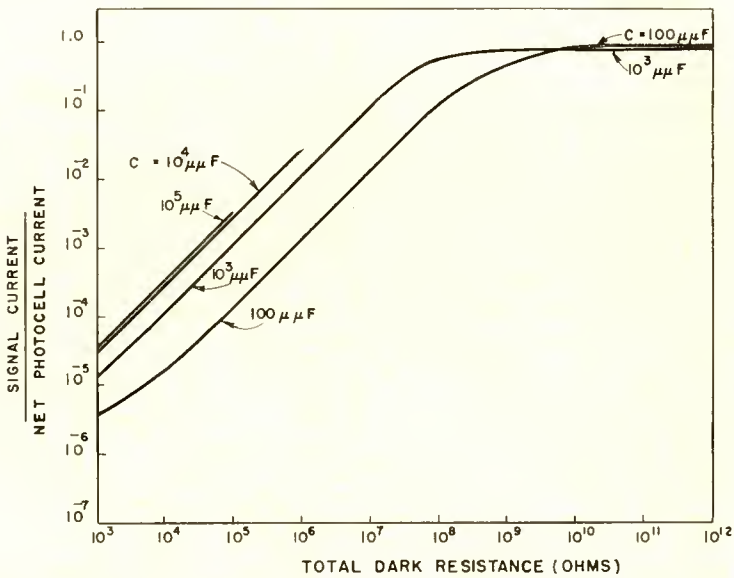


Fig. 4—Efficiency, or ratio of signal current to photocell current, versus total dark resistance for bridge target.

(2) The self-discharging feature of the bridge target frees the beam of its usual function of restoring each target element to a dark potential at the moment of scanning. The total target capacitance is no longer limited to the small values set by the beam resistance. This permits the target to be made unusually large or thin to suit the needs of the photoconductor. Another consequence is that the effective storage period can be reduced to less than a frame time. It thus may become possible to duplicate in a Vidicon the well-known image orthicon characteristic of reproducing a moving object as a series of discrete

images instead of as a smear. However, for rapid self-discharge, the photoconductive lag must be small and the internal time constant of the target must be less than 1/30 second.

(3) The bridge target provides a simple way of producing a video signal corresponding to the *difference* between two signal patterns. For example, Borkan and Weimer¹ have proposed a bridge-type target in which each arm of the bridge is photoconductive and the video signal represents the difference between the signals which either arm would produce separately. The authors show that, with different lag characteristics in the two arms of the bridge, the resultant output signal can have less lag than the signal produced by either component separately.

Bridge-type targets are more difficult to fabricate than conventional Vidicon targets and give poor resolution unless made in exceedingly fine structures. The techniques developed for depositing fine strips of conductors and insulators in the tricolor Vidicon¹ support the view that bridge-type targets with adequate resolution for many purposes could be produced. Operable targets of reasonable size yielding several hundred lines resolution have been built in the laboratory. However, much improvement in fabrication technique will be necessary to achieve targets which are of acceptable uniformity and freedom from defects.

APPENDIX—CALCULATION OF THE EFFECTIVE SENSITIVITY OR "EFFICIENCY" OF BRIDGE TARGETS

In the equivalent circuit for an element of a bridge target, shown in Figure 3A, the action of the scanning beam is represented by the resistance R_b in series with switch K . This switch closes once in a frame time t_f for an elemental time t_c . The representation of the beam by a fixed resistance is sufficiently accurate to give useful results.

The operational cycle of such an element may be considered to begin at the moment when the beam has left the element, i.e., when switch K has just been opened. In the usual case, the center of the bridge is then near cathode potential (0 volts). During the following 1/30 second, S tends toward an equilibrium potential $V(r_f - r_i)/(r_f + r_i)$. The beam now returns to S for a time t_c , deposits a certain number of electrons, and the cycle is repeated.

The two parts of this cycle will now be expressed more quantitatively. Between scans, the potential V_S of S varies according to the relation

¹ H. Borkan and P. K. Weimer, "Differential Method of Lag Compensation in Photoconductive Devices," *RCA Review*, Vol. XIX, p. 62, March, 1958.

$$V_S(t) = \delta V e^{-t/T} + V \frac{r_f - r_l}{r_f + r_l} (1 - e^{-t/T}), \quad (1)$$

where δV is the potential of S at the beginning of the cycle. The time constant T is equal to $r_f r_l (c_1 + c_2) / (r_f + r_l)$. When the beam returns (at $t = t_f$), it finds S at the potential

$$V_{S'} \equiv V_S(t_f) = \delta V e^{-t_f/T} + V \frac{r_f - r_l}{r_f + r_l} (1 - e^{-t_f/T}).$$

The initial beam current landing on the element is $V_{S'}/R_B$. This current approaches the equilibrium value $V(r_f - r_l) / (R_B r_f + R_B r_l + r_f r_l)$ with a time constant $\tau = R_B r_f r_l c / (R_B r_f + R_B r_l + r_f r_l)$. The signal current for a given element is then

$$i_S(t) = \frac{V_{S'}}{R_B} e^{-t/\tau} + V \frac{r_f - r_l}{R_B r_f + R_B r_l + r_f r_l} (1 - e^{-t/\tau}),$$

and the average signal current during the elemental time t_e ,

$$(i_S)_{\text{avg.}} = \frac{1}{t_e} \int_0^{t_e} i_S(t) dt = \frac{\tau}{t_e} \left[\frac{V_{S'}}{R_B} - V \frac{r_f - r_l}{R_B r_f + R_B r_l + r_f r_l} \right] (1 - e^{-t_e/\tau}) + V \frac{r_f - r_l}{R_B r_f + R_B r_l + r_f r_l}.$$

The signal current for the target as a whole is equal to this value reduced by 20 per cent to account for the retrace time.

The "efficiency" of a bridge target was defined before as the ratio of the signal current to the corresponding photocurrent ($V/R_l - V/R_d$) of a comparison photocell. Figure 4 is a graph of this ratio computed as a function of the total dark-resistance of the target, $R_d = r_d/N$, which equals the corresponding fixed resistance, $R_f = r_f/N$. The computation was done for four values of the target capacitance $C = Nc$ and for the following operating conditions. A fixed beam resistance of 10^7 ohms and an elemental time of 10^{-7} second were assumed. V was taken as 10 volts, so that the total voltage applied across the bridge was 20 volts. For each value of R_d , the magnitude of R_l was chosen such that S rises to two volts between scans. In the dark, where $R_d = R_f$, the signal current is zero.

The proper values of R_l were found in the following way. Targets whose time constant T is considerably shorter than the 1/30-second

frame time, reach their equilibrium potential between scans. This is the case if $R_f C$ is less than 10^{-2} second. For these "self-discharging" targets, $V_{s'}$ is equal to two volts if $R_l = 2R_f/3$, regardless of the potential $V_s(t_c)$ at which the beam leaves each element. Targets which do *not* reach an equilibrium potential within $1/30$ second require $R_l < 2R_f/3$, so that a 2-volt potential rise occur between scans. For these cases the appropriate value of R_l was determined from Equation (1) with δV assumed equal to zero. This assumption is not valid for the larger value of C for which the beam leaves S at a voltage considerably higher than cathode potential. If such targets are not self-discharging, lag results. The curves of Figure 4 were discontinued where this effect sets in.

DIFFERENTIAL METHOD OF LAG COMPENSATION IN PHOTOCONDUCTIVE DEVICES*

BY

HAROLD BORKAN AND PAUL K. WEIMER

RCA Laboratories,
Princeton, N. J.

Summary—The slow response time often observed in devices utilizing photoconductivity may be caused by the slow rise and decay of conductivity in the photoconductor, or by the RC time constant of the photoconductor in its associated circuit. In imaging devices such as television camera tubes and light amplifiers, the lag is manifested by smearing of the image for moving scenes. This paper describes a method for reducing the effective response time of the device regardless of the source of lag. By taking the difference of the signals from two photoconductive elements having unlike transient responses, a resultant signal can be obtained having a faster response than either element alone.

Measurements have been taken on pairs of Vidicons set up to view the same scene simultaneously. The lag-corrected video signal formed by the external combination of the two outputs showed improved speed of response with a moderate loss in signal. Similar results have been obtained with pairs of photoconductive cells. The method can also be applied to light amplifiers and to experimental camera tubes designed to yield a lag-corrected signal directly.

INTRODUCTION

DEVICES employing photoconductive materials for transforming light energy into an electrical signal are often limited by a slow response time. Two primary sources of lag are encountered: one due to the inherent response time of the photoconductor and the other due to the capacitance of the photoconductor in the associated circuit. The photoconductive lag, caused by the delay in change of charge carrier density with changes in light levels, varies widely from one material to another and is affected by such factors as temperature and intensity of illumination. The capacitive lag is specified by the product of the capacitance of the photoconductor and the resistance of the measuring circuit. A high-impedance circuit such as the scanning beam in a television camera tube together with a high-capacitance photoconductor, may increase the observed time lag considerably beyond that due to photoconductive lag alone. Conditions imposed by the nature of the device or the properties of the photoconductor may prevent the RC product from being as small as necessary to avoid capacitive lag.

Various methods for compensating for lag in television camera

* Manuscript received October 15, 1957.

tubes and other imaging devices have been under investigation. By lag compensation is meant any basic change in design or method of operation of the device which will reduce the effective time lag to less than that expected from the characteristics of the photoconductor. Lag in imaging devices causes smearing of the image for moving scenes. Lag compensation will involve some reduction in the effective sensitivity of the device but the photoconductor sensitivities are often high enough that such a compromise can be advantageous.

The differential method of lag compensation, which was first proposed many years ago by Korn¹ in attempts to improve the response of selenium cells, has apparently gone unnoticed in modern applications of photoconductivity. The present paper describes the application of the method to imaging devices for the correction of both photoconductive and capacitive lag. Measurements of lag compensation

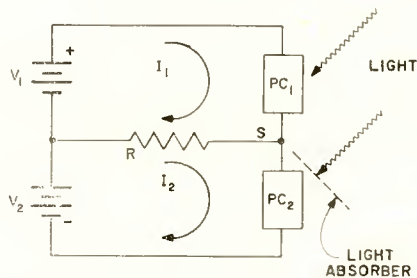


Fig. 1—The basic circuit for differential lag compensation.

using a pair of commercial photocells and a pair of photoconductive camera tubes have been made. The application of the method to a single camera tube is discussed.

THE PRINCIPLE OF DIFFERENTIAL LAG COMPENSATION

Differential lag compensation is a method of producing an improved photoconductive response by taking the difference between two signals obtained by simultaneously illuminating two photoconductors having unlike response times. Figure 1 shows a simple bridge circuit in which the net current flowing through the load resistance, R , is the difference between the currents in the two photoconductors, PC_1 and PC_2 . The larger signal is produced by PC_1 and is assumed to have a typical photoconductive response to a short burst of light as shown by curve (1) in Figure 2. Curve (2) shows the current produced by PC_2 to

¹ A. Korn and B. Glatzel, *Handbuch der Phototelegraphie und Telautographie*, Otto Nemnich, Leipzig, Germany, 1911.

be of smaller magnitude and to have relatively more lag. The total current flowing in R , given by curve (3), represents the lag-compensated difference signal. Curve (4) is the same as curve (3) except that its amplitude has been plotted on a larger scale in order to permit direct comparison of the original uncompensated signal (1) with the final lag-corrected difference signal. It is noted that both the rise and decay times have been decreased at the expense of a moderate loss in sensitivity.

In order to yield an effective improvement in response without appreciable loss in signal, the signal to be subtracted must have more lag than the original uncorrected signal. This condition is readily

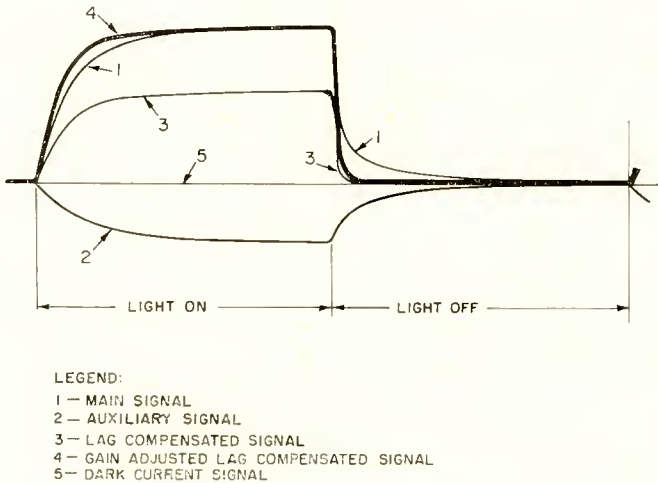


Fig. 2—Typical improvement in response obtained by differential lag compensation.

obtained by proper choice of photoconductors for PC_1 and PC_2 or by operating the same type of photoconductor under different voltage or light level. The improvement is most striking when the photoconductor response shows an initial rapid rate of change followed by a slow change which gradually approaches a steady value. Under these conditions the slow change (which is most objectionable in television camera tube applications) can be subtracted leaving the rapid component unaffected (See Figure 2).

The lag compensation method can be applied to either photoconductive or capacitive lag or to combinations of the two. The subtraction of two exponential decay curves representative of some cases of capacitive lag is discussed in the Appendix.

As the following section on measurements will show, the differential lag-compensation method does not necessarily provide optimum compensation at all light levels. If conditions are chosen to give the best possible compensation in the brightest areas of the picture, the lower light levels may show less improvement. In general, a net improvement could be readily observed in the television camera tube applications without critical adjustment of balance between the two signals.

MEASUREMENTS OF LAG COMPENSATION USING TWO PHOTOCELLS

The basic characteristics of differential lag compensation were studied using two commercial CdS photocells, type 6694-A. The cells were connected as shown in Figure 1, but with convenient means for adjusting the voltages. A cathode-ray oscilloscope capable of slow sweep speeds was connected across the load resistor, R . The value of R was made small compared to the static photocell resistance which is of the order of 10^9 ohms in the dark and 10^6 ohms in the light. The two cells were mounted side by side and illuminated by a uniform source of light interrupted by a motor-driven slotted disc. In the tests made, the lag of PC_2 was made relatively larger than PC_1 by reducing its incident light with a neutral-density filter. Either cell could be used with the filter to compensate for the lag of the other, although it was desirable to select the faster cell for PC_1 .

The typical improvement using two 6694-A cells is shown in Figure 2, which was scaled from a multiply exposed photograph of the oscilloscope. The gain-adjusted lag-corrected signal, curve (4), is shown here as a broader line; in subsequent photographs it is shown as the brightened oscilloscope trace. The rise of signal with light has been improved a moderate amount while the decay of signal when the light was removed has been improved quite markedly. The compensated signal decays to 10 per cent of peak 10 milliseconds after the removal of light as compared with 34 milliseconds for the uncompensated cell. This advantage was obtained at the expense of using a second cell and net reduction in signal level of about 45 per cent.

Figure 3 shows a series of these photographs for various levels of illumination and two different fractions of light passed on to the auxiliary cells, 16 and 32 per cent compared with the amount on the main cell. The cell used for the main signal was a typical type 6694-A while the one used for the auxiliary signal was selected from several as having the greatest amount of lag. The photographs show that the improvement is apparent over the range of light levels tested, but was better at the higher levels. The same pair of cells was used in

tests with 5 to 100 per cent of light incident upon the auxiliary cell compared with the amount on the main cell, with some improvement resulting in each case. Adjusting the operating conditions of the two cells for optimum results was not critical. The above tests were made with the light-on and light-off periods each equal to 0.25 second. The lowest pair of photographs in Figure 3 was taken when the light was alternately on and off for 0.12, 0.06, 0.03 and 0.015 second. In each case faster response resulted indicating that the improvement is also

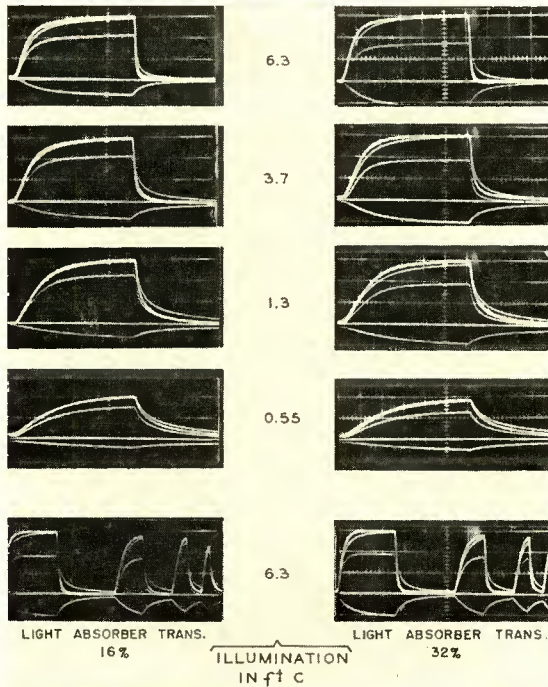


Fig. 3—Relative response times for differential lag-compensated type 6694-A photocells under various levels of illumination and light absorber transmissions. (Refer to Figure 2 for curve identification.)

independent of the length of time the incident light is on.

The usefulness of the differential lag compensation method for photocells depends upon the required application. It would be most effective in cases where the long-term rise and decay characteristics must be minimized. It would be less suitable for high-speed applications where a single conventional cell with associated circuitry to enhance the high-frequency response is adequate. If the differential method is required, the use of two separate photocells would probably be satisfactory in most cases. However, a single three-electrode photo-

cell for this purpose could be made by incorporating two crystals in a single encapsulation or by the use of large-area interdigitated or layered structures as shown in Figure 4.

MEASUREMENTS OF LAG COMPENSATION USING TWO VIDICONS

To evaluate the application of differential lag compensation to image pickup devices, measurements were made using two conventional

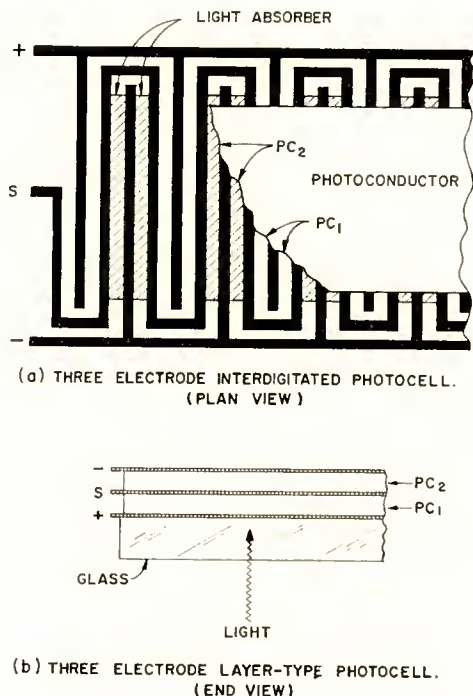


Fig. 4—Large-area photocell structures employing differential lag compensation. (a) Plan view of three-electrode interdigitated photocell. (b) End view of three-electrode layer-type photocell.

Vidicons. Since the two tubes must be in optical and electronic registry, a modified three-tube color camera was used for the actual tests. Figure 5 shows a block diagram of the circuit arrangement used. The signal from each tube was amplified, the signal from the auxiliary tube was inverted, and the two signals combined to form a lag-compensated signal. Misregistry of the two signals would appear not only as lighter or darker edges around stationary objects in the picture but also as uncompensated edges surrounding a moving object in the scene.

Two types of tests have been devised to measure and compare lag in camera tubes. The first method is similar to the one used on photo-cells and employs an interrupted light source and an oscilloscope to display the transient response of the video signal. Since the vertical deflection rate in the camera differs from that of the a-c line, the motor which interrupts the light source was synchronized to the vertical deflection.

The second type of test uses a motor to drive a wheel containing a white spot placed near the edge of a black background. By reflected light the camera views the rotating spot, but due to the lag the bright spot appears as a portion of an annular ring. By photographing the picture on the television monitor with an exposure time approximately

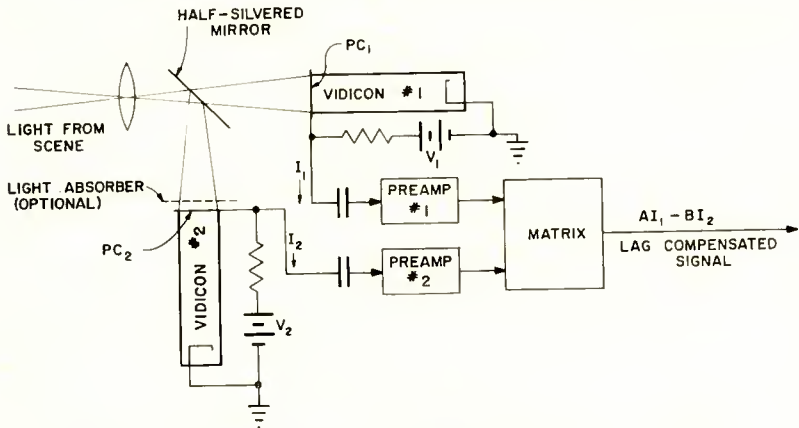


Fig. 5—Two-Vidicon set-up for differential lag compensation.

equal to one vertical period, a permanent record can be made and measurement taken of the number of degrees of arc displayed. Figure 6 shows the data taken for both methods of measuring lag. Two commercial Vidicons, type 6326, were used with two conventional pre-amplifiers. The two signals were combined in a two-channel matrix circuit which could add or subtract adjustable amounts of each signal.

The differential method of lag compensation has been tested with commercial one-inch Vidicons containing a porous antimony tri-sulfide photoconductor as well as with experimental tubes employing the photoconductor developed by Cope² for use in a one-half-inch Vidicon. This new photoconductor has higher sensitivity than the standard one but introduces capacitive lag when used in the one-inch target size. Fig-

² A. D. Cope, "A Miniature Vidicon of High Sensitivity," *RCA Review*, Vol. XVII, p. 460, December, 1956.

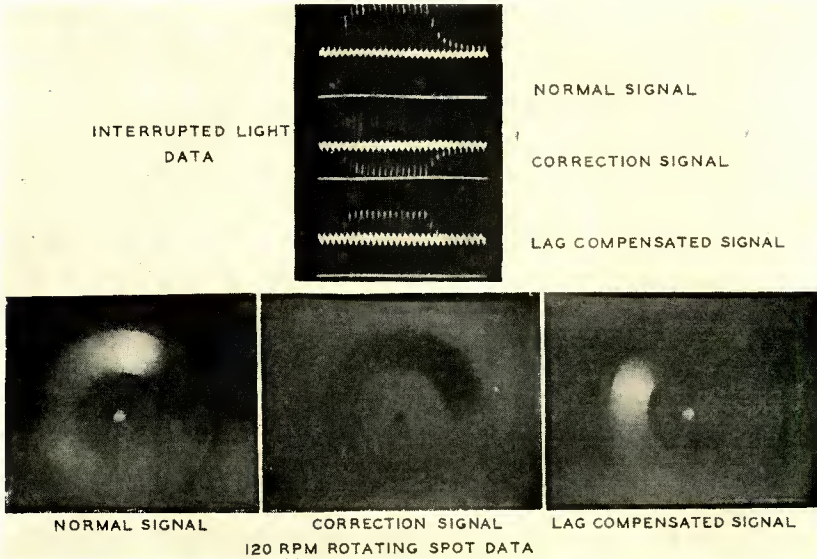


Fig. 6—Typical test results using two type 6326 Vidicons in the arrangement of Figure 5.

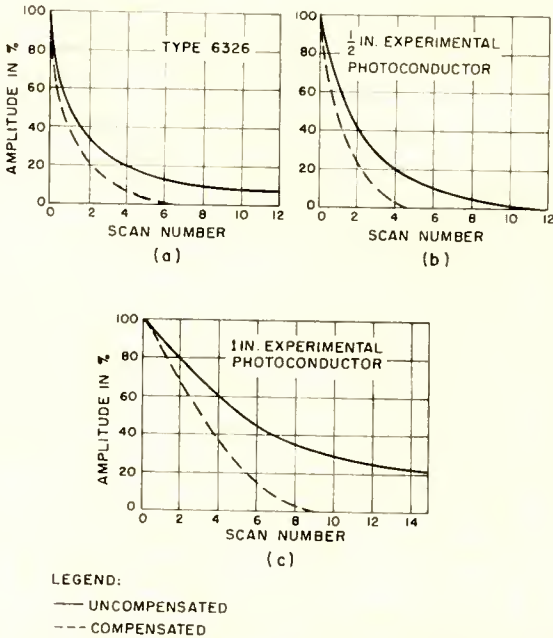


Fig. 7—Measurements of signal decay using several types of Vidicons with differential lag compensation (dashed lines) and without compensation (solid lines).

ure 7 shows the improvement obtained by the differential method of lag compensation when light is removed. Three cases with and without compensation are plotted: (a) the commercial one-inch Vidicon type 6326 with the standard photoconductor; (b) the experimental photoconductor in one-half inch size; and (c) the experimental photoconductor in one-inch size. A comparison of (a) and (b) shows roughly the same amount of lag in each case when uncompensated; about 20 per cent signal remains after the fourth scan by the beam after the light has been removed. This compares to about the second scan for the same residual signal when compensation is applied in each case. Case (c) exhibits greater lag due to capacitance and reaches 20 per cent residual signal at about the fifteenth scan which is reduced to the fifth or sixth scan when compensation is applied. The differential method does not depend on the origin of the lag, but requires that the correction signal has relatively more lag than the main signal. These measurements show that approximately the same relative improvement is obtained with camera tubes as with photocells.

DISCUSSION OF TESTS OF LAG COMPENSATION WITH TWO VIDICONS

The two-Vidicon tests of lag compensation were undertaken primarily to verify the principle involved for image devices and to ascertain that no unexpected spurious effects were visible in the reproduced picture. From this standpoint the tests were successful and seemed to indicate that the method might be incorporated successfully into a single camera tube of the type discussed in the next section.

A noticeable improvement in lag was readily achieved and relatively little difficulty was encountered in determining the proper proportion of signal in each channel. The increased lag in the auxiliary channel was obtained by adjusting the relative illumination on each tube, while signal gains were set for best compensation. The length of the white trail normally left by a moving white spot could substantially be reduced or made to turn black depending on the relative gains. "Burn-in" effects lasting many seconds, which give an illusion of transparency to objects moving in the foreground, could be greatly reduced.

It should be stressed that the differential lag compensation method provides only an approximate correction for the low-light areas. Conversely, if the optimum correction is set for the gray areas of the scene, the bright areas would be over-corrected and give a negative after-image. A satisfactory compromise yielding a net improvement could be reached for a given scene, but the failure to "track" might require some readjustment of relative gains for widely varying scene illuminations.

Further work would be required to determine whether a two-tube monochrome Vidicon camera incorporating differential lag compensation would be of practical value. When the minimum scene illumination is set by the maximum tolerable lag, a means for reducing lag would permit lower scene brightnesses and effectively higher sensitivities.³ On the other hand, the following factors contribute to a loss of signal in the two-tube method:

- (1) Optical losses in the image splitting lens system;
- (2) Diversion of a fraction of the light from the main tube for the auxiliary tube;
- (3) The electrical subtraction process.

The loss from these three causes will be at least 50 per cent. At the same time the subtraction process will increase the noise by about 40 per cent, assuming each channel has the same gain. Although various methods have been proposed for reducing this noise and simplifying the preamplifier circuits, the two-tube camera will suffer a total loss in signal-to-noise ratio of at least three or four for the same light level.

SINGLE CAMERA TUBES EMPLOYING DIFFERENTIAL LAG COMPENSATION

Techniques developed for constructing an experimental tricolor Vidicon⁴ have opened up the possibility of building a monochrome camera tube having a target structure providing differential lag compensation. Although this work, at the present time, has not been carried beyond an early exploratory stage, several experimental target structures have been tested. Such targets can be divided into two classes: those which provide two output signals which must be amplified separately and the difference taken external to the tube, and those which provide directly a single lag-corrected difference signal. The latter type is the more desirable and will be discussed first.

Figure 8 is a form of "bridge" target⁵ whose output is proportional to the difference between the photoconductive signal generated

³ In one qualitative test an increase in light level by twenty times was required to reduce the lag in the uncompensated main channel to the same value as was obtained at the lower light level with compensation.

⁴ P. K. Weimer, S. Gray, H. Borkan, S. A. Ochs and H. C. Thompson, "The Tricolor Vidicon—An Experimental Camera Tube for Color Television," (Abstract) *Proc. I.R.E.*, Vol. 43, p. 370, March, 1955.

⁵ S. A. Ochs and P. K. Weimer, "Some New Structure-Type Targets for the Vidicon—An Analysis of Their Operations," *RCA Review*, Vol. XIX, p. 49, March, 1958.

in the part of the photoconductor labeled PC_1 and the part labeled PC_2 . Each picture element of the target has the equivalent circuit shown in Figure 1. The conducting tabs labeled S (which in some versions may be replaced by a continuous semiconducting layer) assume a potential in the dark corresponding to cathode potential. When light falls on a picture element, the photoconductive current over the positive strips tends to charge the surface S positively while the current over the negative strips acts to reduce the potential to which S can rise in a single scanning period. The video signal generated when the beam returns S to cathode potential is the lag-corrected signal representing the difference between the two currents which flowed in PC_1 and PC_2 .

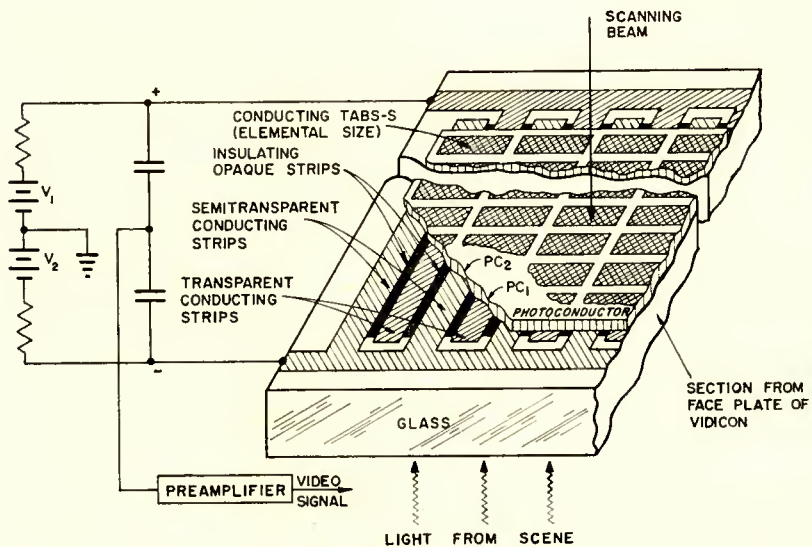


Fig. 8—Bridge target structure for differential lag compensation of a Vidicon-type camera tube.

The photoconductor PC_2 over the negative strips is assumed to have more lag than PC_1 at all light levels, even if the identical photoconductor layer is used for both, because of the light attenuation built into the negative strips of the target.

An advantage of the bridge target is that a negligible amount of noise is introduced in the subtraction process. The noise associated with the signal is small compared with the amplifier noise which is no greater for a bridge target than for a conventional target. The only observed loss in signal-to-noise ratio comes from the signal loss due to the subtraction process itself and the light absorbed in PC_2 .

This factor in a properly designed target should amount to little more than about 2. The best ratio of signal levels for proper compensation is obtained by adjusting the relative voltages applied to the two sets of signal strips. The addition of the negative target-voltage supply represents the only modification which should be necessary in adapting a conventional Vidicon camera for use with a tube having a lag-compensated bridge-type target.

Figure 9 shows the form of a lag-compensated target which provides separate output signals to be combined externally producing the lag-compensated signal. If we assume negligible surface conductivity of the photoconductor,⁶ each set of strips must be biased positively with respect to the gun cathode. The two output signals have the same polarity and must be combined subtractively. As in the tricolor Vidicon,

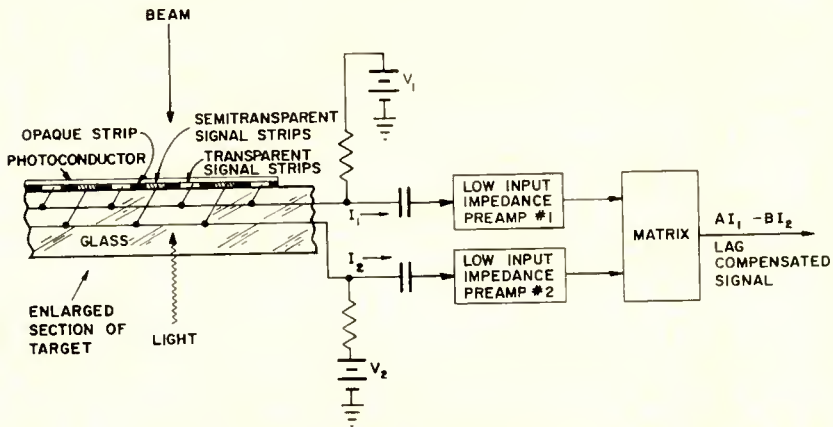


Fig. 9—Two-channel output target for differential lag-compensated Vidicon-type camera tube.

a high capacitance exists between the different sets of strips. Therefore, preamplifiers of low input impedance must be used to obtain independent signals. The noise level in each channel due to this added capacitance is thus considerably higher than normal (by a factor of about 6). Furthermore, the noise in the final difference signal is increased still more by the subtraction process since the two noise currents are 180° out of phase and add directly. This loss in signal-to-noise ratio appears to be too great to make this method of operation attractive.

The problem of fabricating a bridge-type target having strips of

⁶ If the surface of the photoconductor were appreciably more conducting than its bulk conductivity, the target structure of Figure 9 could be operated as a bridge target as discussed for Figure 8.

sufficient fineness and uniformity to produce a high-quality television picture is a serious one. At least 500 strips in each set would be required for normal television standards. Breaks in continuity of the strips would also cause trouble, particularly if the voltage difference between the two sets is too high to permit connections at both ends of each strip. The evaporation techniques developed for the tricolor Vidicon are capable of producing bridge targets of the required fineness, but further refinement in technique is necessary to produce targets free of defects. A tricolor lag-compensated bridge target is also a possibility but would be still more difficult to fabricate.

APPLICATION OF LAG COMPENSATION TO OTHER DEVICES

Differential lag compensation should also be effective in display devices employing photoconductivity. For example, a light amplifier might be constructed with two groups of photoconductive elements having different speeds of response. The electroluminescent light-output elements would be so connected as to be driven by the lag-corrected difference current. The nonlinear character of the presently known electroluminescent and photoconductive powders complicates the design of the structure, however, and the feasibility of the proposal has not been evaluated.

ACKNOWLEDGMENT

The authors wish to express their appreciation to Herman L. Oehme for constructing the equipment used in these experiments.

APPENDIX—COMPUTED LAG COMPENSATION FOR EXPONENTIAL DECAY

For an assumed exponential decay characteristic it is possible to calculate the improvement in response available by the differential method of lag compensation. If both signals decay exponentially with the same time constant, no improvement in speed of response occurs when any fraction of one signal is subtracted from the other. However, if the auxiliary signal has a longer time constant than the main signal, a reduction of lag is indicated. Mathematically, the net gain-adjusted resultant signal is

$$R = \frac{1}{1-x} \left(e^{-\frac{t}{t_0}} - x e^{-b \frac{t}{t_0}} \right),$$

where t_0 is the time constant of the main signal, t_0/b is the time constant of the auxiliary signal, x is the relative amplitude of auxiliary signal, and t is the time after the removal of light. For an assumed

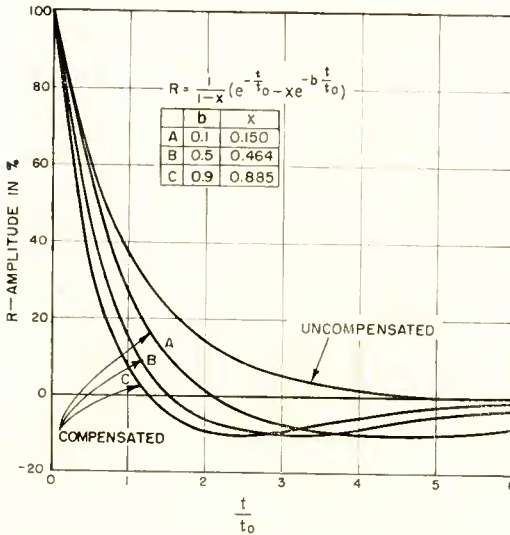


Fig. 10—Theoretical compensation attainable with exponential decays of signal. Parameters selected so that compensated response is tangent to $R = -10$ per cent.

value of b between 0 and 1, R will reach a negative maximum and asymptotically approach the axis. Figure 10 shows the decay characteristic of compensated signals for comparison with the uncompensated signal for various values of b . The condition is imposed that all corrected signals may go no further than 10 per cent negative which specifies the value of x for each value of b . The assumption is made

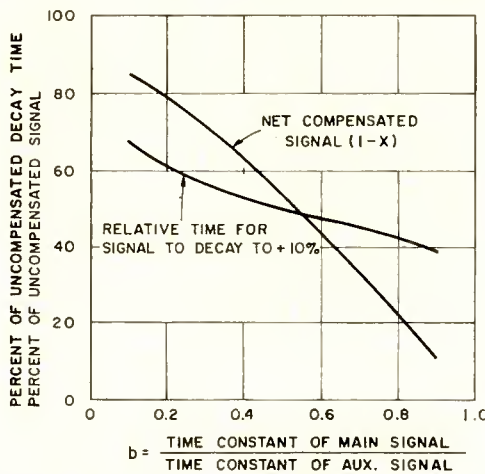


Fig. 11—Response time and residual signal for compensation in Figure 11.

here that a 10 per cent overshoot in the negative direction is the maximum amount which is tolerable.

Figure 11 shows the reduction in the time for the signal to reach the positive 10 per cent value and also the amount of net signal remaining, which is indicative of resultant signal-to-noise ratio. The curves show that the reduction in decay does not change rapidly with b , but loss of signal does increase markedly as b approaches unity.

The above analysis applies to two camera tubes having only capacitive lag with the beam resistance constant. It has been observed however, that in Vidicons having capacitive lag dominating, the decay is slower than exponential. This may be explained by assuming that the

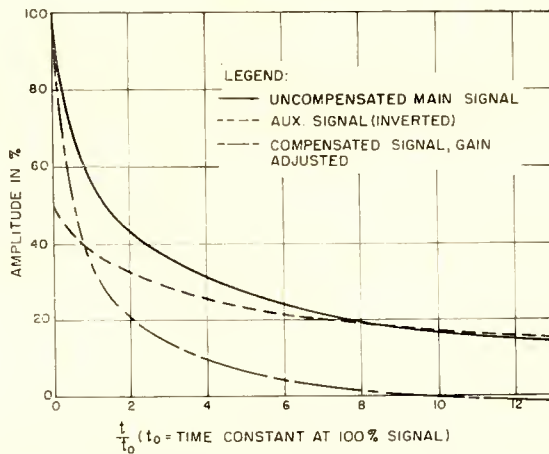


Fig. 12—Calculated compensation attainable for capacitance lag in a Vidicon assuming that the beam resistance is inversely proportional to the signal amplitude.

beam resistance and therefore the time constant increases with decreasing signal level. The relative improvement when assuming that the beam resistance varies inversely as the signal level is calculated in Figure 12. It has been assumed that the time constant of the auxiliary signal is three times that of the main signal while the amplitude of the former is 50 per cent of the latter, which is sufficient compensation to greatly reduce the long tail of decay.

Since the capacitance across the photoconductor can be readily adjusted by choice of photoconductor thickness, the conditions necessary for effective compensation of capacitive lag can be met without great difficulty. Figure 7-C is an example of compensation for capacitive lag.

A HYSTERESIS EFFECT IN CADMIUM SELENIDE AND ITS USE IN A SOLID-STATE IMAGE STORAGE DEVICE*

BY

F. H. NICOLL

RCA Laboratories,
Princeton, N. J.

Summary—A brief description is given of a new hysteresis effect in cadmium selenide photoconductive powder. Photocurrent plotted as a function of voltage has the form of a hysteresis loop, with triggering from low to high currents occurring at a voltage depending on the incident light level. At a suitably chosen voltage, triggering from low to high currents occurs with light pulse excitation. Return to the condition of low current flow is brought about by brief interruption of the supply voltage. Since the triggering is present with a-c or d-c operation, it is possible to use the effect in a series circuit of photoconductor and a-c operated electroluminescent panel. If this is done on an area basis with due attention paid to the impedance match of the photoconductor and electroluminescent layer, it is possible to make an image storage device having no optical feedback. The construction and operation of such a device is described, and a photograph of a stored image on a 3-inch panel is shown.

INTRODUCTION

THE combination of a photoconductive layer and an electroluminescent layer in series with an a-c voltage is now well known as the basis of one type of light amplifier or solid-state image intensifier.¹ These devices have generally employed photoconductive CdS powder. This material has high sensitivity, low dark current, and excellent uniformity when spread in plastic embedded layers. More recently, other photoconductive materials have been made in the form of sensitive powders. Among these is CdSe, which has faster response and comparable sensitivity to CdS. This new CdSe powder has a spectral response which extends further into the infrared than is the case with CdS. When embedded in plastic and operated at relatively high fields, the material exhibits a hysteresis effect in the curve of photocurrent versus voltage. It is this new effect that is discussed, particularly in connection with its use in a light-amplifier structure to give image storing action without any optical feedback.

* Manuscript received November 11, 1957.

¹ B. Kazan and F. H. Nicoll, "An Electroluminescent Light-Amplifying Picture Panel," *Proc. I.R.E.*, Vol. 43, p. 1888, December, 1955.

CURRENT-VOLTAGE CHARACTERISTICS OF CdSe TEST GAPS

The hysteresis curve is most readily examined in a d-c circuit consisting of a microammeter in series with a test gap and voltage source. This arrangement is shown in Figure 1. The CdSe powder is mixed with a 1 per cent plastic binder of ethyl cellulose and is

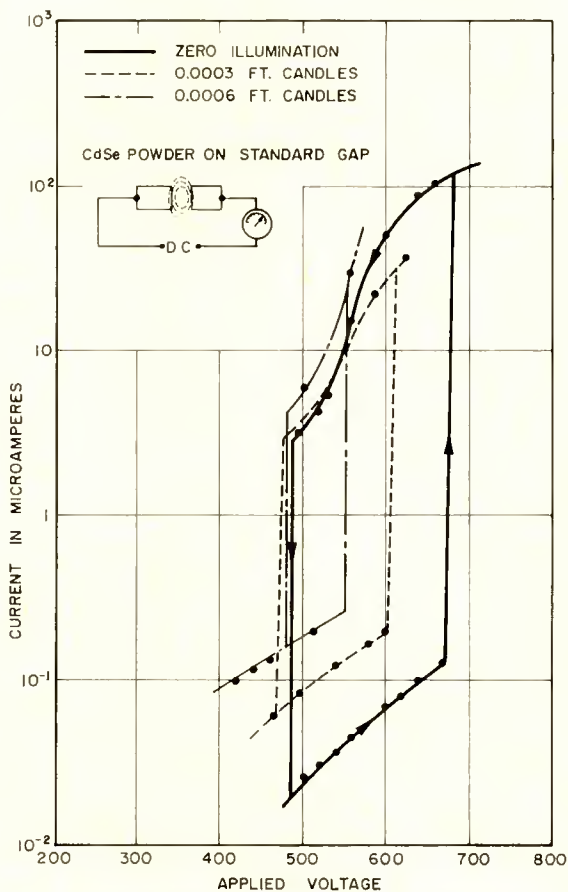


Fig. 1—Hysteresis curves for CdSe powder.

applied to the test gap consisting of two transparent electrodes 5 millimeters long, spaced $\frac{1}{2}$ millimeter apart.

The curves in this figure show plots of current versus applied d-c voltage for no incident light on the powder and for two different low levels of light. The full line curve for no light incident on the photoconductor shows that the dark current of the photoconductor rises normally at first, about as the fourth power of the voltage, but as a

critical value of 670 volts is reached the current suddenly rises by about three orders of magnitude. If the voltage is now lowered, the current decreases until a second critical voltage is reached at which point the current suddenly drops to its original low value. This same type of hysteresis loop is obtained if the photoconductor is exposed to a small amount of light. This is shown in the dashed curve which was taken with steady light excitation of 0.0003 foot candle from a tungsten light source. At low voltages photocurrent is now measurable above the dark current. As the voltage is increased a critical value is again reached where the photocurrent increases by a large amount. The voltage required to trigger the cell into the more conducting state is now lower as a result of the illumination. The third curve of dots and dashes was taken with 0.0006 foot candle illumination on the cell and shows a still further reduction in the triggering voltage required. Thus far, only *voltage* triggering has been considered. However, it is evident from these three curves that if a voltage between 500 and 600 volts is applied to the cell in the dark, then application of light will trigger the cell to higher conductivity. It is this property which is interesting from the point of view of making light-triggered image storage devices.

LIGHT-TRIGGERED STORAGE IN CdSe TEST GAPS

Figure 2 shows this light-triggered effect. The lower curve, taken at 600 volts per millimeter, shows photocurrent as a function of input light level. This is what could be termed normal photoresponse of a photoconductive powder, the current rising slowly with voltage. When the field is raised to a considerably higher value, *normal* photoresponse occurs only at low input light levels, as shown by the dashed curve taken at 1,160 volts per millimeter. As the light level is raised, a point is reached where the photocurrent suddenly rises by a large amount. If the input light is now lowered or removed the triggered photocurrent remains at a high value. To return to the low current level the supply voltage must be interrupted or reduced momentarily.

Light triggering is a function of the product of light level and time, and reciprocity is obeyed in the middle range. A typical exposure figure for triggering the photoconductor is 1/100 second exposure for 0.1 foot-candle illumination with tungsten light, in other words, 0.001 foot-candle second.

The d-c "storage" current flowing when a CdSe powder cell is light triggered to the conducting condition is not a steady current but consists of many oscillations appearing as a noisy current in the left-hand trace of Figure 3. This shows an oscilloscope trace of triggered photo-

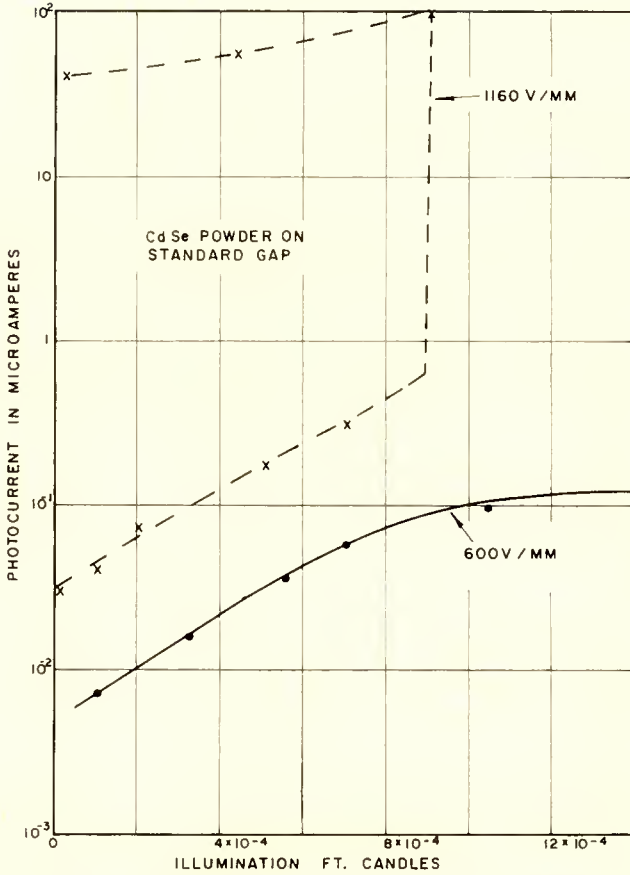


Fig. 2—Light-triggered current in CdSe powder.

current as a function of time. Current remains low until the light has been on a sufficient time to cause triggering, after which the current rises to a high level composed of many oscillations. The right-hand trace of Figure 3 shows the beginning of the triggering action more clearly on an expanded time scale. Rise time to the triggered condition for this sample is about five milliseconds. The ordinate scale on these



Fig. 3—Oscilloscope traces of triggered current in CdSe powder.

traces is linear but the photocurrents shown are 100 to 1,000 times the dark current.

PHOTOCONDUCTIVE CELL IN SERIES WITH ELECTROLUMINESCENT CELL

The triggering action of light is present with a-c operation as well as d-c, and the hysteresis effect is therefore suitable for use in a series circuit composed of a cadmium selenide cell and an electroluminescent panel to give a light-triggered on-off or bistable combination. The simple circuit of such a bistable element is shown in Figure 4.

Light feedback from the electroluminescent cell to the photoconductive cell is prevented by an opaque barrier. When a-c voltage is applied to the combined cells, most of the voltage appears across the

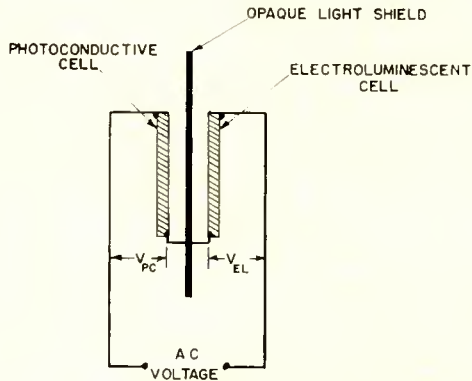


Fig. 4—Storage element with no optical feedback.

photoconductor, since the impedance of the CdSe cell in the dark is much higher than the electroluminescent cell. In the dark, then, V_{pc} is much greater than V_{EL} . If the applied voltage is of the proper value, the photoconductor can be triggered into its conducting or low-impedance condition by a flash of light. After triggering, the photoconductor has lower impedance, and the voltage across it is small; thus the voltage on the electroluminescent layer is increased causing light emission. In this condition V_{pc} may be equal to or less than V_{EL} . Output light will continue to be emitted after the incident flash of light has ceased *only* if the voltage across the photoconductor, V_{pc} , does not fall to a value where the low impedance condition cannot persist. If the voltage falls too much, the photoconductor impedance rises, the "storage" condition ceases to exist, and the combination returns to the off condition with no light emitted from the electro-

luminescent layer. The impedances of the photoconductor cell and electroluminescent cell must be such that the voltage on the photoconductor during triggering remains high, thus allowing the device to remain in the "on" condition when triggered.

Using conventional plastic-embedded electroluminescent layers and the CdSe powder presently available, it was found that with equal electroluminescent and photoconductive areas the photoconductor impedance in the triggered condition is too low to give storage action in the series combination. In other words, the impedance of the electroluminescent cell is too high; therefore, the area of the electroluminescent material must be considerably greater than that of the photoconductor for satisfactory operation. Such an arrangement results in satisfactory bistable elements which can be triggered on by a flash of light and off by brief interruption of the a-c supply.

In the usual light amplifier or image intensifier structure the electroluminescent and photoconductive areas are approximately equal; for this reason the standard structures do not make good picture storage panels when CdSe powder is used as the photoconductor.

Many structures can be visualized in which the electroluminescent areas are larger than the photoconductive areas. These include simple multi-element arrays in which the desired impedance conditions are met. Some such structures have been made and operated, but as element size is reduced it becomes more and more difficult to maintain the necessary impedance conditions.

STORAGE PANEL CONSTRUCTION AND OPERATION

Figure 5 shows a structure which is similar to one previously described.¹ This structure consists of a grooved piece of Lucite fabricated to have fine conducting lines at the bottom of each groove. These grooves are filled with CdSe powder in 1 per cent ethyl cellulose binder. The output side of the device is a conventional plastic-embedded electroluminescent layer on a transparent conductive coating on a piece of glass. On top of the electroluminescent layer is an opaque nonconducting layer for preventing optical feedback. The photoconductive layer and electroluminescent layer are joined electrically by a dry conductive powder layer having the correct electrical properties. This layer is for the purpose of spreading the current from the photoconductive grooves so that the electroluminescent layer will not emit in lines. For this reason the layer has the special property of conducting fairly well transversely, but not so well laterally.

If this panel were operated in the conventional manner with a-c voltage applied between the conducting lines and the conductor under

the electroluminescent layer, the desired impedance relationship between the two layers would not be achieved, and satisfactory storage operation would be lacking. To avoid this difficulty, the storage action in the photoconductor can be largely isolated from the electroluminescent operation by means of the circuit connected to the panel.² The conducting lines at the tops of the ridges are connected alternately to two sides of the center-tapped transformer supply, V_1 . By this means it is possible to apply a high field across the photoconductor so that the storage action can occur in the photoconductor alone as in the simple test gap first described. Under these conditions no drop in voltage occurs when the photoconductor is triggered to the conducting condition. Although storage currents exist in the photoconductor after a picture is flashed on briefly, the result is not visible on the electro-

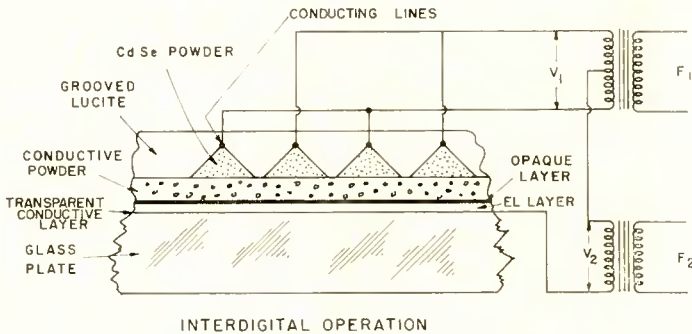


Fig. 5—Construction of image storage panel.

luminescent layer until an additional smaller voltage, V_2 , is added between the center tap of V_1 and the conductor under the electroluminescent layer. If V_2 is small compared with V_1 , the presence or absence of the electroluminescent output picture has little effect on the storage conditions in the photoconductor. This is due to the fact that only a fraction of the full storage current is used to produce the visible image. In addition to choosing suitable voltages V_1 and V_2 , the frequencies F_1 and F_2 can also be chosen for best or most convenient operation.

Typical operating characteristics for this type of storage panel are as follows: The voltage V_1 applied to the photoconductor in the grooves is 600 volts r-m-s at 60 cycles (F_1), while the voltage V_2 applied to the electroluminescent layer is 150 volts r-m-s at about 400 cycles (F_2).

² Application of voltage to alternate sets of lines is described in, "An Improved High-Gain Panel Light Amplifier," by B. Kazan, *Proc. I.R.E.*, Vol. 45, pp. 1358-1364, October, 1957.

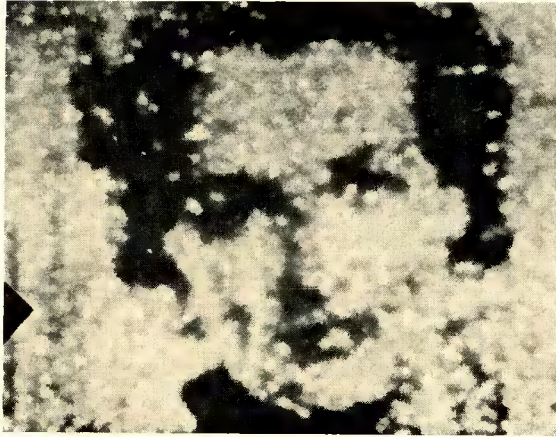


Fig. 6—Output image on 3-inch panel produced by short exposure to half-tone input image.

The choice of these frequencies must be such that no low-frequency beats occur, since they would cause fluctuations in the brightness of the output image.

Figures 6 and 7 show a photograph of two separate stored images on a 3-inch square panel made with the grooved structure and using the circuit and potentials just described. This panel structure has 60-degree grooves spaced 25 mils apart and should, therefore, be capable of 120-line resolution.

The stored image in each case was produced by a 1/100 second exposure to one foot-candle illumination with tungsten light. The storage panel is about ten times less sensitive than the photoconductive

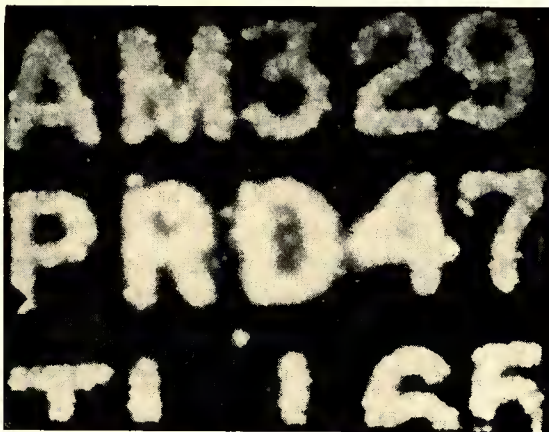


Fig. 7—Output image produced by short exposure to black and white input image.

powder alone. The output image has a luminance of about one foot-lambert. It can be erased by interrupting the photoconductor supply voltage, V_1 , for approximately 1/10 second. The output image can be varied in luminance from zero to one foot-lambert by varying the 400-cycle voltage, V_2 , across the electroluminescent layer from zero to 150 volts r-m-s. Over this range the storage action is unaffected. If this voltage is further increased to increase output brightness, the voltage drop across the photoconductor becomes sufficient to stop the storage action.

Theoretically, this device would be expected to give only a black-and-white picture, but there is some semblance of half-tones in the portrait. This can be explained as due to the presence of particles of various sensitivities throughout the photoconductive powder. The rather heterogeneous CdSe powder here used also accounts in part for the appearance of spots in the picture. In addition, some spots in the otherwise black background are caused by voltage triggering of some of the particles.

This panel can also be used as a conventional image intensifier by simply lowering or removing the voltage V_1 and raising V_2 . Under these conditions amplification without storage occurs. By means of a switch it is possible to change from simple image intensification to image storage.

This experimental panel was made to demonstrate the possibility of using the hysteresis effect in producing image storage devices without the complications of optical feedback. Further improvements in these panels will depend to a considerable extent on the finding of photoconductors having a more pronounced hysteresis and greater homogeneity throughout the powder.

ACKNOWLEDGMENT

The author would like to acknowledge the help of H. F. Ogawa in making many of the measurements. The continued interest of E. W. Herold and D. W. Epstein is also appreciated, and many helpful discussions were had with other members of the laboratory, particularly with B. Kazan, A. Rose, and P. K. Weimer. The CdSe used in these experiments was developed by L. A. Barton and S. M. Thomsen.

AN ELECTROSTATICALLY FOCUSED TRAVELING-WAVE-TUBE AMPLIFIER*

BY

K. K. N. CHANG

RCA Laboratories,
Princeton, N. J.

Summary—By applying the principle of biperiodic beam focusing a new traveling-wave tube, entirely electrostatically focused, has been achieved through the use of a pair of concentric bifilar helices and an annular gun. Design curves for choice of an optimum geometry of the tube for a given beam perveance using a minimum focusing field are given. Experimental d-c focusing results have agreed very well with theory. With a non-optimized gun, a beam of perveance 2×10^{-6} amp/volt^{3/2} has been focused to 97 per cent current transmission. An r-f gain of 10 decibels has been obtained at a power level of 100 milliwatts at 2,970 megacycles.

INTRODUCTION

SINCE the introduction of traveling-wave tubes, their use has been limited by the weight and inconvenience of the beam-focusing means which had to be used. During the last several years, work has been done attempting to reduce the weight or the size of the focusing mechanism by using either a periodic magnetic field or a periodic electrostatic field.¹⁻⁴ Although considerable success was achieved in these attempts, no tube was operated as an amplifier at a high power level without a magnet. It has been felt that any attached outside magnet, however small or light it may be, would add to the alignment problems. For commercial use, especially for airborne application, it would be convenient to have a traveling wave tube which is equipped with a "built-in," entirely electrostatic, focusing means.

* Manuscript received October 15, 1957.

¹ J. R. Pierce, "Spatially Alternating Magnetic Fields for Focusing Low Voltage Electron Beams," *Jour. Appl. Phys.*, Vol. 24, p. 1247, September, 1953.

² J. T. Mendel, C. F. Quate, and W. H. Yocum, "Electron Beam Focusing With Periodic Permanent Magnet Fields," *Proc. I.R.E.*, Vol. 42, p. 800, May, 1954.

³ P. K. Tien, "Focusing of a Long Cylindrical Electron Stream by Means of Periodic Electrostatic Fields," *Jour. Appl. Phys.*, Vol. 25, p. 1281, October, 1954.

⁴ K. K. N. Chang, "Confined Electron Flow in Periodic Electrostatic Fields of Very Short Periods," *Proc. I.R.E.*, Vol. 45, p. 66, January, 1957.

A built-in focusing technique has been described in a recent paper⁵ which analyzes a biperiodic electrostatic field recommended for high-current-density beam focusing. The present paper discusses an S-band traveling-wave tube which uses this biperiodic focusing principle. The tube has the following novel features:

- (1) an outer bifilar helix and an inner bifilar helix
- (2) an annular gun
- (3) a hollow cathode with a doughnut-shaped coiled heater
- (4) a unique quartz supporting structure which gives a self-contained alignment between the gun and the helices.

Direct-current tests have shown a current transmission of more than 97 per cent with a beam perveance in the order of 2×10^{-6} amp/volt^{3/2}. A 10-decibel gain has been observed at a frequency of 2,970 megacycles. These experiments show that a new traveling-wave tube, entirely electrostatically focused, has been achieved.

BEAM PERVEANCE

The beam perveance of a focused hollow electron beam in a biperiodic electrostatic field⁵ formed by an outer bifilar helix and an inner bifilar helix can be computed as follows.

The inward radial force, F_2 , acting on electrons at the radius, r , due to the periodic electrostatic field produced by the outer bifilar helix is

$$F_2 = \frac{2\pi\eta}{LV_0} C_1^2 \left[\frac{7}{4} I_1 \left(\frac{2\pi r}{L} \right) + \frac{1}{4} I_3 \left(\frac{2\pi r}{L} \right) \right] \times \left[\frac{1}{2} I_0 \left(\frac{2\pi r}{L} \right) + \frac{1}{2} I_2 \left(\frac{2\pi r}{L} \right) \right], \quad (1)$$

where

$$C_1 = \frac{4 \sin \pi\sigma}{\pi^2\sigma} \cdot V \cdot \frac{K_1 \left(\frac{2\pi r_2}{L} \right) - K_1 \left(\frac{2\pi r_1}{L} \right)}{I_1 \left(\frac{2\pi r_1}{L} \right) K_1 \left(\frac{2\pi r_2}{L} \right) - I_1 \left(\frac{2\pi r_2}{L} \right) K_1 \left(\frac{2\pi r_1}{L} \right)} \quad (2)$$

⁵ K. K. N. Chang, "Biperiodic Electrostatic Focusing for High-Density Electron Beams," *Proc. I.R.E.*, Vol. 45, p. 1522, November, 1957.

In this expression, I and K are modified Bessel functions, L is the period, V_0 is the average d-c potential on both the inner and outer helices, r_2 and r_1 are respectively the radii of the outer helix and the inner helix; $2V$, the potential difference between adjacent turns on both the outer bifilar helix and the inner bifilar helix; σ , the ratio of the spacing between bifilar helices to the period; and η , the ratio of electron charge to mass. Similarly, the outward radial force F_1 acting on electrons at the radius r due to the periodic electrostatic field produced by the inner bifilar helix is

$$F_1 = \frac{2\pi\eta}{LV_0} D_1^2 \left[\frac{7}{4} K_1 \left(\frac{2\pi r}{L} \right) + \frac{1}{4} K_3 \left(\frac{2\pi r}{L} \right) \right] \times \left[\frac{1}{2} K_0 \left(\frac{2\pi r}{L} \right) + \frac{1}{2} K_2 \left(\frac{2\pi r}{L} \right) \right], \quad (3)$$

where

$$D_1 = \frac{4 \sin \pi\sigma}{\pi^2\sigma} \cdot V \left[\frac{I_1 \left(\frac{2\pi r_1}{L} \right) - I_1 \left(\frac{2\pi r_2}{L} \right)}{I_1 \left(\frac{2\pi r_1}{L} \right) K_1 \left(\frac{2\pi r_2}{L} \right) - I_1 \left(\frac{2\pi r_2}{L} \right) K_1 \left(\frac{2\pi r_1}{L} \right)} \right] \quad (4)$$

The period L of the inner bifilar helix is assumed to be the same as that of the outer one. The space-charge force, F_s , for a hollow beam with radii r_0 and r_i has been computed⁵ as

$$F_s = - \frac{4\eta}{r} \frac{\rho}{2\epsilon_0} (r^2 - r_e^2), \quad (5)$$

where ρ is the space charge density, ϵ_0 is the dielectric constant and r_e is the equilibrium radius at which the space charge force is zero:

$$r_e^2 = \left[r_0^2 \ln \left(\frac{r_2}{r_0} \right)^2 + r_i^2 \ln \left(\frac{r_i}{r_1} \right)^2 + r_0^2 - r_i^2 \right] / \ln \left(\frac{r_2}{r_1} \right)^2 \quad (6)$$

The force balance is accomplished at $r = r_e$; i.e.,

$$F_s(r_e) + F_1(r_e) + F_2(r_e) = 0. \quad (7)$$

Since by Equation (5), $F_x(r_e) = 0$, it follows that

$$F_1(r_e) + F_2(r_e) = 0. \tag{8}$$

That is,

$$\left[\frac{I_1\left(\frac{2\pi r_1}{L}\right) - I_1\left(\frac{2\pi r_2}{L}\right)}{K_1\left(\frac{2\pi r_2}{L}\right) - K_1\left(\frac{2\pi r_1}{L}\right)} \right]^2 =$$

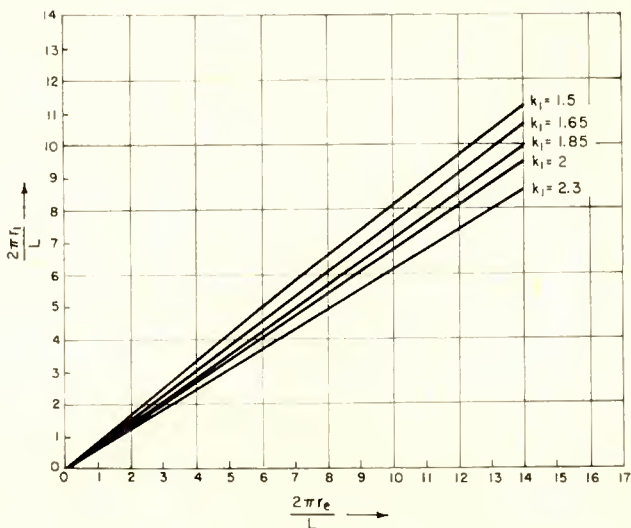


Fig. 1—The ratio of the inner helix radius to the period versus the ratio of the equilibrium radius to the period.

$$\left[7I_1\left(\frac{2\pi r_c}{L}\right) + I_3\left(\frac{2\pi r_c}{L}\right) \right] \left[I_0\left(\frac{2\pi r_c}{L}\right) + I_2\left(\frac{2\pi r_c}{L}\right) \right] \\ \left[7K_1\left(\frac{2\pi r_c}{L}\right) + K_3\left(\frac{2\pi r_c}{L}\right) \right] \left[K_0\left(\frac{2\pi r_c}{L}\right) + K_2\left(\frac{2\pi r_c}{L}\right) \right] \tag{9}$$

Equation (9) is a transcendental equation, and r_1 is solved for in terms of r_c with the aid of a computer. The results are plotted as Figure 1, with various values of the ratio $K = r_2/r_1$. The curves shown enable the designer to choose the geometry of the helices once the equilibrium radius is given.

Equation (9) gives one relation between r_1 , r_2 and r_e . Hence r_1 and r_2 are not uniquely defined. A second relation between these variables may be obtained by balancing the forces at a second radius perturbed around r_e in the beam. Then it becomes possible to determine r_1 and r_2 independently in terms of r_e , the beam perveance and the voltage between adjacent wires of the bifilar helices. The second relation is obtained as follows:

Expand F_1 , F_2 and F_s around r_e by writing

$$r = r_e + \hat{r} \quad \hat{r} \ll r_e \quad (10)$$

$$\begin{aligned} F_1(r) &= F_1(r_e) + F_1'(r_e) \hat{r} \\ F_2(r) &= F_2(r_e) + F_2'(r_e) \hat{r} \\ F_s(r) &= F_s(r_e) + F_s'(r_e) \hat{r}. \end{aligned} \quad (11)$$

The force balance then occurs in a first-order approximation if

$$F_1'(r_e) + F_2'(r_e) + F_s'(r_e) = 0. \quad (12)$$

It then follows from Equation (12) that

$$\begin{aligned} \left(\frac{V}{V_0} \right)^2 \left(\frac{4 \sin \sigma \pi}{\sigma \pi^2} \right)^2 \left(\frac{2\pi r_e}{L} \right)^2 \left[\ln \left(\frac{r_2}{r_1} \right)^2 - \frac{r_0^2}{r_e^2} \ln \left(\frac{r_2}{r_0} \right)^2 \right. \\ \left. - \frac{r_i^2}{r_e^2} \ln \left(\frac{r_i}{r_1} \right)^2 \right] \\ \left[\frac{K_1 \left(\frac{2\pi r_2}{L} \right) - K_1 \left(\frac{2\pi r_1}{L} \right)}{I_1 \left(\frac{2\pi r_1}{L} \right) K_1 \left(\frac{2\pi r_2}{L} \right) - I_1 \left(\frac{2\pi r_2}{L} \right) K_1 \left(\frac{2\pi r_1}{L} \right)} \right]^2 f_t(r_e) \\ = \frac{4P}{\pi \epsilon_0 \sqrt{2\eta}}. \end{aligned} \quad (13)$$

where P is the beam perveance defined as beam current/(beam voltage)^{3/2} and

$$f_t(r_e) = \frac{1}{16} [7I_1 + I_3] [3I_1 + I_3] + \left[\frac{7}{8} I_0 + I_2 + \frac{1}{8} I_4 \right] \left[\frac{I_0 + I_2}{2} \right]$$

$$\begin{aligned}
 &+ \left[\frac{7I_1 + I_3}{7K_1 + K_3} \right] \left[\frac{I_0 + I_2}{K_0 + K_2} \right] \left\{ \frac{1}{16} (7K_1 + K_3) (3K_1 + K_3) + \left(\frac{7}{8} K_0 \right. \right. \\
 &\quad \left. \left. + K_2 + \frac{1}{8} K_4 \right) \left(\frac{K_0 + K_2}{2} \right) \right\}. \tag{14}
 \end{aligned}$$

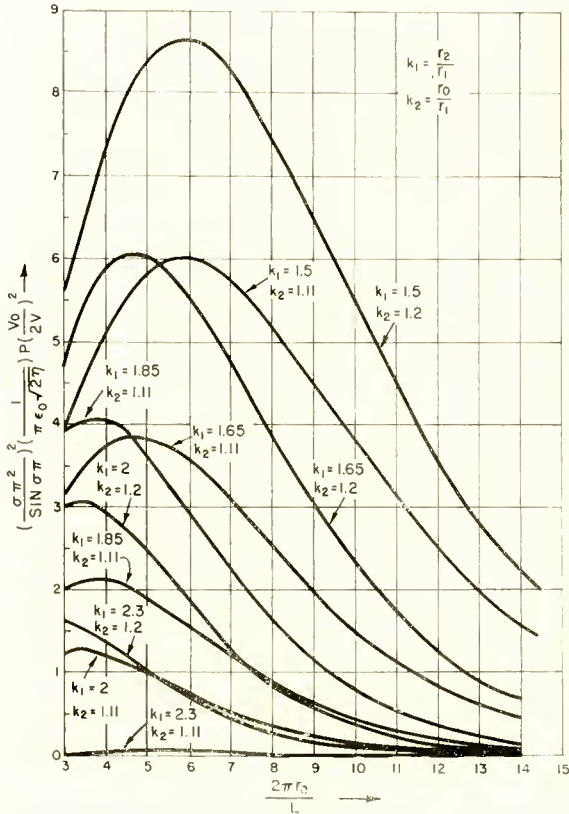


Fig. 2—Beam perveance as a function of percentage voltage variation, equilibrium radius, helix radii, and beam radii.

The arguments of all Bessel functions I and K in Equation (14) are $2\pi r_0/L$. The ratio $2\pi r_0/L$ appearing in Equation (13) is plotted versus $P/(2V/V_0)^2$ in Figure 2 by assuming the ratio of the outer helix diameter to the outer beam radius, r_2/r_0 , to be 1.25 and by assigning the ratio of the outer beam radius to the inner beam radius, r_0/r_1 , at the two values, 1.11 and 1.2. It is indicated by the peaked curves in Figure 2 that an optimum geometry exists with a maximum perveance

and a minimum focusing field. Those geometries larger than the optimum produce stronger outside stray fields and thus result in small perveances and large focusing fields. The curves shown in Figure 2 will help the designer find the potential parameter from a given value of the beam perveance. For example, for the particular value $2\pi r_o/L$ equals 9.0, which was chosen for the experimental tube to be discussed ($r_o/r_i = 1.75$, $r_o/r_i = 1.11$), the relationship between P and $2V/V_o$ is shown by the solid curve in Figure 5.

FIELD EQUATION IN THE ELECTRON BEAM

Rigrod and Lewis⁶ arrived at the conclusion that wave propagation along a cylindrical beam with Brillouin flow is accompanied by swelling and contracting of its boundary, with *constant* space-charge density, rather than by space-charge bunching. Another interesting result they found is that the dynamics and field equations for the focussed beam are identical with those for a beam with zero d-c magnetic field, except for the angular component of a surface current density. This angular surface current density is formed because the beam has been focused by a Brillouin magnetic field. If the beam were focused by a pure electrostatic field such that no electron rotation is involved, there would not be any angular surface current density. This situation is realized by the use of the present biperiodic electrostatic focusing. It is of interest to investigate the r-f field which would appear on a beam which has been focussed by the biperiodic electrostatic field. The equations of motion of electrons in a biperiodic electrostatic field in cylindrical coordinates (r , ϕ , z) are as follows:

$$\ddot{r} = \eta \frac{\partial V}{\partial r} - \eta E_r + \frac{\eta \rho}{2r\epsilon_0} (r^2 - r_o^2), \quad (15)$$

$$r \ddot{\phi} + 2 \dot{r} \dot{\phi} = 0, \quad (16)$$

$$\ddot{z} = \eta \frac{\partial V}{\partial z} - \eta E_z, \quad (17)$$

where V is the d-c potential, E_r and E_z are, respectively, the r-f radial field and the r-f axial field.

⁶ W. W. Rigrod and J. A. Lewis, "Wave Propagation Along a Magnetically-Focused Cylindrical Electron Beam," *Bell Sys. Tech. Jour.*, Vol. 33, March, 1954.

In a biperiodic field, where the beam is perturbed by a small d-c periodic field and is also modulated by a small a-c signal, the electron coordinates are found to be as follows:^{4,6}

$$r = r_0 + \hat{r} \cos \left(\frac{2\pi}{L} z \right) + \tilde{r}(r_0) e^{j[\omega t - \gamma(z_0 + \mu_0 t)]}, \quad (18)$$

$$\theta = 0, \quad (19)$$

$$z = z_0 + \mu_0 t + \hat{z} \sin \left(\frac{2\pi}{L} z \right) + \tilde{z}(r_0) e^{j[\omega t - \gamma(z_0 + \mu_0 t)]}, \quad (20)$$

where peaks indicate perturbations due to the d-c field and tildes indicate modulations due to r-f field. ω is the angular frequency; γ is the propagation constant; $(r_0, 0, z_0)$ is the initial position of an electron in question, with an axial d-c velocity μ_0 .

Since the space-charge field is cancelled to the first approximation by the average biperiodic electrostatic field according to Equation (12), the a-c space-charge density, $\tilde{\rho}$, is equal to zero exactly as in the Brillouin flow case which was calculated by Rigrod and Lewis. Omitting the factor $e^{j[\omega t - \gamma(z_0 + \mu_0 t)]}$ for brevity from all a-c terms, Equations (15) and (17) can be rewritten as follows:

$$\ddot{\tilde{r}} = -\eta E_r, \quad (21)$$

$$\ddot{\tilde{z}} = -\eta E_z. \quad (22)$$

After replacing the time derivatives by multiplication by $j(\omega - \gamma\mu_0)$, these become

$$\tilde{r} = \eta E_r / (\omega - \gamma\mu_0)^2, \quad (23)$$

$$\tilde{z} = \eta E_z / (\omega - \gamma\mu_0)^2. \quad (24)$$

These are exactly the same results which have been obtained for the Brillouin flow case. Essentially, all the field equations and the r-f performance associated with them are identical with those derived for the Brillouin flow case. The only difference is that in the present case the electron beam is focussed by a biperiodic electrostatic field instead of by a magnetic field and thus no electron rotation takes place.

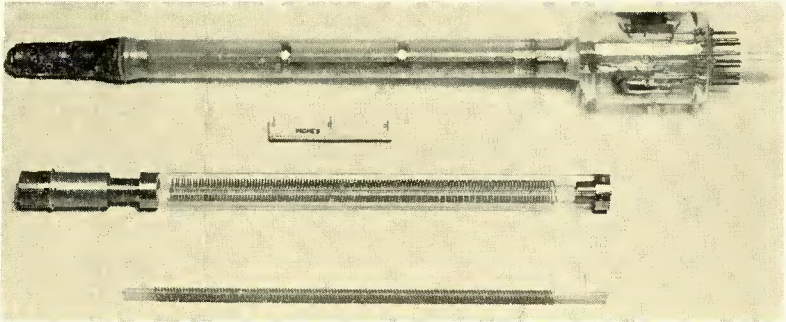


Fig. 3—The experimental tube.

EXPERIMENTAL RESULTS

An experimental traveling-wave tube shown in Figure 3 was built for testing the focusing performance and the r-f performance. The tube uses an inner bifilar helix, an outer bifilar helix and an annular electron gun. Figure 4 is a sketch of the tube assembly. The outer bifilar helix is wound with .020-inch tungsten wire on a mean diameter of .380 inch and a pitch of 10 turns per inch. To eliminate all possible undesirable r-f interaction with the inner bifilar helix, the inner helices are wound with .020-inch resistance wire on a mean diameter of .200 inch and 10 turns per inch. As shown by Figure 4, the alignment

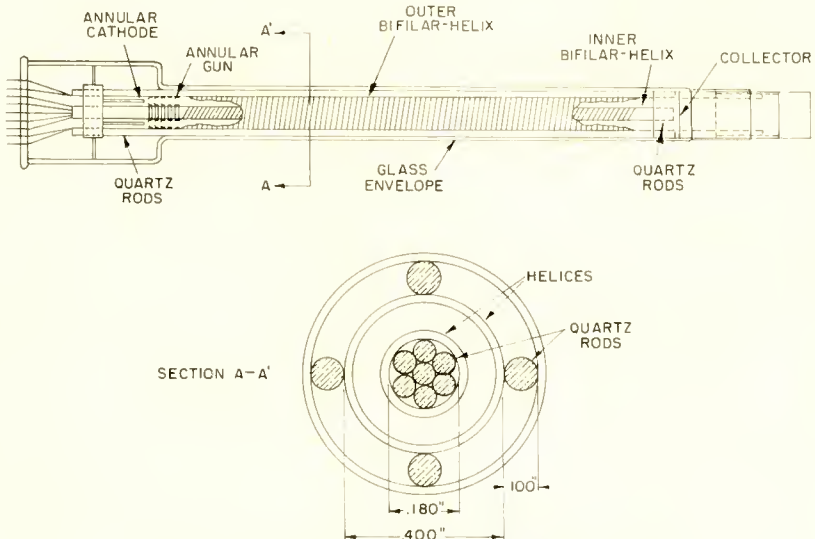


Fig. 4—Assembly of the experimental tube.

between the gun and the helices is uniquely determined by a set of precision quartz rods.

The tube was tested first for its focusing performance. The results obtained are tabulated in Table I.

Table I—Experimental Results

D-C Performance	
Average helix voltage	200 volts
Bifilar helix voltage	100 volts, 300 volts
Collector current	4 milliamperes
Helix-intercepted current	less than .11 milliampere
Current transmission	97%
R-F Performance	
Frequency	2,970 megacycles
Synchronizing voltage	1,850 volts
Gain	10 decibels
Output power	100 milliwatts

The current-transmission is more than 97 per cent with a beam perveance of the order of 2×10^{-6} amp/volt^{3/2} if the current intercepted in the gun is ignored. The observed focussed beam perveance agrees in general very well with the theoretical curve shown by Figure 5. The interception in the gun causes no surprise since the construction of the gun was not optimum.

Measurements made at r-f are very encouraging. A 10-decibel net gain has been observed at an output power of 100 milliwatts and a frequency of 2,970 megacycles with a beam current of 1.3 milliamperes. The r-f synchronizing helix voltage was found to be 1,850 volts. The measured gain figure is somewhat higher than that which corresponds to a confined flow case. This agrees with the result of Rigrod and Lewis, presumably because of transverse electron motion in the present Brillouin case.

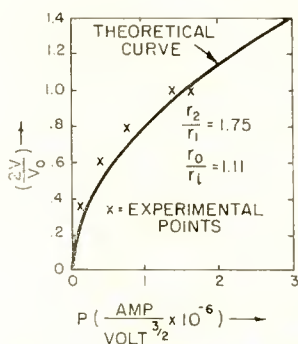


Fig. 5—Percentage voltage variation versus perveance for the experimental tube.

Because of the large diameter of the present tube envelope, the coupling and attenuation could not be optimized. Hence, the above results are considered particularly promising.

The experimental setup for measurement is shown in Figure 6. Since the tube is entirely electrostatically focused, it can be mounted vertically, as shown, on the chassis just as are conventional low-frequency tubes. All of the r-f testing equipment is on the left and the power-supply units are on the right.

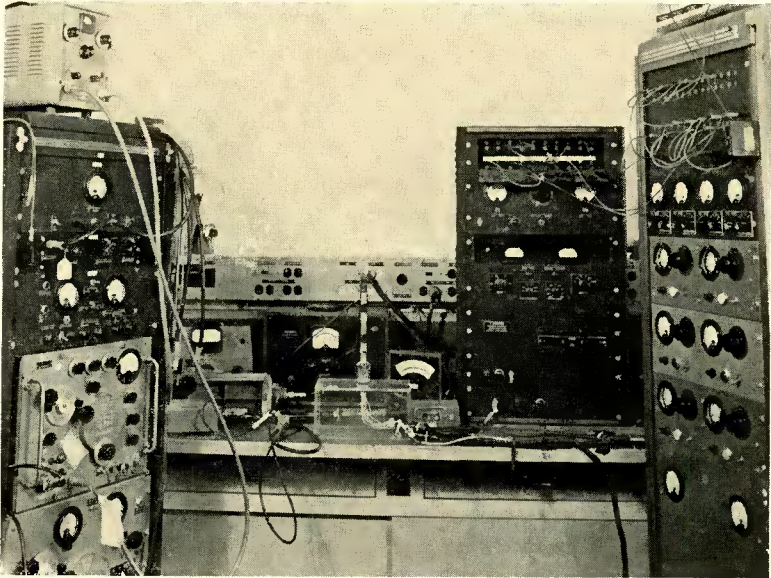


Fig. 6—Experimental setup.

CONCLUSION

A new traveling-wave tube, entirely electrostatically focused, has been achieved through the use of a pair of concentric bifilar helices and an annular gun.

Design curves for optimum geometries of the tube for a given perveance using a minimum focusing field are given. Experimental d-c focusing results have checked the theoretically calculated results very well. With a periodic voltage variation of 5 per cent on the beam, it is theoretically possible to focus, with an ideal gun, an electron beam of perveance in the order of 10^{-5} amp/volt^{3/2}. With a non-optimized gun, a beam of perveance 2×10^{-6} amp/volt^{3/2} has been focused to a 97 per cent current transmission.

Preliminary r-f tests are encouraging. A gain of 10 decibels has been obtained at a power level of 100 milliwatts and at 2,970 megacycles.

ACKNOWLEDGMENT

The author wishes to give credit to R. E. Chamberlain for construction of the tube and to R. D. Hughes for assistance in the tube design and the experimental setup. He also wishes to thank the Computing Laboratory, particularly F. Edelman, for programming and computing the design curves.

LARGE-AREA GERMANIUM POWER TRANSISTORS*

BY

B. N. SLADE[†] AND JANE PRINTON[‡]

Summary—Both p-n-p and n-p-n experimental alloy-junction power transistors have been developed to operate at collector currents of 10 amperes or more. Depending on design factors (polarity, low or high voltage operation), collector-to-base current ratios range up to 200 at 1 ampere and to 60 at 10 amperes. Thermal resistances are about 1 to 2°C per watt. The extension of the operating current range by an order of magnitude has been accomplished by increasing the junction area (0.24-inch diameter). Base-lead resistance is reduced by a factor of 6 by the use of ring emitters with axial and co-axial base contacts. Due to the transverse field developed in the base, wide variations (16 to 1) in the collector-to-base current ratios result from the use of the different base contacts (axial or co-axial contact) alone.

Diffusion techniques were applied to an alloy-emitter-diffused-collector transistor. This construction combines the high injection efficiency of an alloy emitter with the advantages of the diffusion techniques to obtain a uniformly flat large-area collector of controlled penetration.

Early work reported here has given results comparable to alloy-junction transistors of similar geometry. The diffusion technique has also been applied to obtain a reduction in the base-lead resistance by a factor of 3 through the diffusion of a heavily doped layer in the base wafer before alloying.

INTRODUCTION

THE extension of the high-current performance of alloy-junction transistors through the use of high-emitter-efficiency alloys, and the design of high-current and high-voltage power transistors have been discussed previously.^{1,2} The purpose of this paper is to discuss work leading to further extension of the high-current and power performance of p-n-p and n-p-n germanium power transistors. This performance has been obtained principally through an increase in junction area, but also through the application of improved alloying and diffusion techniques. Three types of power transistors are dis-

* Manuscript received January 10, 1958.

[†] Formerly, RCA Laboratories, Princeton, N. J.; now with International Business Machines, Poughkeepsie, N. Y.

[‡] Formerly, RCA Semiconductor Division, Somerville, N. J.

¹ L. D. Armstrong, C. L. Carlson and M. Bentivegna, "P-N-P Transistors Using High-Emitter-Efficiency Alloy Materials," *Transistors I*, RCA Laboratories, Princeton, N. J., 1956, p. 144.

² B. N. Slade, "Recent Developments in Power Transistors," *Transistors I*, RCA Laboratories, Princeton, N. J., 1956, p. 150.

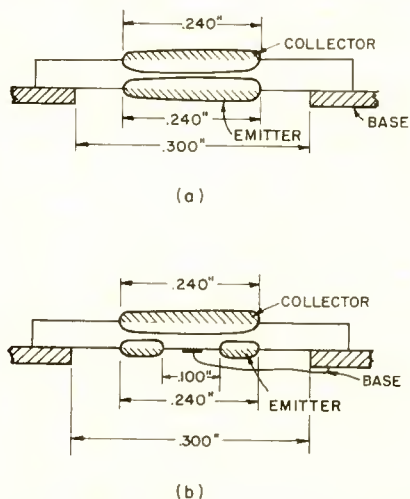


Fig. 1—Cross sections of large-area power transistors.

cussed. The first two types are p-n-p and n-p-n large-area alloy-junction transistors; the third type is a hybrid construction consisting of an alloy emitter and a collector formed by diffusion from a vapor. Supplementary techniques for the reduction of base-lead resistance are also described.

P-N-P AND N-P-N ALLOY JUNCTION POWER TRANSISTORS

Construction

Figure 1 shows cross-sectional diagrams of two junction geometries used for experimental p-n-p and n-p-n transistors. Significant differences between the solid and ring emitter constructions will be discussed.

Figure 2 shows a photograph of a cross section of a large-area p-n-p transistor of the type shown schematically in Figure 1a. The mechanical design features have been described elsewhere² but are shown for reference in Figure 3. The high-emitter-efficiency alloys described earlier^{1,2} are used in the present transistors.

High-Current Performance

At high currents the collector-to-base current transfer ratio de-



Fig. 2—Cross section of large-area power transistors.

pends primarily on the injection efficiency of the emitter which in turn varies inversely as the current density.³ Hence, good injection efficiency at high currents may be obtained by increasing the emitter area in order to decrease current densities. The achievement of improved operation at higher currents through an increase in junction area can be seen in the curves of Figures 4a and 4b. Here the collector-to-base

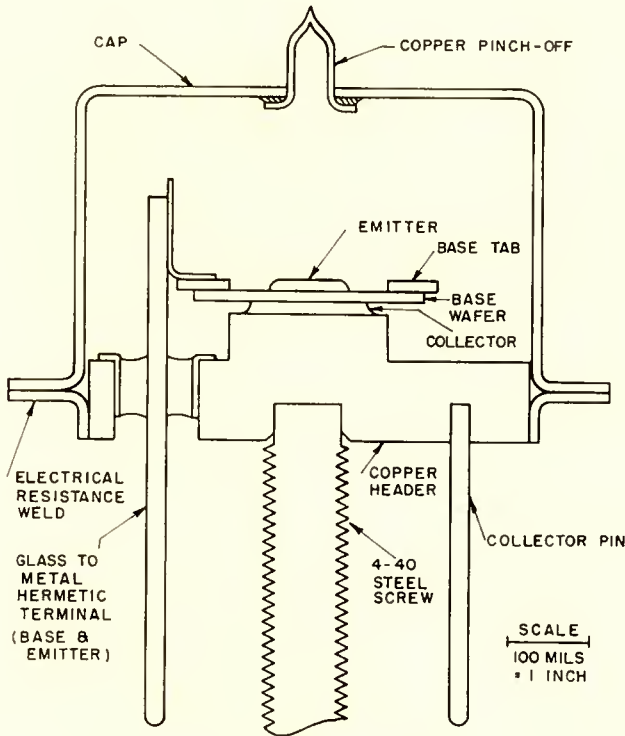


Fig. 3—Power transistor.

current transfer ratio (d-c alpha) is plotted as a function of emitter current for p-n-p and n-p-n transistors. The data compare the performance of transistors having a solid 0.060-inch diameter emitter with units having a ring emitter of 0.100- and 0.240-inch inner and outer diameters, respectively. The emitter areas are in the ratio of 1 to 15. The smaller area solid-emitter transistors are those described in Reference (2). The collector diameter of the large area units is

³ W. M. Webster, "On the Variation of Junction Transistor Current Amplification Factor with Emitter Current," *Proc. I.R.E.*, Vol. 41, p. 914, June, 1954.

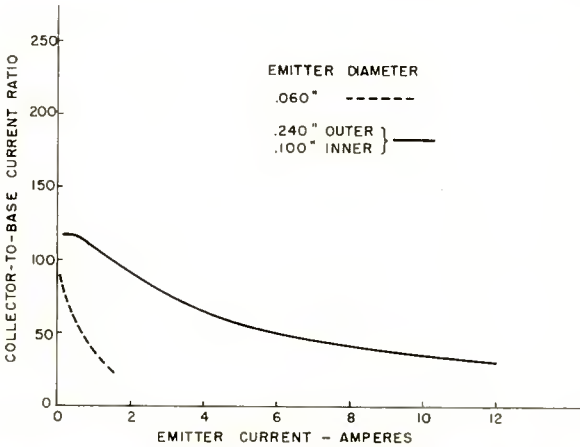


Fig. 4a—Collector-to-base current ratio versus emitter current for p-n-p transistors.

0.240-inch. The curves of Figure 4a and 4b show that the larger-area transistors are capable of operation with high gain at currents of 10 amperes or more.

Table I shows other electrical characteristics of the p-n-p and n-p-n large-area transistors. Although the large-area junctions present additional wetting and etching problems in fabrication, the data indicate that the techniques used permit the fabrication of these junctions with essentially no degradation in the reverse junction characteristic as compared with that obtained on smaller power transistors.²

The n-p-n and the p-n-p high-voltage types designated in Table I use germanium of the same resistivity and have similar spacing be-

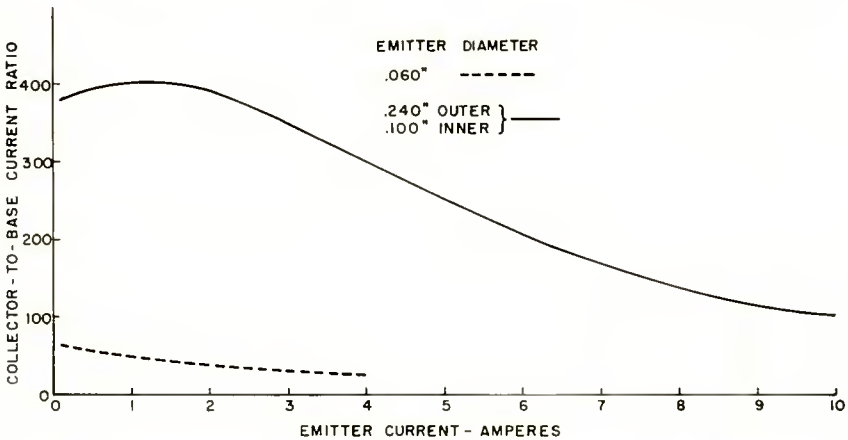


Fig. 4b—Collector-to-base current ratio versus emitter current for n-p-n transistors.

tween junctions. The p-n-p low-voltage type has been modified for higher current operation. Closer junction spacings (about 2.8 mils) than those listed in the table have resulted in n-p-n units with 1-ampere current ratios ranging from 200 to 500. A few units have been made with values as high as 1,000.

Thermal Resistance

The increase in junction area also decreases the thermal resistance between the collector junction and the copper mounting stud (Figure 3). The p-n-p transistors have a thermal resistance of approximately 2 to 2.6°C per watt. Most of this thermal resistance occurs in the indium collector dot which is approximately 0.240-inch diameter and 0.010-inch thick. The n-p-n type has a thermal resistance ranging from about 1.8 to 2.1°C per watt. This lower value results from the higher

Table I — Electrical Characteristics* of P-N-P and N-P-N Large-Area Transistors

Type	Ge base material Resistivity ohm-cm	W (mils)	Collector Current with zero emitter current (μ a)		Breakdown Voltage	Collector-to-base Current Transfer Ratio	
			-1v	-25v		$I_c = 1$ amp	$I_c = 10$ amps
P-N-P high volt.	4-6	3.3	30	50	125	45	15
P-N-P low volt.	2-3	2.5	18	65	60	80	30
N-P-N	4.6	3.3	80	120	80	200	60

* Average values.

thermal conductivity of the lead-arsenic collector alloy used in the n-p-n transistor.

A considerable reduction in the thermal resistance of the p-n-p transistor has been achieved by removing approximately $\frac{3}{4}$ of the indium collector dot before soldering to the copper stud. Thermal resistance measurements on these transistors range from 0.8 to 1.30°C per watt.

Base-Lead Resistance

The base-lead resistance ($r_{bb'}$) at high currents can be reduced considerably by reducing the extrinsic portion which exists between the junction edges and the base connection. This resistance remains relatively constant at high currents while the intrinsic base resistance which exists between the junctions decreases to a very small value due to conductivity modulation. The geometry shown in Figure 1b offers a method of reducing the base-lead resistance by paralleling two ex-

trinsic lead-resistance components, namely, that existing between the outer base ring and the outer edge of the emitter and the component between the edge of the inside base dot and the inner diameter of the emitter ring. A comparison of the base-lead resistance for the solid and ring emitter constructions of Figure 1a and 1b for transistors having the same values of junction spacing and germanium resistivities can be seen in Figure 5, in which I_{base} versus V_{base} is plotted. The values of $r_{bb'}$ at emitter currents of 1 ampere, computed from the

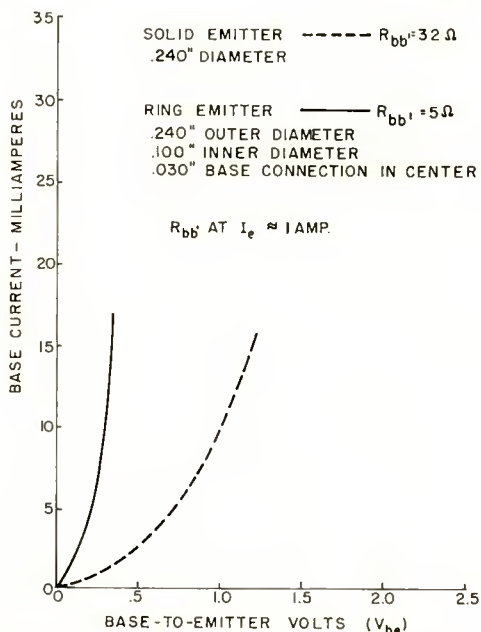


Fig. 5—Input characteristic of p-n-p power transistor with solid and ring emitters.

slope of the curve, are approximately 32 ohms for the solid emitter and 5 ohms for the ring-emitter geometry.

Figure 6 illustrates a second technique for reducing the base-lead resistance. This technique has been applied only to the p-n-p type, but, in principle, should also be useful for n-p-n transistors. In this method, a high-conductivity n-type layer is diffused onto the conventional n-type pellets used for power transistors. The diffusion process is carried out in an antimony vapor and results in a layer of approximately 0.0005-inch thickness. Figure 6a shows the pellet cross section after diffusion. Emitter and collector dots of Ga-In-Au are then alloyed through the n layer as shown in Figure 6b. The base ring contact is fired on

during or subsequent to the alloying process. Finally, the emitter and collector junctions are electrolytically etched to form a groove around the junctions to isolate the n layer from the p-type recrystallized region, thus preserving the breakdown voltages normally obtained with the base germanium used. An alternate technique is to remove the n layer from the collector side before alloying.

Figure 6c shows the final geometry of the transistor. Since the conductivity of the diffused layer near the surface is very high, the base contact has been effectively moved much closer to the emitter region, thus reducing the extrinsic base-lead resistance. The effectiveness of such a process is illustrated in Table II which gives values of $r_{bb'}$ at 1 milliampere and 1 ampere for a transistor processed in the

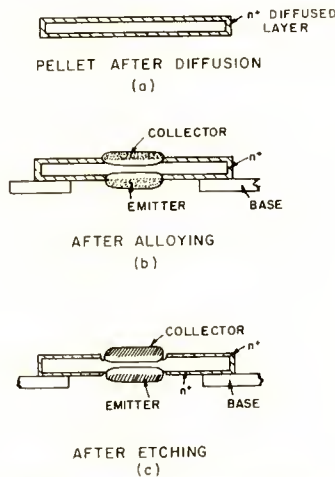


Fig. 6—Method of reducing base-lead resistance.

above manner. These values are compared with values measured after the diffused layer has been etched away. A substantial increase in the extrinsic value of base resistance has occurred even though the cross-sectional area of the base region was not substantially changed by the light etching used to remove the diffused layer.

This technique was applied to a transistor employing a 0.100-inch diameter emitter, a base ring having an inside diameter of 0.200-inch, and a germanium resistivity of 4-6 ohm-centimeters. The average value of $r_{bb'}$ at 1 ampere for units without the diffused layer was 50 ohms. For units using the prediffused pellets the average value was about 20 ohms. This process might be expected to show a comparable improvement in $r_{bb'}$ on transistors having other geometries and resistivities. Other characteristics such as junction leakage, breakdown and

Table II — Effectiveness of a Diffused Layer for Reducing the Base-Lead Resistance

Emitter Current	Base Lead Resistance with Diffused Layer	Base Lead Resistance after Removal of Diffused Layer
1 ma.	80	112
1 ampere	16	50

current transfer ratio are not significantly affected by this process. However, extreme care must be taken in etching to preserve the thin diffused layer on the emitter side.

Effect of Location of Base Contact

Interesting observations have been made on the effect of the location of the base contact on operation of the transistor shown in Figure 1b.

Figures 7a, 7b, and 7c show three configurations of large-area power transistors, (a) with a solid emitter (similar to Figure 1a), (b) with a ring emitter, and (c) a ring emitter with an inside base connection in addition to the outside ring base contact as in Figure 1b. If the two bases in Figure 7c are not connected together, the high-current performance obtained with each base connection differs considerably.

Table III shows the dependence of the one-ampere collector-to-base current transfer ratio upon the location of the base contact.

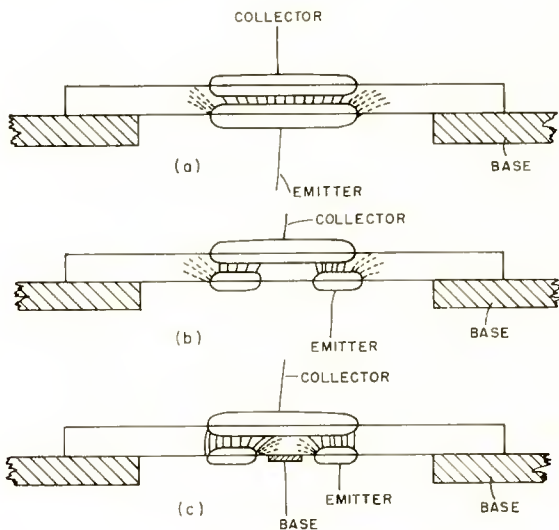


Fig. 7—Cross section of large-area power transistor with different base connections

This phenomenon may be explained as follows. In high-current transistor operation, there is a transverse electric field (parallel to junction plane) in the base region due to the base current and resistance. This field is sufficiently strong and in such a direction as to cause minority carriers injected at the edge of the junction to acquire a drift component towards the base contact. These deflected carriers do not reach the collector and are lost by recombination. For instance, in the case of the n-p-n transistor, the base is positive with respect to the emitter, thus pulling the electron minority carriers toward it. The dotted lines in Figure 7a represent the flow paths of the current having a component toward the base contact while the solid lines represent the diffusion current toward the collector. Now, if the center portion of the emitter in Figure 7a is removed as in 7b, two factors tend to cause a decrease in gain. First, the current density is increased for a given current. Second, much of the minority carrier flow leaving the emitter will occur around the periphery of the junctions increasing the effective spacing between junctions. If, however, a base contact is placed inside the emitter ring, as in Figure 7c, the transverse electric field in the

Table III — Collector-to-Base Current Transfer Ratios for Different Base Connections

<u>Outside Base Only</u>	<u>Inside Base Only</u>	<u>Bases Tied Together</u>
6	100	80

base will be in such a direction to pull the current carriers inward toward the center; thus few carriers are lost around the edges. With the two base connections tied together, an intermediate condition is obtained as indicated by the data of Table III.

According to this explanation, the small-signal current-transfer ratio at low currents, should be independent of the base-contact position since, at low currents, the electric field in the base region will be very small. Measurements confirm this expectation; the current transfer ratio at 1 milliamperes is approximately the same regardless of the base connection used. This phenomenon does not occur if the collector is larger than the emitter since the larger collector would catch most of the carriers leaving the emitter. Measurements on transistors having a 0.240-inch diameter collector and a emitter of 0.150-inch outer diameter show no difference in current-transfer ratios between the inner and the outer base connections.

ALLOYED-EMITTER, DIFFUSED-COLLECTOR TRANSISTOR

A combination of the techniques of alloying and diffusion in the vapor phase has also been used to fabricate power transistors. Solid-

state diffusion offers important advantages in making large-area n-p-n power transistors. First, the technique lends itself well to the formation of large-area flat junctions, and to the close control of junction penetration and spacing between junctions. Secondly, it makes possible the elimination of the indium or lead alloy which is the largest source of thermal resistance between the collector junction and the heat sink in the alloy-junction units. Lower thermal resistances should lead to higher allowable dissipation.

In the case of the emitter junction, the results of the alloy transistors just described demonstrate the high values of injection efficiency obtained with the use of a lead-arsenic alloy. By combining the advantages of an alloyed junction for the emitter with the advantages of the diffused collector, a transistor of improved characteristics may be expected.

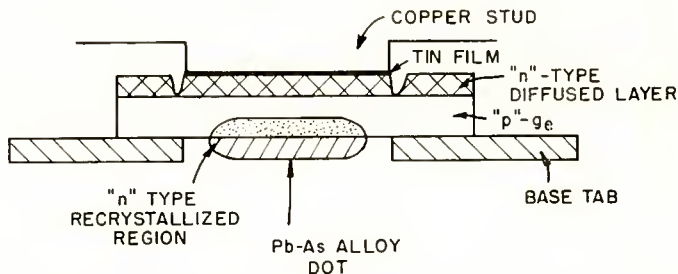


Fig. 8—Cross section of alloy emitter, diffused-collector power transistor.

Figure 8 shows a cross-sectional diagram of an n-p-n transistor of such construction. The emitter is formed by alloying a 0.060-inch diameter Pb-As dot. The collector is formed by diffusion in antimony vapor. The depth of diffusion is about 1.5 mils. A 0.100-inch diameter tin dot serves as the solder between the diffused surface and the copper mounting stud. Electrolytically etching a groove around the dot through the diffused layer serves to define the periphery of the collector. Table IV shows characteristics of these transistors for base materials of two different resistivities. Experience so far indicates that higher breakdown voltages can be achieved with diffused junctions than are obtained with alloyed junctions of the same size using the same germanium resistivity. The high-current transfer characteristics are comparable with those of n-p-n alloyed units of similar geometry described in Reference (2). This is to be expected since this characteristic is primarily determined by the injection efficiency of the emitter.

Table IV — Characteristics of Alloy-Emitter Diffused-Collector Transistors

Ge.	Sat. currents (μa)		Reverse Junction Currents (μa) (+25v)		Breakdown Voltage		Collector-to-Base Current Trans. Ratio	
	ohm-cm	Emitter	Collector	Emitter	Collector	Emitter	Collector	100 ma. 1 amp.
1.8	14	25	40	35	60	100	70	60
5	50	60	100	100	80	130	80	60

A few transistors of this type made with a ring emitter geometry (0.240-inch outer and 0.100-inch inner diameters) and 0.240-inch diameter diffused collectors had current ratios of 100 to 500 at 1 ampere.

CONSIDERATIONS AFFECTING THE RISE AND DECAY OF CATHODE CURRENTS IN RECEIVING TUBES*

By

EDWARD R. SCHRADER

RCA Electron Tube Division,
Harrison, N. J.

Summary—Curves showing the rise and decay of cathode current resulting from the application and removal of heater power in receiving tubes are analyzed to determine the dependence of these curves upon various tube properties. In the case of diodes and some multi-electrode tubes, changes in cathode activation appear as shifts of the temperature-limited region of the curves and sometimes as transient changes in the space-charge-limited region. Because of its inception from equilibrium current conditions, cathode current decay is a somewhat more reproducible quantity than rise current. Also, since most cathodes take longer to cool than to heat, the time for decay is usually longer than for rise, permitting better resolution of any differences between tubes.

Experiments with a diode having a rotating anode are used to illustrate the effects of cathode poisoning and reactivation. The results of rise-time measurements made during life tests are summarized. Because of the trend toward the use of "operation time" as a specification for certain tube types, there is given an analysis of the increase of cathode temperature with time in which energy transfer by radiation alone is assumed.

INTRODUCTION

THIS paper presents the results of an investigation conducted to determine the factors which affect the cathode current of electron tubes from the instant heater power is applied, through equilibrium, to the time the cathode is cool. The investigation was prompted by several considerations, including (a) the necessity for tight control of warm-up time of series-string tubes to prevent development of excessive voltage across a given tube;¹ (b) reduction of the warm-up time of television picture tubes to minimize delay in the appearance of the picture; (c) military requirements that tubes of certain types reach operating condition within specified times after application of heater power. The data presented should be of value in the design of tubes where some time quantity for transient currents is specified.

In this paper the terms "rise" and "decay" are used to describe

* Manuscript received January 9, 1958.

¹ R. L. Pear and A. Szilasi, "The Effect of Heater Coating Thickness on Warm-Up Time," *Electronic Design*, Vol. 3, September, 1955.

the transient cathode or plate currents which result, respectively, from the application and removal of heater power, and the term "warm-up" is used only to describe the variation in cathode temperature resulting from the application of heater power. The term "operation time" represents the time in seconds required for the plate or cathode current of a tube to reach a specified percentage of its value after several minutes.

When power is applied to the heater of an electron tube, the temperature of each element of the tube, from the heater out, begins to increase. If all electrodes of the tube are fixed at normal operating potentials, the increase in the temperature of the cathode results first in temperature-limited and then in space-charge-limited currents. As other parts of the tube get hot, they may release adsorbed gases which react with and poison the cathode; also, the resistances of semiconducting films which may be present on some electrodes will vary to a degree determined by their states of activation and temperatures. The behavior of the cathode current of a tube as a function of time is the resultant of all of these factors. Since the effects of poisoning and semiconductor resistances vary with the relative contamination of the tube parts and the tube geometry, they do not always affect the same portion of the cathode-current curve. Consequently, a cathode-current curve cannot be completely specified by a single number, such as "operation time." Expression of cathode-current rise time as a single number, however, still is useful as an indication of the departure of a particular tube from a statistical norm, even though it may not be a true indication of tube quality.

Most of the rise and decay data presented in this paper were obtained with the aid of a Brown recorder, using as a signal source the voltage developed across a small resistance in the plate or cathode circuit of the tube under test. All tests were conducted using fixed electrode potentials, including grid bias. Heater power was obtained from a regulated direct-current supply. The resulting curves of cathode current make it possible to determine almost any of the desired measures of rise and decay. Among the characteristics investigated were the time required for the *rate of change* of cathode current to reach a maximum value as well as to reach arbitrary specified values. These characteristics are potentially useful for automatic testing since the equilibrium current need not be known.

RISE CURVES

Study of the rise curves of hundreds of tubes of at least 16 different types indicate that these curves fall roughly within the four types

shown in Figure 1. Type A, by far the most prevalent, or "normal" type, has a fairly steep initial increase and a rounded knee. Type B, the second most prevalent, rises very slowly, sometimes taking many minutes to reach equilibrium. Type C has a steep slope and rounded knee similar to that of type A, but begins to slump at a point on or just beyond the knee, although it usually starts to rise again within the first few minutes of operation. Type D is a relatively rare type which starts to rise noticeably later than the normal or type A curve but has a steeper slope and a sharper knee.

The "normal" or type A rise curve is produced by a current which is initially temperature limited and then gradually becomes space-

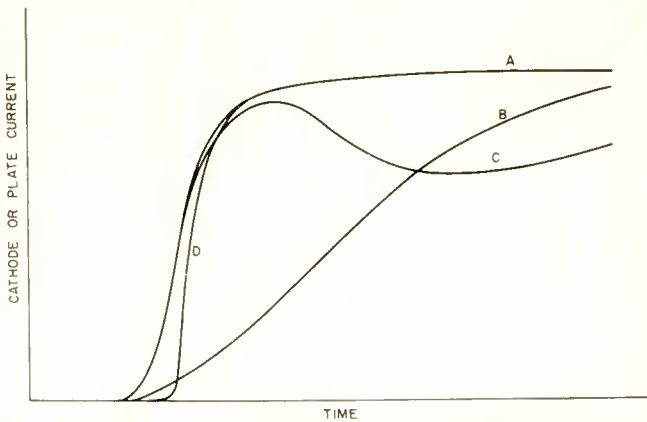


Fig. 1—The four major types of cathode-current-rise curves obtained in tests for several hundred receiving tubes of various types.

charge limited at some point below the knee. In curves for most diodes the transition between the two regions of the curve is masked by the effects of surface roughness and temperature differences along the length of the cathode which also tend to round off the knee of the rise curve. In curves for triodes or multi-grid tubes the transition is even more difficult to see because the distortion of the field at the cathode due to the presence of the grid does not permit a sudden transition from temperature-limited to space-charge-limited operation.

R. M. Matheson,* in an unpublished report, conclusively shows that longer-than-normal rise times, such as those represented by type B curves, can occur in picture tubes as a result of accumulations of electrons on semiconducting films on grid surfaces. Such films usually consist of materials evaporated from the cathode and may contain other

* RCA Laboratories, Princeton, N. J.

constituents produced by reactions between the cathode and grid materials. The films tend to limit electrode current until they have been heated sufficiently to decrease their resistance. There is little doubt that similar conditions exist in receiving tubes. Matheson, and another unpublished report by Hui*, suggest that slowly rising curves may also be caused by poor cathode activation.

Type C rise curves, it is believed, indicate partial deactivation of the cathode by poisoning agents released from other tube parts as the temperature rises. In trials with successively higher heater voltages, the dip becomes more pronounced and occurs sooner after power is applied. At very high heater temperatures, however, the deactivating action ceases, probably because of more efficient gettering action by the cathode. Tubes which produce type C curves, when operated at rated heater voltages, generally exhibit conventional rise behavior for the conditions when operated at low heater voltages—that is, their curves show a slow rise with no dip. Type C curves are usually not repeatable, and most tubes which produce such curves initially show normal, or type A, behavior after some high-temperature aging. In a small percentage of the tubes which produced type C rise curves, cathode current slumped steadily with time after a short initial recovery, and the cathodes eventually became completely inactive.

The reason for the delayed type D curves has not been determined because of the rarity and nonrepeatability of these curves. The few curves observed became normal type A curves after several runs. The only explanation that can be offered at this time is that under certain conditions, a cathode can be poisoned and then relatively quickly reactivated. If the reactivation occurs after the cathode has reached a fairly high percentage of its final temperature, there will be a sudden increase in current, such as occurs in the type D curve. Since so little can be offered at this time to explain this behavior, it will not be treated further in this paper.

DECAY CURVES

Because most cathodes take longer to cool than to warm up, a decay curve presents the total change in cathode current on a longer scale than does a rise curve and permits correspondingly better resolution. Consequently, the decay curves of most diodes and low- g_m triodes show the break between the space-charge-limited and temperature-limited regions which is not usually evident on rise curves. Only in certain cases does a factor which affects the shape of a rise curve also affect the shape of the corresponding decay curve. For example, a cathode-

* RCA Electron Tube Division, Marion, Ind.

poisoning agent which causes a very slow rise can easily cause a sudden decay if it is still active at the instant heater power is removed. Also, the rise and decay characteristics of tubes which have close-spaced grids shielding the cathode are apparently highly dependent upon the same factors which determine the space-charge-limited equilibrium current: that is, if the equilibrium current is low, the rise time will be long and the decay short. Rise and decay curves in these cases offer very little information. On the other hand, it is easily possible for certain effects, such as deactivation occurring during long shelf life, to clear up during the short time the tube is operated under equilibrium conditions before decay is initiated. Furthermore, temperature-sensitive factors such as the semiconductor grid films previously mentioned are unlikely to have the same effects on rise and decay curves because the temperature relationship between the contaminated grid and the cathode is not the same during the rise and decay intervals. Decay tests, rather than rise tests, therefore, are most likely to reflect conditions important to the equilibrium efficiency and life of a tube.

DIODE TESTS

The effects of cathode poisoning were studied with the aid of a special diode having a rotatable nickel plate and a picture-tube-type cathode approximately $\frac{1}{4}$ -inch in diameter, spaced 1 millimeter from the plate. The tube had been used for other work, and its plate had a brownish "activation" spot at one position (arbitrarily called 0 degrees) and a thick white film resulting from the flash of a getter in air at the 180-degree point. Although the other areas of the plate surface appeared "clean," repeatable retarding-potential readings taken every 45 degrees around the periphery of the plate showed significant differences in either the plate work function or film resistance, indicating that the apparently clean portions of the plate did not have identical surface conditions. Impedance measurements made with the aid of a Wagner pulse tester showed that when the plate was in its 90-degree position, the cathode was deactivated to a degree determined by the duration of plate-current flow. At any other position of the plate the cathode was either unaffected or reactivated, depending upon its previous state.

Starting with the cathode in an intermediate state of activation, recordings were made of the rise and decay of cathode current at points 45 degrees apart around the periphery of the plate. The resulting curves are shown in Figure 2. The break between space-charge-limited and temperature-limited currents can be clearly seen on the decay curves. The rise and decay curves for the 0-degree and 45-degree

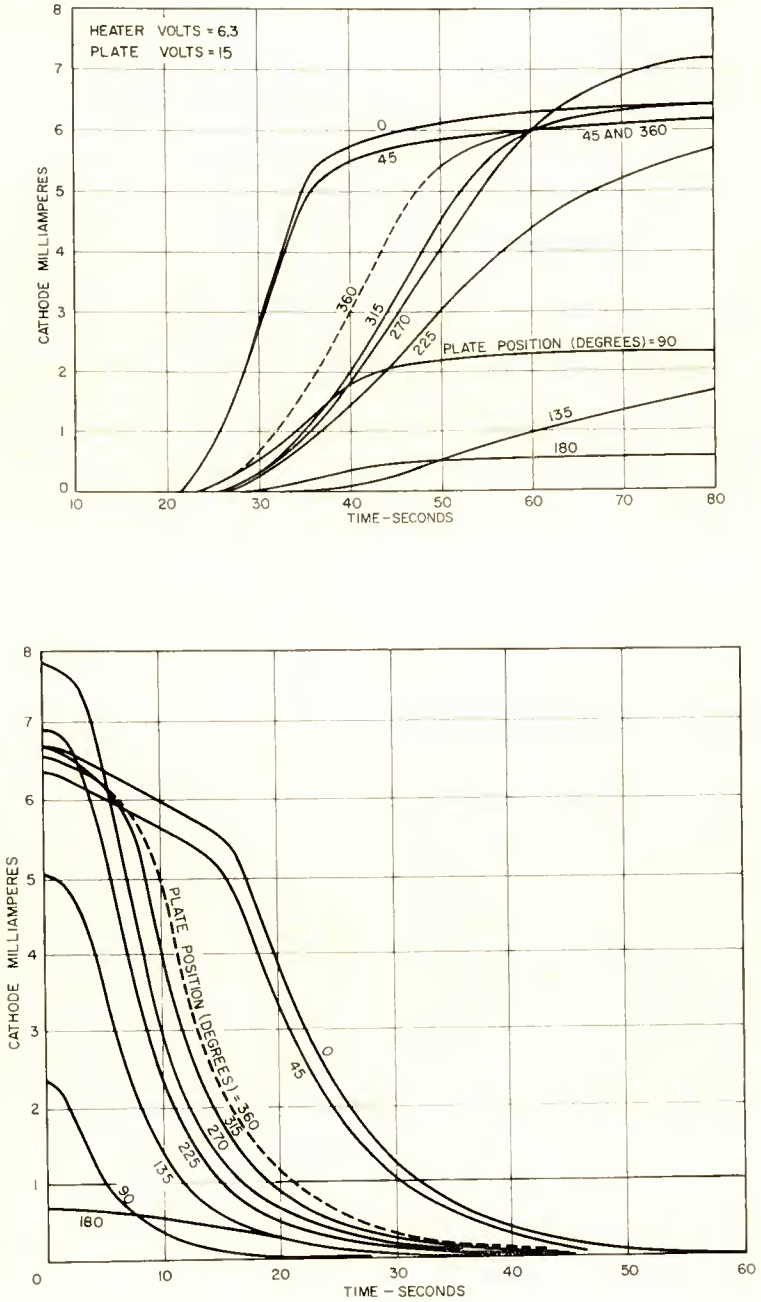


Fig. 2—Cathode current as a function of time of a special diode having a rotatable plate: (a) current rise; (b) current decay.

positions are very similar, the rise curve for the 45-degree position showing the effects of slight deactivation due to the proximity of the poisoning area surrounding the 90-degree position. The curve for the 90-degree position rises very slowly because of this poisoning, and levels off (i.e., reaches equilibrium) at a low value of current. The rapid decay in the 90-degree position suggests that the cathode current was probably temperature limited at the instant heater power was removed. The fact that the curve for 135 degrees rises even more slowly than that for 90 degrees shows the effects of the poisoning which took place during the 90-degree test. The continuous rise of the 135-degree curve, however, indicates that some reactivation is taking place. Although each subsequent test shows further reactivation taking place during the short time the cathode is at rated temperature, the cathode never recovers its original activity during the series of tests.

The rise and decay curves shown in Figure 2—that is, poisoning at the 90-degree position and reactivation at all subsequent positions—could be repeated at will. The low value of the equilibrium current at the 180-degree position is undoubtedly due to the voltage drops across the thick white film at this position. However, the initial position of the rise curve and the final portion of the decay curve for 180 degrees evidently maintain the proper sequence dictated by the progressive cathode activation. The differences in equilibrium value of cathode current not reasonably attributable to changes in cathode activation, and other differences between the curves, can be ascribed to slight differences in plate-to-cathode spacing and in the work function of the plate at the various positions.

Figure 3 shows the effect on the decay curves of variations in plate voltage (Figure 3a) and heater voltage (Figure 3b). The curves were obtained at a plate position where the degree of cathode activation was not affected. As expected, all the curves of Figure 3a decay into a common line representing the temperature-limited emission characteristic of the cathode. Figure 3b shows that the transition to temperature-limited emission is delayed as the cathode temperature is increased. The relatively flat slopes of the initial portions of the decay curve show that the space-charge-limited current is only slightly dependent on temperature and current. In some cases, decay curves of triodes and multi-grid tubes have steeper initial slopes which are concave upward, much like those of the temperature-limited portion of the decay curves. Since Matheson's study has shown that temperature-dependent semiconducting grid films can materially affect the rise curves, it is logical that such films, when present, will affect the

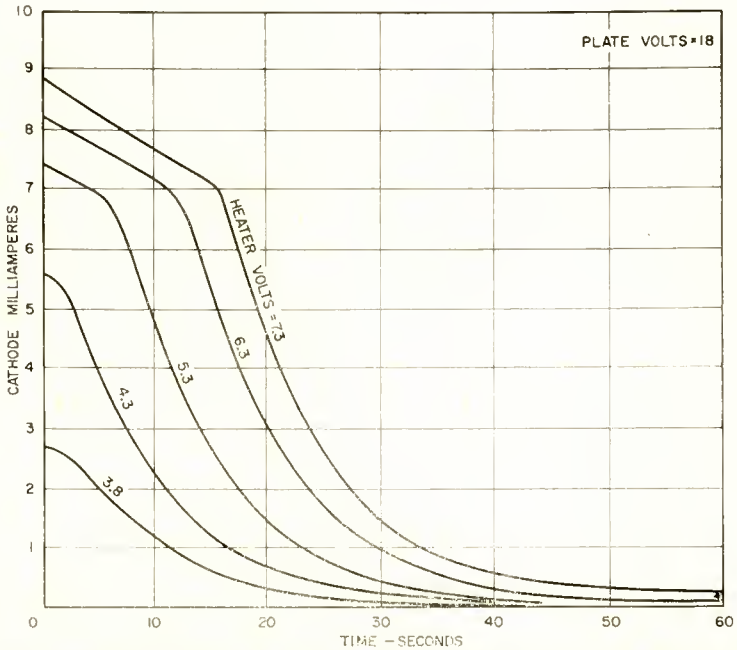
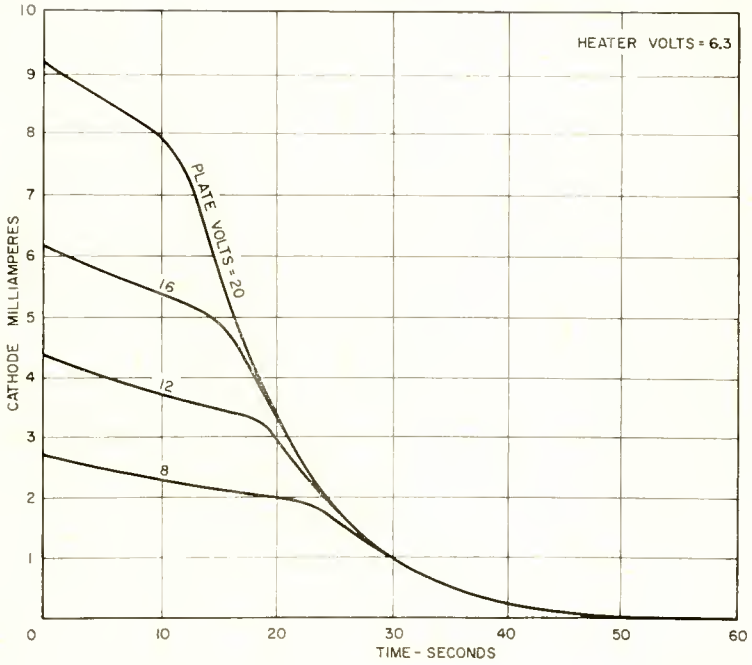


Fig. 3—Cathode-current-decay curves of rotatable-plate diode at plate position where no deactivation of cathode occurs: (a) effects of variation in plate voltage; (b) effects of variation in heater voltage.

decay curves of receiving tubes which have grids. The equation describing the temperature dependence of a semiconductor² is essentially equivalent in form to the de Boer equation for temperature-limited emission.³ In a private communication, L. S. Nergaard* has pointed out that if the voltage-current characteristics of the space-charge-limited region of the curves of Figure 3(a) are plotted with time as a parameter, information can be abstracted about contact-potential shifts due to the thermoelectric effect and the bulk resistance of the oxide. Further manipulation of the data shown in Figure 3(b) permits an approximation of the activation energy for cathode resistance. When the initial portion of the decay curve is affected by the voltage drop across the temperature-dependent semiconducting cathode coating, or any other semiconducting film, it can look like the later (lower) portion of the curve, although there would still be a distinct transition between the two portions. Curves for triodes and multi-grid receiving tubes may also be modified by the variation, with temperature, of local space-charge fields. The effects of this variation can dominate the shape of the entire curve and, as mentioned before, obliterate any recognizable transition from space-charge-limited to temperature-limited operation.

Figure 4 shows decay curves for a 6CG7 twin triode. These curves are similar to the diode curves shown in Figure 3a except that as a result of the variable field distortion created by the grid, the lines for various voltages do not decay into a common curve representing the temperature-limited-current characteristics of cathodes but into individual pseudo-saturation lines.

In the case of a diode, a rough approximation of the saturated emission at operating temperatures can be obtained by projection of the temperature-limited-current portion of the decay curves back to zero time. If the logarithm of the saturated current, I_s , (corrected to unit area) is plotted against the time of decay, t , a straight line results which can conveniently be extrapolated to zero time. The value derived for the cathode used with the rotating anode in its highest state of activation was 0.1 ampere per square centimeter. The value for the cathode of a 6AU4-GT diode was 7.5 amperes per square centimeter, a reasonable value for this tube. Since plots of $\log I_s$ versus the reciprocal of the cathode temperature, T , theoretically also yield

² F. Seitz, *The Modern Theory of Solids*, McGraw-Hill Publishing Co., New York, N. Y., 1940, p. 65.

³ I. G. Herrmann and P. S. Wagener, *The Oxide Coated Cathode*, Vol. II, Chapman & Hall, London, England, 1951, p. 179.

* RCA Laboratories, Princeton, N. J.

straight lines, the cathode temperature must decay as $A/(B + Ct)$ for the lower temperatures. Radiation laws predict a different decay of the higher temperatures, making it probable that the extrapolation gives only approximate values.

Operation Time

In life tests of ten 6AF4-A and ten 6X8 tubes, the times required for the cathode current to reach 80 per cent of its 2-minute value, and

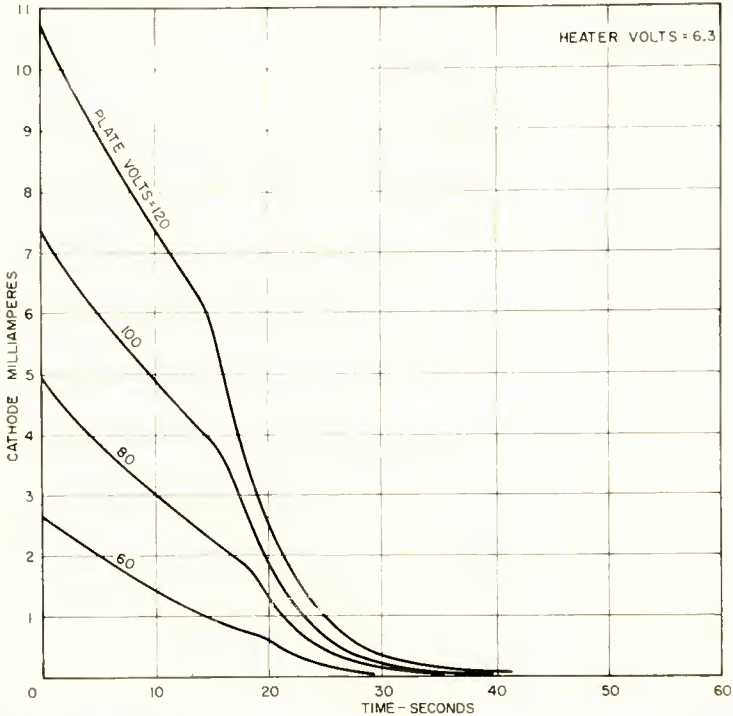


Fig. 4—Cathode-current-decay curves of type 6CG7 twin triode for different plate voltages.

to reach a rate of change of 0.2 milliamperes per second were measured at regular intervals. The resulting data for the ten tubes of each type tested were then averaged. The measurements involving the rate of change of cathode current showed practically no change during life. In the case of the 6AF4-A tubes, the average time required for the cathode current to reach 80 per cent of its 2-minute value was 13 seconds at 0 hours, 10 seconds at 2 hours, 16 seconds at 500 hours, and 14 seconds at 1,000 hours. None of the other conventional tests which accompanied these measurements gave any clue as to why the rise time peaked at 500 hours. The time required for the cathode current

to decay to 20 per cent of its 2-minute value was also measured on all tubes, but added little information to the rise data. While these results are probably indicative of the normal run of factory-produced tubes, other, less formal tests have shown wide variations of rise and decay data in the early hours of life.

Because operation time will probably become an increasingly important requirement in receiving-tube specifications, it is desirable to have some quantitative design data on this characteristic. To do this explicitly for all types of rise-time measurements is difficult because of (1) the intractable nature of heat conduction and radiation equations and (2) the lack of knowledge of cathode current during the transition between temperature-limited and space-charge-limited operation in practical cathodes. Because some rise-time measurements can involve this region, calculations which would give results for only the pure temperature-limited and space-charge regions were avoided. Instead, the rise of the cathode temperature is approximately calculated, and the time to get to any arbitrary temperature is used in place of the conventional rise time measurements. The calculations of cathode current are best avoided because it is the variations of cathode current rather than the variations in cathode temperature which are mainly responsible for the large differences sometimes found between rise curves of the same type.

A first-order approximation of changes in cathode temperatures (or rise time) sufficiently accurate for most purposes can be obtained if it is assumed that all the power expended in the heater is transferred to the cathode and then to other tube parts by radiation. The large differences between the equilibrium temperatures of the heater and cathode make it necessary to derive an expression for the increase of the heater temperature with time, and with the results in a general form, to apply the power radiated from the heater as the power input to the cathode. Following a general procedure set forth in an unpublished report by A. G. F. Dingwall* on the calculations of the heater warm-up characteristics of series-string tubes,

$$[ei - K_h (T_h^4 - T_o^4)] dt = 4.18 \sum_h C_h g_h dT_h \quad (1)$$

where e is the heater voltage (assumed to be constant);
 i is the instantaneous heater current in amperes;
 T_h is the heater temperature in degrees Kelvin;
 T_o is the ambient temperature in degrees Kelvin (this term will be neglected for most purposes);

* RCA Electron Tube Division, Harrison, N. J.

$\sum_h C_h g_h$ is the sum of the products of the specific heat in calories per gram and the weight in grams of each heater constituent (denoted by the subscript h);

K_h is a constant of proportionality relating radiated power to the fourth power of heater temperature;

4.18 is a constant used to convert joules to calories; and

t is time in seconds.

The instantaneous heater power is

$$ei = \frac{e^2}{r \frac{L}{A}} = \frac{W_f r_f}{r}, \quad (2)$$

where r is the heater resistivity in ohm-centimeters;

L is the length of the heater wire in centimeters;

A is the cross-sectional area of the heater wire in square centimeters;

W is the heater power input in watts; and

subscript f denotes the equilibrium value of a variable.

Equation (1), therefore, becomes

$$dt = 4.18 \frac{\sum_h C_h g_h dT_h}{W_f \frac{r_f}{r} - K_h (T_h^4)}. \quad (3)$$

The temperature dependence of the specific heat can be taken into account by application to the specific heat at the final temperature of a correction factor based on equal weights of heater wire and coating.

$$\sum_h C_h g_h \approx \sum_h (C_h g_h)_f \frac{C_h}{(C_h)_f} \equiv S_h a_h, \quad (4)$$

$$\text{where } S_h \equiv \sum_h (C_h g_h)_f, \text{ and } a_h = \frac{C_h}{(C_h)_f}.$$

When the numerator and denominator of Equation (3) are divided by $W_f = K_h T_{hf}^4$, and Equation (4) is applied, the result, expressed in incremental form, is

$$\Delta t = \frac{4.18 S_h}{W_f} \left[\frac{a_h \Delta T_h}{r_f \overline{T_h^4}} \right] \quad (5)$$

where $\overline{T_h^4}$ is the average value of T_h^4 for the interval ΔT_h (the ambient term T_o^4 being neglected).

The quantity in the parentheses in Equation (5) depends only on the heater composition and consequently is independent of the heater dimensions. In order to plot this general term on a suitable scale, a new variable is defined which includes the specific heat and power terms. This new variable is an "equivalent time" with the unit of degrees. It is divided by 1,000 to bring the calculations conveniently in accord with values commonly met with in receiving tubes.

$$\Delta \tau = \frac{W_f \Delta t}{1,000 S_h} = \frac{.00418 a_h \Delta T_h}{r_f \overline{T_h^4}} \text{ (degrees)}. \quad (6)$$

$\Delta \tau$, therefore, is expressed directly in seconds for a heater where $S_h/W_f = 0.001$. To convert the units of a graph of Equation (6) to true time, multiply the $\Delta \tau$ axis by 1,000 S_h/W_f , evaluated for the heater of interest.

Equation (6) was evaluated for tungsten heaters having alumina insulation, assuming small values for the increment ΔT_h and using corresponding values for a and r derived from information given in appropriate handbooks. This evaluation was carried out for equilibrium heater temperatures of 1,500°K and 1,700°K and is shown in Figure 5. Because of the small difference in the times required for the two curves to reach the same percentage of equilibrium temperature, the lower curve ($T_{hf} = 1,500^\circ\text{K}$) is used in all subsequent calculations involving the temperatures of cathodes having conventional tungsten heaters. Tests have shown that there is generally very good agreement (within approximately 15 degrees) between heater-temperature changes evaluated from Figure 5 and those calculated from the change in heater current with time. In these tests the equilibrium temperatures of the heaters were normalized to 1,500°K to allow direct comparison of the temperature changes. An example of such a comparison for a 35Z5-GT is given in Figure 6. To use Figure 5 for any tungsten heater, multiply the abscissa by 1,000 S_h/W_f and read the result directly in seconds.

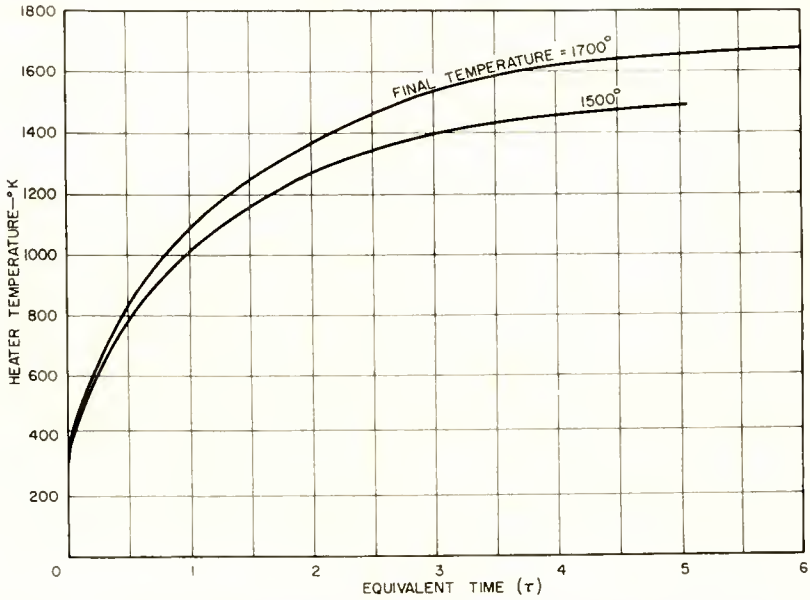


Fig. 5—Temperature of a tungsten heater as a function of equivalent time for final temperatures of 1700°K and 1500°K.

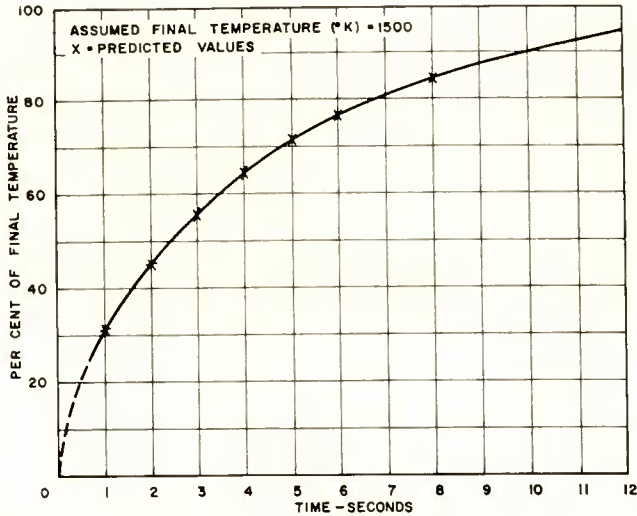


Fig. 6—Measured per cent increase with time of the temperature of a 35Z5-GT heater, compared with increase predicted from Figure 5. Assumed final temperature = 1500°K.

WARM-UP CONSIDERATIONS

The temperature transient (i.e., "warm-up") characteristics of a cathode may also be calculated by the general principles set forth above. The energy radiated from the heater is the input to the cathode which, at equilibrium, is equaled by the energy radiated from the cathode. Transfer by conduction is neglected because it can vary significantly from one tube to another and, therefore, would require knowledge of unavailable information. If it is assumed that there are no end losses, the power transferred by radiation alone at equilibrium can be expressed by

$$(K_h T_h^4)_f = (K_k T_k^4)_f = W_f, \quad (7)$$

where T_k is the absolute cathode temperature. As with the heater, the ambient temperature term, T_0^4 , will be neglected except when T_k is close to T_0 , where it will be understood that the T_k^4 term will be $(T_k^4 - T_0^4)$;

K_k is a constant of proportionality relating the power radiated from the cathode to the fourth power of the cathode temperature; and

subscript f denotes the final, or equilibrium value of a variable.

A heat-balance equation, similar to Equation (1), can also be written for the cathode;

$$(K_h T_h^4 - K_k T_k^4) dt = 4.18 \sum_k C_k g_k dT_k, \quad (8)$$

where $\sum_k C_k g_k$ is the sum of the products of the specific heat in calories per gram and the weight in grams of each cathode constituent (subscript k). Equation (8) divided by Equation (7), rearranged, and expressed in incremental form, becomes

$$\Delta t = 4.18 \frac{\sum_k C_k g_k}{W_f} \frac{\Delta T_k}{\frac{\overline{T_h^4}}{T_{hf}^4} - \frac{\overline{T_k^4}}{T_{kf}^4}}, \quad (9)$$

where, as before, the average values of the fourth power of the temperature during the interval Δt are used. The temperature dependence

of the specific heat of the cathode can be taken into account in the same manner as in Equation (4);

$$\sum_k C_k g_k = \sum_k (C_k g_k)_f \frac{C_k}{(C_k)_f} \equiv S_k a_k, \quad (10)$$

$$\text{where} \quad S_k \equiv \sum_k (C_k g_k)_f, \quad \text{and} \quad a_k = \frac{C_k}{(C_k)_f}.$$

For all practical purposes, the summation in a_k is negligible since the only cathode constituent which need be taken into account for the correction is the cathode nickel. When this correction is applied to Equation (9) and the result multiplied by $0.001 W_f/S_h$,

$$\frac{0.001 \Delta t W_f}{S_h} = \Delta \tau = \frac{0.00418 a_k \Delta T_k}{R \left(\frac{\overline{T_h^4}}{T_{hf}^4} - \frac{\overline{T_k^4}}{T_{kf}^4} \right)}. \quad (11)$$

$$\text{where} \quad R = \frac{S_h}{S_k}.$$

Physically, T_h is the independent variable, the cathode temperature T_k being related to it through τ and R . Although Equation (11) provides a relation for ΔT_k versus $\Delta \tau$ for any practical value of $\overline{T_h^4}/T_{hf}^4$ less than 1, only one of these solutions will correspond to the actual T_h reached by the heater.

Equation (11) can be evaluated in the incremental form by simultaneous solution with Equation (6) and substitution of values of a_k obtained from tables of specific heats. This evaluation has been performed for an assumed equilibrium cathode temperature of 1030°K and is shown in Figure 7. The abscissa is in terms of equivalent time τ and may be converted to time in seconds by multiplication by $1,000 S_h/W_f = 1,000 \left(\sum_h C_h g_h \right)_f / W_f$. The abscissa, therefore, depends only on the constants of the heater. The ordinate is in terms of $R = \sum_h (C_h g_h)_f / \sum_k (C_k g_k)_f = S_h/S_k$ which relates the heater and cathode constants. Equivalent times required to reach a constant cathode temperature are shown for various temperatures up to 970°K, each curve being drawn through three points calculated for $R = 0.2, 0.6,$ and 2.0 .

The calculated results shown in Figure 7 were compared with measured increases of cathode temperature, using the heater and cathode of a 6080-WA tube. A 0.005-inch chromel-alumel thermocouple was welded to the cathode at a point approximately one quarter the length

from one end, and the cathode then sprayed with conventional triple carbonates and processed in a vacuum. Because of some unexplained darkening around the thermocouple weld, the equilibrium temperatures were a little lower than usual and were, therefore, normalized to 1030°K. The measured values are shown in Figure 8 and show poor agreement with those predicted from Figure 7. A disturbing fact is

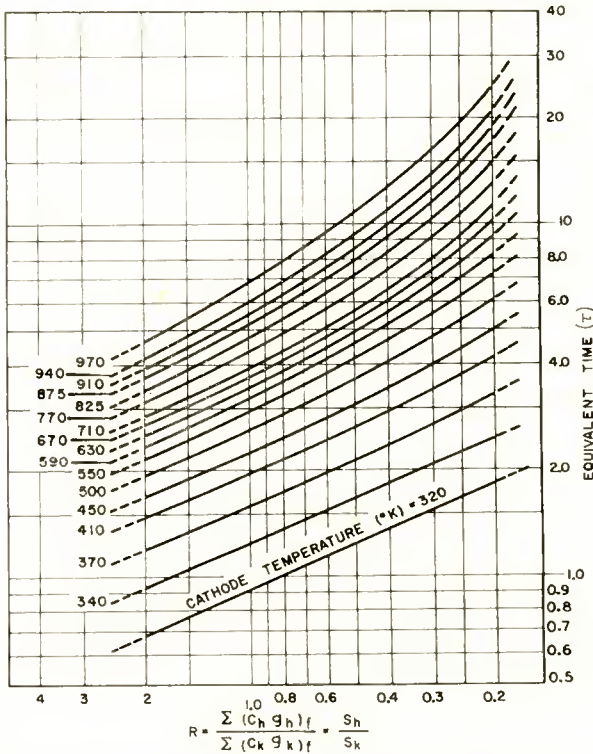


Fig. 7—Equivalent time required for a cathode to reach various temperatures as a function of heater and cathode properties. Transfer of heat by radiation only is assumed.

that there is little agreement between values obtained from different cathodes of the same type. Since a similar lack of agreement was observed in other cathode structures, it was assumed that not enough consideration was given to the effects of heater-cathode heat conduction.

The importance of heater-cathode conduction was tested using a 6080-WA heater suspended by tungsten springs in the center of a large cylindrical cathode in such a manner that no part of the heater touched the cathode. The results of this test are also shown in Figure 8. The fact that these results are in good agreement with the calcu-

lated values indicates that heater-cathode conduction can play an important part in cathode current rise characteristics of some commercial receiving tubes. It is logical, therefore, to question the good agreement between the measured and calculated values of heater temperature rise shown in Figure 6 for heater-cathode structures in which, presumably, the same conduction processes are going on. Part of this good agreement is due to the fact that it is only the temperature change of the tungsten wire which was measured (by changes in resistivity). The outside surface of the alumina coating is at a different temperature than the wire, the actual value at any point depending upon the degree

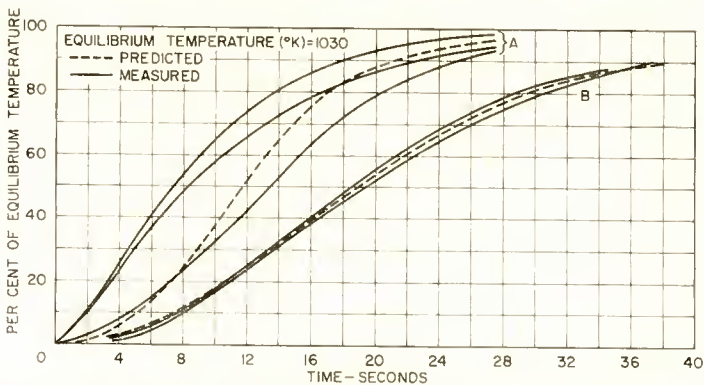


Fig. 8—Measured and predicted changes with time in temperatures of experimental cathodes, expressed in per cent of equilibrium temperature: Group A—conventional type 6080-WA heater-cathode assemblies, with physical contact between heater and cathode; Group B—special assemblies having type 6080-WA heaters suspended so as to eliminate physical contact between heater and cathode.

of contact with other heater strands and the inner surface of the cathode. Furthermore, because the equilibrium temperature of the heater is of the order of 500°K higher than that of the cathode, the integrated effect of radiation will be greater during heater warm-up than during cathode warm-up, making it more likely that the equations based on radiation fit the measured value.

Because of the variability of cathode temperature transients among tubes of the same type, and of the difficulty in uniquely determining the cathode current for the complete temperature range, it is impractical to calculate cathode or plate currents from the temperatures of Figure 7. However, to evaluate *changes* in rise time which are likely to result from given changes in cathode and heater construction, it is only necessary to choose, by measurement or experience, a particular cathode temperature at which the current is a desired percentage of the equilibrium value, for example, 875°K for 80 per cent of the

current. The line may then be selected from the family of constant-temperature lines in Figure 7 relating the heater and cathode weights and specific heats to a time in seconds required to reach 875°K. Such information is generally sufficient for design changes since some rise-time data are almost always available and it is only necessary to calculate changes rather than an absolute value of rise time.

CONCLUSION

From the results of many tests of receiving tube rise and decay currents, it has become evident that no simple interpretation will suffice to explain the large variations found. They result from the integrated effect of all phenomena which influence the effective electrode potentials and state of activation of the cathode.

Generally, the complexity of the curves and degree of nonrepeatability increases with the number of electrodes. The rise times of well-activated production diodes of any one type almost always agree within a few seconds. It is not uncommon, however, to have 5- to 15-second differences between triodes of the same type.

The time required for the rate of change of cathode current to reach a specified value sometimes shows similar changes, from tube to tube, as does operation time. The agreement between the two types of measurement is best when the arbitrary rate of change of current is chosen so that, on the average, it falls on the same portion of the rise curve as defined by operation time. The maximum rate of change, which has been used in some tests, occurs so soon after heater power is applied that most of the factors affecting the operation time have not yet fully acted. The maximum rate is therefore not satisfactory as a choice.

Variations in rise time due to changes in the construction of tungsten and alumina heaters and nickel cathodes can be predicted with accuracy sufficient for most commercial design purposes. Probable large differences in the degree of heater-to-cathode heat conduction between tubes make more accurate analysis unprofitable.

ACKNOWLEDGMENTS

The writer would like to thank E. G. Widell for the benefit of his knowledge and experience in the interpretation of this investigation and E. J. Hannig for making pulse measurements for the determination of cathode impedence. I. F. Stacy and A. G. F. Dingwall gave generously of their time to review the text. Mrs. D. A. Yanchusk has been extremely helpful in reducing the data and preparing many of the figures as well as in the construction of the experimental structures.

RCA TECHNICAL PAPERS†

Fourth Quarter, 1957

Any request for copies of papers listed herein should be addressed to the publication to which credited.

"An Equivalent Circuit for Microwave Noise at the Potential Minimum," S. Bloom (coauthor), <i>Trans. I.R.E. PGED</i> (October)	1957
"Anomalous Variation of Band Gap with Composition in Zinc Sulfide and Seleno-Tellurides," S. Larach, R. E. Shrader, and C. F. Stocker, <i>Phys. Rev.</i> (November 1)	1957
"Automatic Test Systems for Production," H. S. Dordick, <i>I.R.E. Wescon Convention Record, Part 5, Instrumentation, Telemetry and Remote Control</i>	1957
"Biperiodic Electrostatic Focusing for High-Density Electron Beams," K. K. N. Chang, <i>Proc. I.R.E.</i> (November)	1957
"The Bizmac Trancoder," D. E. Beaulieu, D. P. Burkart and C. H. Propster, Jr., <i>I.R.E. Wescon Convention Record, Part 4, Automatic Control and Computers</i>	1957
"Black Level—The Lost Ingredient in Television-Picture Fidelity," R. G. Neuhauser, <i>Jour. S.M.P.T.E.</i> (October)	1957
"A Carrier-Energized Bistable Circuit Using Variable-Capacitance Diodes," E. O. Keizer, <i>RCA Review</i> (December)	1957
"Circuitry Report On 21-Inch Color-TV Chassis Using Glass Picture Tube," J. A. May, <i>Service</i> (October)	1957
"Coherent Spontaneous Microwave Emission by Pulsed Resonance Excitation," L. E. Norton, <i>Trans. I.R.E. PGMTT</i> (October)	1957
"Color TV Recording on Black and White Lenticular Film," J. M. Brumbaugh, E. D. Goodale, and R. D. Kell, <i>Trans. I.R.E. PGBTR</i> (October)	1957
"Comparison of the Semiconductor Surface and Junction Photovoltages," E. O. Johnson, <i>RCA Review</i> (December)	1957
"A Constant Input-Impedance RF Amplifier for VHF," H. B. Yin and H. M. Wasson, <i>Trans. I.R.E. PGBTR</i> (October)	1957
"Conversion of AM Transmitters to DSB Operation," C. A. West, <i>CQ</i> (November)	1957
"Depot Test Equipment Concepts," D. B. Dobson, <i>Trans. I.R.E. PGANE</i> (December)	1957
"Design of a High-Speed Transistor Decimal Counter with Neon-Bulb Read-Out," R. D. Lohman, <i>I.R.E. Wescon Convention Record, Part 5, Instrumentation, Telemetry and Remote Control</i>	1957
"Designing Relays for High Reliability," D. H. Cunningham, <i>I.R.E. Wescon Convention Record, Part 6, Component Parts, Industrial Electronics and Production Techniques</i>	1957
"Effect of Impurity Scattering on the Magnetoresistance of n-Type Germanium," M. Glicksman, <i>Phys. Rev.</i> (October 15)	1957
"Effective Magnetic Anisotropy and Magnetostriiction of Monocrystals," P. K. Baltzer, <i>Phys. Rev.</i> (November 1)	1957
"Effects of Nuclear Radiation on Transistors," A. J. Schwartz, <i>Electronic Design</i> (December 15)	1957

† Report all corrections or additions to *RCA Review*, RCA Laboratories, Princeton, N. J.

"Electron Mobility in the Germanium-Silicon Alloys," B. Goldstein, <i>RCA Review</i> (December)	1957
"Electron Tubes," E. P. Bertin and I. F. Stacy, <i>The Encyclopedia of Chemistry</i> , Reinhold Publishing Corp., New York, N. Y.....	1957
"Erasing Magnetic Film for Noise-Free Splices," C. Shipman and C. Hittle, <i>Jour. S.M.P.T.E.</i> (November)	1957
"Experimental Facsimile Communication Utilizing Intermittent Meteor Ionization," W. H. Bliss, R. J. Wagner, Jr., and G. S. Wickizer, <i>Proc. I.R.E.</i> (December) (Letter to the Editor)....	1957
"Field Service Experiences with Color-TV Receivers," W. H. Powell, R. Scattergood, and J. W. Mills, <i>Service</i> (November).....	1957
"Future Circuit Aspects of Solid-State Phenomena," E. W. Herold, <i>Proc. I.R.E.</i> (November)	1957
"Glass Envelope 21-Inch Picture Tube For Color-TV," L. B. Headrick, <i>Service</i> (October)	1957
"Guided Missile Instrumentation Radar," I. Stokes and D. K. Barton, <i>Broadcast News</i> (October)	1957
"Heat Transfer in Power Transistors," I. G. Maloff, <i>Electronic Industries</i> (December)	1957
"Impact Noise Isolation in Television Studios," M. Rettinger, <i>Broadcast News</i> (October)	1957
"An Improved High-Gain Panel Light Amplifier," B. Kazan, <i>Proc. I.R.E.</i> (October)	1957
"Influence of Hydration-Dehydration of the Germanium Oxide Layer on the Characteristics of P-N-P Transistors," J. T. Wallmark and R. R. Johnson, <i>RCA Review</i> (December)	1957
"Installation Checks For Latest Color-TV Chassis," J. R. Meagher, <i>Service</i> (October)	1957
"Interrogation in the Bizmac System," D. E. Beaulieu and C. H. Propster, Jr., <i>I.R.E. Wescon Convention Record, Part 4, Automatic Control and Computers</i>	1957
"An Investigation of the Discharge Characteristics of Groups Ib-Vb Oxides in an Alkaline Electrolyte," R. Glicksman and C. K. Morehouse, <i>Jour. Electrochem. Soc.</i> (October)	1957
"Low-Noise Transistor Microphone Amplifier," J. J. Davidson, <i>Audio</i> (October)	1957
"Measurement of Minority Carrier Lifetimes with the Surface Photovoltage," E. O. Johnson, <i>Jour. Appl. Phys.</i> (November)....	1957
"A Method of Accurate Thickness Determination of Germanium Wafers Suitable for Transistor Production," A. R. Moore, <i>Trans. I.R.E. PGED</i> (October)	1957
"Monaural Tape Recorder-Stereotape Player," S. F. Pusey, <i>Service</i> (December)	1957
"Monovibrator Has Fast Recovery Time," A. I. Arcanson and C. F. Chong, <i>Electronics</i> (December)	1957
"Multiple Antenna Systems," I. T. Newton, Jr., <i>Broadcast News</i> (October)	1957
"New Approaches to the Amplification of Microwaves," J. P. Wittke, <i>RCA Review</i> (December)	1957
"100-Watt TV Transmitter Type TTL-100AL/AH," R. S. Jose, <i>Broadcast News</i> (December)	1957
"Orbiters Extend Image Orthicon Life in Color and Monochrome Operation," S. L. Bendell and K. Sadashige, <i>Broadcast News</i> (December)	1957
"A Packaged 4-Speaker Hi-Fi Radio-Phono," R. S. Fine, <i>Service</i> (November)	1957
"The Physics of the Cathode," L. S. Nergaard, <i>RCA Review</i> (December)	1957
"A Plea for Maximum Utility in Government Contract Reports Covering Research and Development," E. W. Herold, <i>Advisory Group on Electron Tubes News Bulletin</i> (October 1).....	1957

- "Pomsee Puts Them to Work," J. R. Jackson, *Signal* (December) . . . 1957
- "Predicting Performance of Candelabra Antennas by Mathematical Analysis," M. Siukola, *Broadcast News* (October) 1957
- "Proposed Reference Signals for Broadcast Television Transmission," J. W. Wentworth, *Broadcast News* (October) 1957
- "Puncher Transcribes Computer Output," J. E. Palmer, J. J. O'Donnell, and C. H. Proppster, Jr., *Electronics* (December) 1957
- "Qualitative Performance Evaluation of Land Mobile Systems," J. R. Neubauer, *I.R.E. Wescon Convention Record, Part 8, Aeronautical and Navigational Electronics, Communication Systems, Military Electronics, and Vehicular Communications* . . . 1957
- "Quantitative Estimation of Graphite in Refractory Carbon Deposits by X-ray Technique," P. G. Herold (coauthor), *Nature* (Letter to the Editor) (December 7) 1957
- "Radio Foundation Day 1957," D. Sarnoff, *Proc. I.R.E. (Australia)* (December) 1957
- "Realistic Tube Testing," J. M. Lowery, *Electronic Design* (December 15) 1957
- "Recent Developments in TV Camera Tubes," F. S. Veith, *Trans. I.R.E. PGPTS* (December) 1957
- "Reduction of Image Retention in Image Orthicon Cameras," S. L. Bendell and K. Sadashige, *Trans. I.R.E. PGPTS* (December) 1957
- "Report on the Second Symposium on the Physics of Semiconductors," F. Herman, *The Physics and Chemistry of Solids*, Vol. II, No. 1 1957
- "Simplified Treatment of Electric Charge Relations at a Semiconductor Surface," E. O. Johnson, *RCA Review* (December) 1957
- "Solid-State Light Amplifiers," B. Kazan and F. H. Nicoll, *Jour. Opt. Soc. Amer.* (October) 1957
- "Some Engineering of the Past and for the Future," T. A. Smith, *Jour. S.M.P.T.E.* (November) 1957
- "Some Graphical Approaches to Coding Problems," J. Dutka, *RCA Review* (December) 1957
- "Space Charge Neutralization in the Ionizing Beam of a Mass Spectrometer," R. H. Plumlee, *Rev. Sci. Instr.* (October) . . . 1957
- "On Spiral Etch Pits in Germanium and Silicon," S. G. Ellis, *Philosophical Magazine* (October) 1957
- "Surface Studies on Single-Crystal Germanium," S. G. Ellis, *Jour. Appl. Phys.* (November) 1957
- "Sync and Sweep Selection in CRO Applications," R. Samuel, *RCA Rad. and Tele. Serv. News* (December) 1957
- "Telemetering Receiving System at the Air Force Missile Test Center," H. A. Rcloff, *Trans. I.R.E. PGTRC* (December) 1957
- "The Television Color Translating Microscope," V. K. Zworykin, *I.R.E. Wescon Convention Record, Part 7, Audio, Broadcast and Television Receivers and Broadcast Transmission Systems* 1957
- "Television Receiver Picture-Area Losses," C. L. Townsend, *Jour. S.M.P.T.E.* (December) 1957
- "Theory of a Wide-Gap Emitter for Transistors," H. Kroemer, *Proc. I.R.E.* (November) 1957
- "Theory of Parametric Amplification Using Nonlinear Reactances," S. Bloom and K. K. N. Chang, *RCA Review* (December) . . . 1957
- "A Time Domain Synthesis for Optimum Extrapolators," C. W. Steeg, Jr., *Trans. I.R.E. PGAC* (November) 1957
- "The TM-21—A Stabilized Color Monitor," E. E. Gloystein and N. P. Kellaway, *Broadcast News* (December) 1957
- "The Transition from Engineer to Supervisor," H. M. Elliott, *I.R.E. Wescon Convention Record, Part 10, Engineering Management and Reliability and Quality Control* 1957
- "The Traveling-Wave VHF Television Transmitting Antenna," M. S. Siukola, *Trans. I.R.E. PGBTR* (October) 1957

“The Traveling-Wave VHF Television Transmitting Antenna,” M. S. Siukola, <i>I.R.E. Wescon Convention Record, Part 7, Audio, Broadcast and Television Receivers and Broadcast Transmission Systems</i>	1957
“Triboluminescence in Semiconductors,” D. A. Jenny, <i>Jour. Appl. Phys.</i> (Letter to the Editor) (December)	1957
“The Ultraviolet Color-Translating Television Microscope,” <i>Broadcast News</i> (December)	1957
“The Utilization of Domain Wall Viscosity in Data-Handling Devices,” V. L. Newhouse, <i>Proc. I.R.E.</i> (November)	1957
“The VTVM . . . Its Care and Repair,” R. Samuel, <i>Radio-Electronics</i> (December)	1957
“Why the Television Service Man Should Be a Color-TV Booster,” C. E. Walter, <i>Service</i> (October)	1957

AUTHORS



HAROLD BORKAN received the B.S. degree in Electrical Engineering from Rutgers University in 1950. During 1945 and 1946 he served in the U. S. Navy. In June 1950 he joined the technical staff of RCA Laboratories at Princeton N. J. He did graduate work at Rutgers on a part-time basis, receiving the M.S. degree in Electrical Engineering in 1954. Since 1952 he has been with the Electronic Research Laboratory and is concerned with circuit problems pertaining to television camera tubes. Mr. Borkan is a member of the Institute of Radio Engineers and Eta Kappa Nu.

K. K. N. CHANG received the B.S. degree from the National Central University, Nanking, China, in 1940; the M.S. degree in Electrical Engineering from the University of Michigan in 1948, and the D.E.E. degree in 1954 from the Polytechnic Institute of Brooklyn. From 1940 to 1945, he was associated with the Central Radio Manufacturing Works, Kunming, China, working on radio receivers and from 1945 to 1947, he was a radio instructor in the Office of Strategic Service, U. S. Army, China Theatre. Since 1948, he has been at RCA Laboratories, Princeton, N. J., where he has engaged in research on magnetrons, traveling-wave tubes, beam-focusing devices, and parametric amplifiers. Dr. Chang is a member of Sigma Xi.



KARL G. HERNQVIST received the Civilingenjor degree in Electrical Engineering from the Royal Institute of Technology, Stockholm, Sweden, in 1945, and the Teknologic Licentiat degree in 1951. From 1946 to 1952 he was employed by the Research Institute of National Defense in Stockholm working in the field of microwave electronics. From 1948 to 1949, Mr. Hernqvist was a trainee of the American-Scandinavian Foundation at RCA Laboratories, to which he returned in 1952; he is presently working in the field of gaseous electronics.

BENJAMIN KAZAN received the B.S. degree in Physics from the California Institute of Technology in 1938 and the M.A. degree in Physics from Columbia University in 1940. In 1940 he joined the Signal Corps Engineering Laboratories and was engaged in early experimental work with radar equipment. From 1944 to 1950 he was Chief of the Special Purpose Tube Section at the Evans Signal Laboratory, responsible for the development work and application engineering in traveling-wave tubes, klystrons, cathode-ray and storage tubes, crystal rectifiers, and transistor devices. Since 1951, Mr. Kazan has been engaged in research on television tubes and solid-state display devices at the RCA Laboratories, Princeton, N. J. Mr. Kazan is a member of the American Physical Society, Sigma Xi and Tau Beta Pi.





FREDERICK H. NICOLL received the B.Sc. degree in Physics from Saskatchewan University, Canada, in 1929 and the M.Sc. degree in 1931. He held an 1851 Exhibition Scholarship to Cambridge University, England for three years research and received the Ph.D. degree from that university in 1934. He was a research physicist with Electric and Musical Industries, Ltd. in London from 1934 to 1939. From 1939 to 1941 he was with the RCA Victor Division at Camden, N. J. as a research engineer. Since 1942 he has been with the RCA Laboratories in Princeton, N. J. engaged in research on cathode-ray

tubes and electron optics and, more recently, photoconduction and electroluminescence. Dr. Nicoll is a Senior Member of the Institute of Radio Engineers and a Member of the American Physical Society and of Sigma Xi.

STEFAN A. OCHS received the B.S. degree in Mechanical Engineering from Columbia University in 1943. After service in the U. S. Army, he did graduate work in physics at Columbia and obtained the A.M. degree in 1949 and the Ph.D. degree in 1953. In 1952, he joined the RCA Laboratories at Princeton, N. J., where he is engaged in research on television camera tubes. Dr. Ochs is a member of the American Physical Society, the Institute of Radio Engineers, and Sigma Xi.



EDWARD R. SCHRADER received the B.A. degree in Physics from Columbia University in 1950 and the M.S. degree in Physics in 1953 from the Polytechnic Institute of Brooklyn. He is now working toward a Ph.D. degree. He was engaged in oceanographic research for the American Museum of Natural History from 1950 to 1951. As an engineer for the Sperry Gyroscope Company he worked on aircraft instrument research and development from 1951 to 1954. Since 1954 he has been with the Receiving-Tube Chemical and Physical Laboratory of the RCA Electron-Tube Division at Harrison. His work is

chiefly concerned with the investigation of cathode and grid problems. Mr. Schrader is a member of the American Physical Society and of the Society of the Sigma Xi.

BERNARD N. SLADE received the B.S. degree in Electrical Engineering from the University of Wisconsin in 1948, and the M.S. degree from Stevens Institute of Technology in 1954. He joined the RCA Victor Division in Harrison, N. J. in 1948 where he was associated with the Advanced Development Group of the Tube Department. In 1953 he became Manager of the Semiconductor Advanced Development group, and in 1955 he joined RCA Laboratories in Princeton, N. J. In July 1956 he joined the International Business Machines Corporation at Poughkeepsie, N. Y. where he is presently Manager of Transistor Engineering. Mr. Slade is a senior Member of the Institute of Radio Engineers and a member of Sigma Xi.





HAROLD STARAS received the B.S. degree in Physics from the City College of New York in 1944, the M.S. degree from New York University in 1948, and the Ph.D. degree from the University of Maryland in 1955. From 1944 to 1947 he was with NACA at Langley Field, Va.; during the years 1947-1948 he was doing full-time graduate work at New York University; and from 1948 to 1954 he was on the staff of the National Bureau of Standards. In 1954 he joined the Advanced Development Section of RCA at Camden, N. J., and in 1956 he transferred to RCA Laboratories at Princeton, N. J. where his work

has been in the field of propagation and communications. Dr. Staras is a Senior Member of the Institute of Radio Engineers, and a member of the American Physical Society, Sigma Xi, the U. S. National Committee of URSI Commission II, and Study Group V of U. S. CCIR Preparatory Committee. He is also a lecturer in mathematics and physics at LaSalle College, Philadelphia.

PAUL K. WEIMER received the B.A. degree from Manchester College in 1936, the M.A. degree in Physics from the University of Kansas in 1938, and the Ph.D. degree in Physics from Ohio State University in 1942. During 1936 and 1937 he was a graduate assistant in physics at the University of Kansas. From 1937 to 1939, he taught physics and mathematics at Tabor College, Hillsboro, Kansas. Since 1942 he has been engaged in television research at RCA Laboratories Division at Princeton, N. J. Dr. Weimer is a Fellow of the Institute of Radio Engineers, and a Member of the American Physical Society and Sigma Xi.



